RL-TR-95-67, Vol II (of two)
Final Technical Report
April 1995

ULTRA WIDE BAND (UWB) RADAR DETECTION ANALYSIS AND DEMONSTRATION PROGRAM, PHASES I AND II

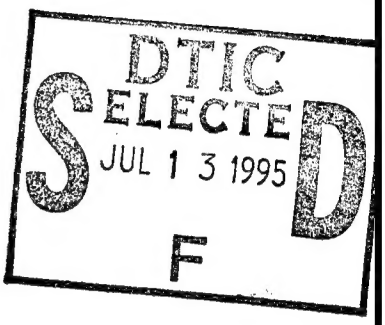

Technology Service Corporation

Sponsored by
Advanced Research Projects Agency
ARPA Order No. 9721

APPROVED FOR PUBLIC RELEASE; DISTRIBUTION UNLIMITED.

Rome Laboratory
Air Force Materiel Command
Griffiss Air Force Base, New York

This report has been reviewed by the Rome Laboratory Public Affairs Office (PA) and is releasable to the National Technical Information Service (NTIS). At NTIS it will be releasable to the general public, including foreign nations.

RL-TR-95-67, Vol II (of two) has been reviewed and is approved for publication.

APPROVED: Gerard J. Genello

GERARD J. GENELLO
Project Engineer

FOR THE COMMANDER: Donald W. Hanson

DONALD W. HANSON
Director of Surveillance & Photonics

If your address has changed or if you wish to be removed from the Rome Laboratory mailing list, or if the addressee is no longer employed by your organization, please notify RL (OCTS) Griffiss AFB NY 13441. This will assist us in maintaining a current mailing list.

Do not return copies of this report unless contractual obligations or notices on a specific document require that it be returned.

ULTRA WIDE BAND (UWB) RADAR DETECTION ANALYSIS AND DEMONSTRATION PROGRAM, PHASES I AND II

Allan Corbeil
Lee R. Moyer
Dr. Charles J. Morgan

Contractor: Technology Service Corporation (Subcontractor)
Syracuse University (Prime Contractor)
Contract Number: F30602-91-C-0035
Effective Date of Contract: 15 February 1991
Contract Expiration Date: 15 December 1994
Short Title of Work: UWB Radar Detection

Period of Work Covered: Feb 91 - Dec 94

Principal Investigator: Dr. Donald D. Weiner
Phone: (315) 443-4428

RL Project Engineer: Clifford Tsao
Phone: (315) 330-3576

This research was supported by the Advanced Research Projects Agency of the Department of Defense and was monitored by Clifford Tsao, RL (OCTS), 26 Electronic Pky, Griffiss AFB NY 13441-4514.

REPORT DOCUMENTATION PAGE

Form Approved
OMB No. 0704-0188

1. AGENCY USE ONLY (Leave Blank)	2. REPORT DATE	3. REPORT TYPE AND DATES COVERED
	April 1995	Final Feb 91 - Dec 94

4. TITLE AND SUBTITLE
ULTR WIDE BAND (UWB) RADAR DETECTION ANALYSIS AND DEMONSTRATION PROGRAM, PHASES I AND II

5. FUNDING NUMBERS
C - F30602-91-C-0035
PE - 63737D
PR - 1706
TA - 06
WU - 02

6. AUTHOR(S)
Allan Corbeil, Lee R. Moyer, and Dr. Charles J. Morgan

7. PERFORMING ORGANIZATION NAME(S) AND ADDRESS(ES)
Technology Service Corporation
6515 Main Street
Trumbull CT 06611

8. PERFORMING ORGANIZATION REPORT NUMBER
N/A

9. SPONSORING/MONITORING AGENCY NAME(S) AND ADDRESS(ES)
Advanced Research Projects Agency
3701 N. Fairfax Dr.
Arlington VA 22203-1714
Phillips Lab/WSH
3550 Aberdeen Ave SE, Kirtland NM 87117-5776
Rome Laboratory (OCTS)
26 Electronic Pky
Griffiss AFB NY 13441-4514

10. SPONSORING/MONITORING AGENCY REPORT NUMBER
RL-TR-95-67, Vol II (of two)

11. SUPPLEMENTARY NOTES
Rome Laboratory Project Engineer: Clifford Tsao/OCTS/(315) 330-3576

Prime Contractor: Syracuse University

12a. DISTRIBUTION/AVAILABILITY STATEMENT
Approved for public release; distribution unlimited.

12b. DISTRIBUTION CODE

13. ABSTRACT (Maximum 200 words)
A unique concept for UWB radar operation is presented. Advantages of the postulated concept are described. An innovative, computationally efficient signal processing technique utilizing wavelet transforms that has been developed by TSC is discussed. An example is presented in which actual UWB data that has been interpolated to simulate a high-PRF waveform is processed to validate the concept. A demonstration concept for the postulated UWB modulation is proposed.

14. SUBJECT TERMS
Ultra Wide Band Radar, high-PRF waveform

15. NUMBER OF PAGES
140

16. PRICE CODE

17. SECURITY CLASSIFICATION OF REPORT	18. SECURITY CLASSIFICATION OF THIS PAGE	19. SECURITY CLASSIFICATION OF ABSTRACT	20. LIMITATION OF ABSTRACT
UNCLASSIFIED	UNCLASSIFIED	UNCLASSIFIED	UL

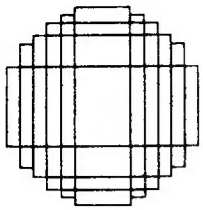

Technology Service Corporation

6515 Main Street, Trumbull, Connecticut 06611 Phone: (203) 268-1249

PHASE I, VOLUME II

TECHNOLOGY SERVICE CORPORATION

FINAL TECHNICAL REPORT

AIR FORCE ROME LABORATORY
CONTRACT NO. F30602-91-C-0035
SYRACUSE UNIVERSITY
SUBCONTRACT NO. 352-1272

TABLE OF CONTENTS

TABLE OF CONTENTS (Continued)

TABLE OF CONTENTS (Concluded)

LIST OF FIGURES

LIST OF FIGURES (Concluded)

LIST OF TABLES

1.0 INTRODUCTION

This final technical report presents the results of the first phase of the Ultra-Wide Bandwidth (UWB) Radar Detection Analysis and Demonstration Program. This work was performed by the Connecticut Operation of Technology Service Corporation (TSC) under Subcontract No. 353-1272 to Syracuse University (SU). The SU prime contract, No. F30602-91-C-003, is being conducted for the Air Force Rome Laboratory (AFRL) and the Defense Advanced Research Projects Administration (DARPA). The period of performance for Phase I of this program was from 15 February to 30 September 1991, and the TSC principal investigators were Messrs. Allan Corbeil and Lee Moyer.

TSC received an additional funding increment to support DARPA contractors performing UWB signal processing. This effort was performed during the period of 20 April to 14 July, 1992. Appendix A of this report describes the supplementary work that was performed under this effort. Mr. Lee Moyer and Dr. Charles Morgan of TSC performed the research on the supplemental effort.

1.1 Program Objective

The purpose of this program is to analyze UWB radar signatures of aircraft targets, and to use the insight gained to develop reliable moving target detection (MTD) algorithms. The intended application of these MTD algorithms is a new type of UWB surveillance radar that provides high range resolution (HRR) measurements of targets and clutter. Such UWB radars are currently being considered for development because they offer a number of advantages compared to conventional radars. Depending on radar implementation and interference conditions, these advantages include low probability of intercept (LPI), much greater subclutter visibility, and less susceptibility to multipath [1].

Although both coherent and noncoherent processing algorithms were

investigated on this program, TSC concentrated on noncoherent and hybrid noncoherent/coherent techniques. These algorithms can offer nearly the same performance as optimal coherent processing at modest signal-to-noise ratios when preceded by clutter prefiltering, and should generally have lower signal processing requirements.

The MTD algorithmsms developed on this effort are applicable to a wide variety of air and ground targets. The targets include low observable (LO) cruise missiles and manned, stealth aircraft that can penetrate conventional radar defensive networks. The results described in this report should thus be of interest to other contractors and Government investigators involved in the Balanced Technology Initiative (BTI) program being sponsored by DARPA.

1.2 Technical Approach

TSC's approach on Phase 1 of this program was to make maximum use of previously collected UWB radar data taken at S-band. This measured radar data was originally recorded by TSC and Syracuse Research Corporation (SRC) on the Real-Time Multisensor algorithms Experiment (RTAE) program, AFRL Contract No. F30602-88-C-0125 [2]. The S-band measurements include signatures of a variety of small and large commercial aircraft. On the present effort, the signatures were extracted from high density tape to create a more convenient VAX computer database. This database was then analyzed to determine the key characteristics of UWB target returns.

These S-band measurements include little clutter interference because of the look-up viewing geometry and narrow, pencil beam of the S-band tracking radar. In addition, the data was originally collected at a high signal-to-noise ratio (SNR) for real-time Inverse Synthetic Aperture Radar (ISAR) imaging experiments. Therefore, both receiver noise and clutter interference were simulated by TSC and combined with the measured data to evaluate candidate MTD algorithms. In this

way, a wide variety of realistic operating scenarios and interference conditions could be investigated using the same set of S-band target measurements.

A preliminary analysis of S-band signatures found that most UWB target returns consist of 2 to 4 dominant scatterers. Together, these scatterers make up 60 to 80% of the total target Radar Cross-Section (RCS). The amplitude and phase characteristics of these scatterers were also found to remain relatively constant from pulse-to-pulse over short coherent processing intervals (CPI).

Based on this scattering phenomenology, MTD algorithms which first identify the primary scatterers were developed. This is accomplished, for example, by thresholding the returns and selecting the largest signal peaks in each pulse. Regression analysis is then performed on the peak locations in each pulse to search for linear target motion.

A variety of peak-finding and linear regression algorithms were investigated on this program. Each algorithms employs unique rules for associating the peaks in different pulse returns, and some form of coincidence logic to declare a target detection. To evaluate each algorithm, Monte Carlo computer experiments were conducted using simulated, noise-only and measured target-plus-simulated noise data.

Each candidate MTD algorithm was also tested against selected clutter-only and target-plus-clutter conditions. Of particular interest were low SCR conditions because these stress the MTD algorithms the most. Linear distributions of clutter discretes and intermixed target and clutter returns, both of which can degrade the performance of linear regression algorithms, were also tested. To overcome these clutter limitations, MTI filtering algorithms to reject clutter prior to regression processing were also investigated.

1.3 Algorithm Overview

In Phase I, TSC developed several, reliable linear regression

algorithms to detect moving targets in UWB radar returns. A hybrid regression and Coherent Doppler Filtering (CDF) technique was also developed.

The linear regression algorithms developed on this effort involved the following five basic steps:

1. Apply a threshold to the magnitude detected UWB signals.
2. Determine the location and features of scattering peaks.
3. Associate peaks from different pulses by a set of matching rules.
4. Define a candidate line of motion for each match that is found.
5. Declare a detection based on the degree of alignment with other peaks.

Individual linear regression algorithms are distinguished by the matching rules used to associate peaks, and by the procedures for testing peak alignment.

A clutter rejection prefiltering algorithm was also developed to address severe clutter conditions. Conventional delay line cancellers (DLC) eliminate clutter by subtracting radar returns on a pulse-by-pulse basis. In UWB returns, however, the target moves between range cells on consecutive pulses. Thus subtraction cancels stationary clutter but produces a doublet for each target scatterer. TSC therefore developed a modified DLC algorithm that recombines this doublet prior to MTD algorithm processing.

1.4 Multiband Polarization Demonstration

As part of its subcontract, TSC also supported SU in collecting S-band radar data to investigate multiband polarization cancelling (MBPC) algorithms. The MBPC technique employs a multi-frequency transmit waveform to discriminate targets from clutter based on differences in their polarization states. The use of multiple frequency bands improves the probability that the clutter and target signal

will have a significantly different polarization angle in at least one band.

For the experimental test, TSC assisted AFRL engineers in setting up the radar equipment, recording the received data, and identifying suitable target-in-clutter measurement events. TSC then installed a MBPC processing demonstration on the Sun workstation at AFRL that describes this experiment. This automated demonstration displays a sequence of viewgraphs and analysis plots prepared by SU researchers using the MATLAB and FRAMEMAKER software tools. The plots show the MBPC waveform, processing block diagram, and a target-in-clutter detection example. Further information on this MBPC processing investigation can be found in SU's Final Report and Mr. C.J. Lee's Ph.D. Research Proposal [3].

1.5 Further Research

During the course of this effort, several areas were identified where further research is warranted. These areas include collecting additional UWB data on targets and clutter, developing high performance Moving Target Indication (MTI) algorithms to reject severe clutter interference, and developing a real-time implementation of the hybrid regression CDF technique.

The S-band radar at AFRL has recently been upgraded to a 640 MHz bandwidth, providing a nominal 0.234m range resolution. This radar could be very effectively used to gather data on a wide variety of commercial, private and military aircraft flying near Griffiss Air Force Base (AFB). Clutter measurements can also be collected on several types of terrain cover including urban, farmland, and forested regions. TSC is in an excellent position to make such measurements because of our recent clutter modeling and validation work for the Federal Aviation Agency (FAA), under Contract No. B52-0634 [4]. On this effort, TSC obtained a digital terrain and cultural feature database for the area surrounding Griffiss AFB, and collected S-band radar data to validate various clutter scattering models.

TSC's initial work on clutter prefiltering algorithms should also be continued. Such algorithms are required to reject the most severe clutter interference prior to regression analysis. TSC has identified several promising techniques based on conventional Constant False Alarm Rate (CFAR) and DLC algorithms. These techniques must now be evaluated against a UWB database of measured clutter returns.

Finally, the hybrid regression/CDF algorithm that was developed on this program should be validated in a real-time processing experiment at AFRL. For this purpose, the algorithm can be readily implemented on either the ST-100 Array Processor (STAR) or a Sun workstation and attached SKYbolt i860-based processor. High speed processing on these platforms is also the most efficient way to conduct further performance evaluations.

1.6 Report Organization

The remainder of this report is organized as follows. Section 2 describes the UWB database that was generated using previously collected S-band radar measurements. This required extracting radar returns for each target aircraft from high density tape, and then simulating receiver noise and clutter discretes to degrade the high SNR data. Section 3 presents the analysis of UWB target signatures that are contained in this database.

Section 4 is a review of coherent and noncoherent techniques suitable for UWB signal processing. Section 5 describes the new regression analysis algorithms that were developed on this program. These include the peak-pair matching (PPM), peak alignment counting (PAC), and the hybrid regression/CDF techniques. Section 6 discusses clutter rejection filtering which must precede both of these regression-based MTD algorithms.

Section 7 of this report presents the results of a detailed performance evaluation carried out for the PAC regression algorithms. The evaluation

procedure, performance against individual aircraft types, and observed trends are discussed here. Section 8 then presents an analysis of the detection performance and processing requirements of a UWB surveillance system based on the S-band radar at AFRL.

Finally, Section 9 presents the conclusions of this study, and outlines areas identified for further work in more detail. Section 10 contains a list of references, and for convenience, Table 1.6-1 contains a list of acronyms that are used throughout this report. Additional information on any of the topics covered here can be obtained from Mr. Allan Corbeil or Mr. Lee Moyer of TSC at (203) 268-1249.

TABLE 1.6-1 LIST OF ACRONYMS

ALGORITHMS

AR	-	Autoregressive Model
CDF	-	Coherent Doppler Filtering
CFAR	-	Constant False Alarm Rate Processing
DLC	-	Delay Line Canceller
FFT	-	Fast Fourier Transfer
ISAR	-	Inverse Synthetic Aperture Radar
MBPC	-	Multiband Polarization Cancelling
MDLC	-	Modified DLC Algorithm
MEM	-	Maximum Entropy Method
MF	-	Morphological Filtering
MTD	-	Moving Target Detection
MTI	-	Moving Target Indication
NCTI	-	Non-Cooperative Target Identification
PAC	-	Peak Alignment Counting
PC	-	Pulse Compression
PPM	-	Peak Pair Matching
TBD	-	Track-Before-Detect

HARDWARE

ADC	-	Analog-to-Digital Converter
DHI	-	Dedicated Hardware Interface
FIFO	-	First-In First-Out Buffer
HBR	-	High Bit Rate 3000 Tape Recorder
HG	-	Header Generator
IBIS	-	1.4 Gbyte Disk Attached to STAR

MISCELLANEOUS

ECM	-	Electronic Counter Measures
ESM	-	Electronic Support Measures Receiver
HRR	-	High Range Resolution
IFF	-	Identification Friend or Foe System
I/O	-	Input/Output
JSS	-	Joint Surveillance System
LO	-	Low Observable Target
LOS	-	Line of Sight to Radar
LPI	-	Low Probability of Intercept
RMS	-	Root Mean Square
ROC	-	Receiver Operating Curve
UWB	-	Ultra-Wide Bandwidth

TABLE 1.6-1 LIST OF ACRONYMS (Continued)

ORGANIZATIONS

AFB	-	Air Force Base
AFRL	-	Air Force Rome Laboratory
DARPA	-	Defense Advanced Research Projects Administration
FAA	-	Federal Aviation Administration
KSC	-	Kaman Science Corporation
SRC	-	Syracuse Research Corporation
SU	-	Syracuse University
TSC	-	Technology Service Corporation

PROCESSORS

HP	-	Hewlett Packard 2117F or A900 Computer
SKY	-	SKYbolt i860-based Vector Processor Attached to SUN
STAR	-	ST-100 Array Processor
SUN	-	SPARCserver 470 Workstation
VAX	-	VAX 8650 or MicroVAX 3300 Computer

PROJECTS

BTI	-	Balanced Technology Initiative
RTMSAE	-	Real-Time Multisensor Algorithm Experiment

QUANTITIES

CPI	-	Coherent Processing Interval
CNR	-	Clutter-to-Noise Ratio
KW	-	Kilowatts
MDV	-	Minimum Detectable Velocity
P_D	-	Probability of Detection
P_{FA}	-	Probability of False Alarm
PRF	-	Pulse Repetition Frequency
PRI	-	Pulse Repetition Interval
RCS	-	Radar Cross Section
SCR	-	Signal-to-Noise Ratio
SNR	-	Signal-to-Clutter Ratio

TABLE 1.6-1 LIST OF ACRONYMS (Concluded)

SIGNALS

DC	-	Direct Current (Zero-Frequency)
H	-	Horizontal Polarization
I	-	In-Phase Component
IF	-	Intermediate Frequency
Q	-	Quadrature Component
RF	-	Radio Frequency
V	-	Vertical Polarization

SOFTWARE

APCL	-	Array Processor Control Language for STAR
DBMS	-	Database Management Software
MATLAB	-	Mathematics Laboratory by Mathworks, Inc.
RSW	-	Radar Software Workbench
RTP	-	Run-Time Parameter Files
SPLEX	-	Signal Processing Laboratory Executive Program on HP
SRCIM	-	Syracuse Research Corporation's Image Processing Package
UT	-	UWB Target Files
WASP	-	Waveform Analysis and Signal Processing Package at TSC
TBD	-	Track Before Detect

UNITS

dB	-	decibels
GFLOPS	-	Billions of Floating Point Operations per Second
kHz	-	Thousands of Hertz
km	-	Thousands of Meters
m	-	Meters
MFLOPS	-	Millions of Floating Point Operations per Second
MHz	-	Millions of Hertz
MIPS	-	Millions of Instructions per Second
MOP	-	Millions of Operations
m/s	-	Meters per Second
msec	-	Milliseconds
nmi	-	Nautical Miles
µsec	-	Microseconds

WAVEFORMS

NB	-	Narrowband 40 µs, 2.5 MHz LFM Chirp Pulse
WB	-	Wideband 76.8 µsec, 320 MHz LFM Stretch Pulse
LFM	-	Linear Frequency Modulation

2.0 UWB DATABASE

Readers not concerned with the data collection details may skip over this section without any loss in understanding this report.

On this program, TSC developed an extensive VAX computer database of UWB target signatures at S-band. The primary purpose for generating this database was to analyze target signatures to better understand UWB scattering phenomenology. A second purpose was to evaluate candidate MTD algorithms. To address realistic surveillance conditions, it was necessary to degrade the SNR of the measured signatures and to add clutter interference signals. For this purpose, TSC developed several new database management software (DBMS) tools, and utilized our existing Waveform Analysis and Signal Processing (WASP) software package.

2.1 S-band Measurements

High range resolution (HRR) measurements of aircraft targets of opportunity were originally collected at AFRL on the RTMSAE effort by TSC and SRC. The measurements were made with the assistance of AFRL engineers in February and October 1990 to support real-time ISAR experiments. An example HRR image of an unknown aircraft is shown in Figure 2.1-1. The S-band radar parameters for these HRR ISAR experiments are presented in Table 2.1-1. Note that the 320 MHz waveform bandwidth represents 10% of the S-band radar operating frequency. The AFRL S-band radar has now been upgraded to support a 640 MHz (20%) bandwidth waveform.

The aircraft targets for which UWB measurements were collected include a diverse set of small and large commercial aircraft. Of most interest, however, were small aircraft moving at low radial speeds. These are the most challenging targets to detect, since they have the fewest number of scatterers and the smallest range movement per pulse.

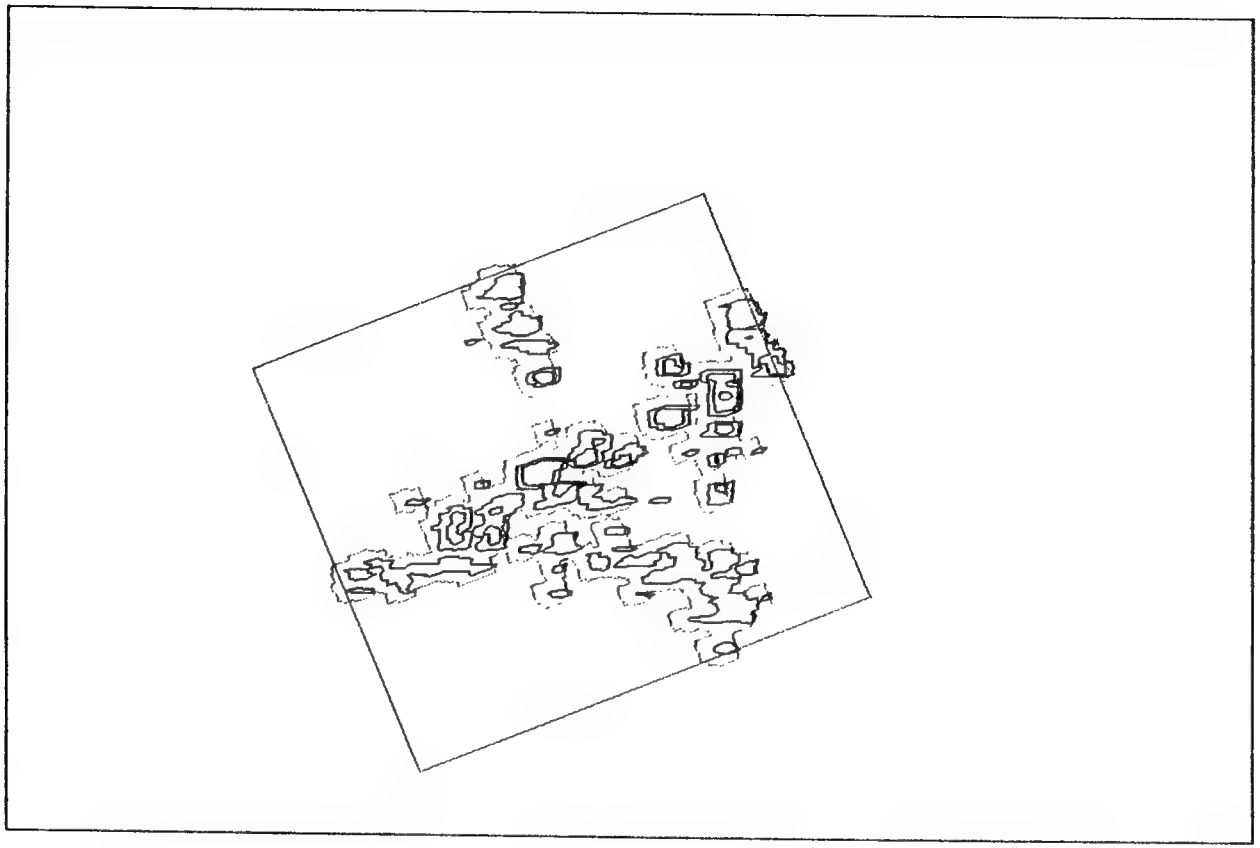

Figure 2.1-1 HRR ISAR Image of Unknown Aircraft

TABLE 2.1-1 HRR ISAR EXPERIMENT PARAMETERS

S-Band Frequency	=	3.35 GHz
Transmit/Receive Polarization	=	Vertical
LFM Pulse	=	76.8 μsec Duration, 320 MHz BW Upramp
PRI	=	4 ms (Interleaved by a NB Track Pulse)
A/D Clock Rate	=	13.33 MHz
Number ADC Bits	=	12 (I & Q)
FIFO Load Signal	=	Track Range Gate
FIFO Dump Signal	=	NB Pulse at 2 ms
FIFO Reset/HG Trigger	=	WB Pulse
FIFI Read/HBR Record Clock	=	1 MHz

Special SPLEX Setup: S-Menu, Item #4 = Interleaved Mode: On
M-Menu, Item #8 = Header Select: Track Range

Hardware Connections: 1 MHz Clock to HBR Recorder
Track Gate to FIFO Load
NB PRI to FIFO Dump
WB PRI to FIFO Reset
5 MHz Range Counter to HG Input

Table 2.1-2 presents a summary of the S-band HRR ISAR measurements, including the target type, High Bit Rate (HBR) recorder tape positions, and operator notes from the test log. These data recordings were reviewed by TSC to select representative radar dwells for each aircraft. Note that each target was recorded over a time period lasting only a few minutes, and were viewed primarily at near-tangential aspect angles. This aspect which was purposely selected to maximize target rotation angle for ISAR imaging, but fortuitously provides a low radial velocity. Since most of the targets were commercial, passenger-carrying aircraft, their speed and direction did not change significantly over the recording period. Therefore, to create the UWB database, it was sufficient to extract a few "snapshots" of the slowly changing target signature.

The S-band viewing geometry for ISAR imaging is not ideal for evaluating all aspects of MTD algorithm performance. The S-band tracker has a narrow pencil beam of 0.8° beamwidth, and operates primarily at look-up elevation angles. This is because Griffiss AFB is located in a valley, and most targets flew at medium-to-high altitudes. Therefore little clutter interference is present, except that which enters through the 20 dB one-way S-band antenna sidelobes. In fact, only one instance of clutter was measured in the narrow (500m) range window where the target signals were acquired.

2.2 HRR Data Extraction

The signal processing sequence for the real-time ISAR experiments is described in detail in the RTMSAE Final Report. This sequence consists primarily of: 1) STRETCH pulse-compression (PC) processing on the STAR to produce HRR sweeps, and 2) range alignment/Doppler integration on the VAX computer to produce an ISAR image. To extract the HRR sweeps in a form suitable for UWB signature analysis, it was necessary to modify the real-time STAR software code. To understand these modifications, the wideband mode of the S-band radar must

TABLE 2.1-2 SUMMARY OF HRR TARGET MEASUREMENTS

TEST DATE	AIRCRAFT	IFF ID	TAPE HBR LOCATIONS (ft)	RANGE (nm)	ALTITUDE (kft)	OPERATOR NOTES
FEB. 90	Unknown	4156	500-1060	46-67	33	-
	DC-10	6642	1060-2116	52-77	28	-
	Beechcraft-1900	4655	2116-2554	27-20	7.6	-
	DC-9	1111	2554-4130	29-55	31	-
	B-52	324	4130-4834	5-11	3.6	12 dB Attenuation Frequent Saturation
	L-1011	3341	4834-5707	37-75	37	-
	Cessna 402	5365	5707-6002	22-29	8.5	-
	Cessna 310	4502	6002-6312	17-22	11.6	Poor Track
	Beechcraft 99	5360	6312-7700	31-80	6.7	-
OCT. 90	Unknown	4614	0-500	25-10	31	No Attenuation
	DC-10	3520	580-1800	10-30	35	3 dB Attenuation, Some Saturation
	Unknown	7461	1800-2480	27-31	19.7	3 dB Attenuation

first be explained.

2.2.1 Wideband Radar Mode

In wideband mode, the AFRL S-band tracking radar transmits an interleaved narrowband (NB) and wideband (WB) pulse waveform. The NB pulse is a standard 40 μs, 2.5 MHz Linear Frequency Modulated (LFM) chirp which is pulse-compressed in hardware to support monopulse angle measurements that keep the target centered in the S-band radar beam. The WB range track is used to trigger a deramp signal at the proper target range on the next WB pulse. This provides a HRR range acquisition window roughly centered at the target position and substantially simplifies real-time STRETCH PC processing. The overall system configuration for this WB mode is illustrated in Figure 2.2.1-1, and the waveform timing diagram is shown in Figure 2.2.1-2.

For each WB pulse, radar In-phase and Quadrature (I/Q) samples within a 500m range window are acquired at a 13.33 MHz Analog-to-Digital Converter (ADC) rate. These WB samples are sent via a First-In First-Out (FIFO) buffer to a Hewlett Packard (HP) computer-controlled Header Generator (HG) module at a 1 MHz rate. The FIFO buffer load and dump gates are controlled by the deramp trigger and NB pulse, respectively. This 13.33:1 reduction in clock speed permits the digital data to be recorded on HBR tape and/or transferred to the STAR via a Dedicated Hardware Interface (DHI). The size of the FIFO buffer and present clock rates are sufficient for up to 2000 I/Q samples to be stored and read out at the 1 MHz clock rate during each interleaved 2 ms NB pulse period.

Note that the HG adds several header words to each pulse record including time and date, HBR tape position, and the S-band tracker elevation, azimuth and range. This information was read back from the high density AMPEX tapes to determine the original radar measurement conditions.

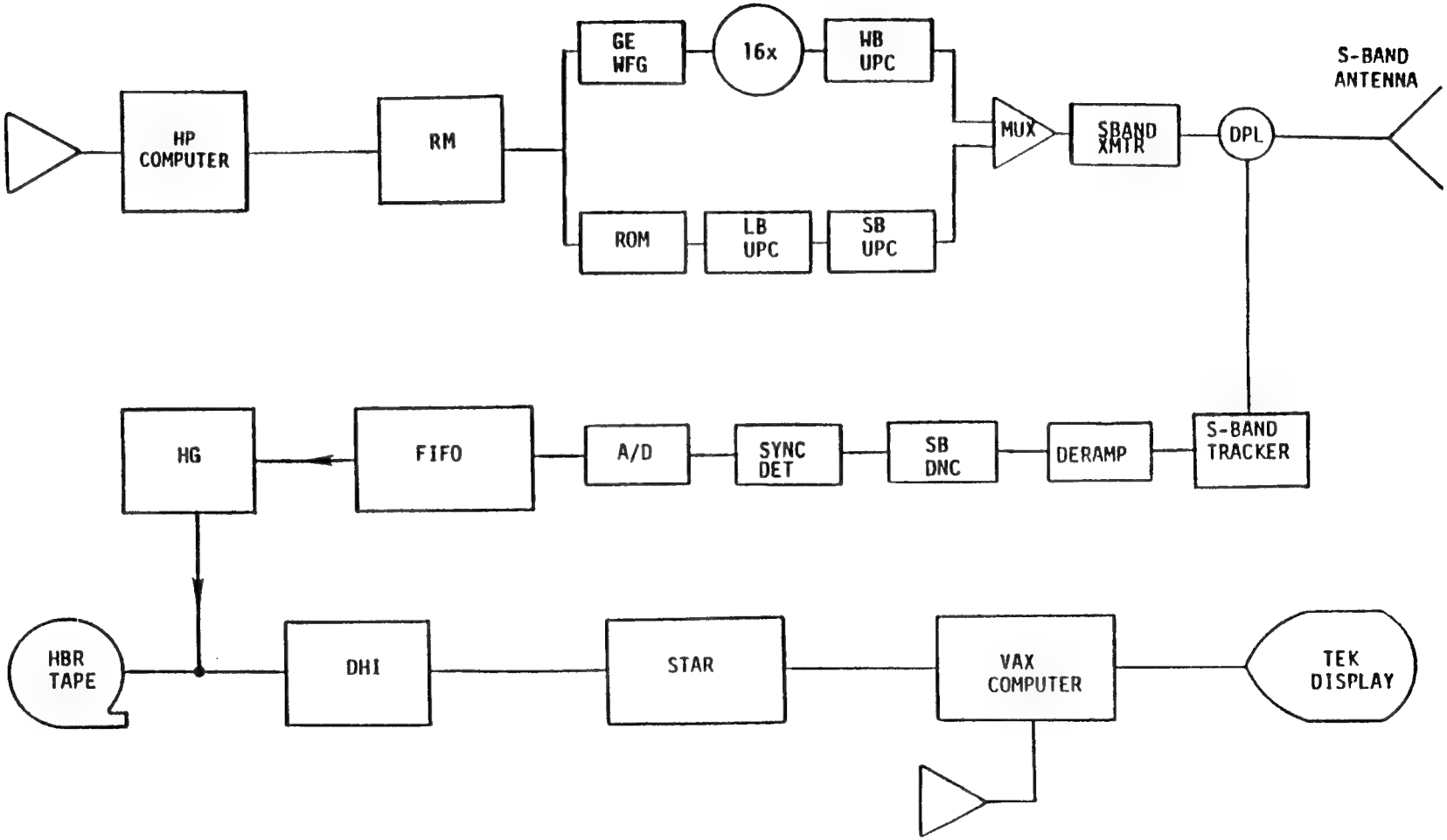

Figure 2.2.1-1 Wideband System Configuration

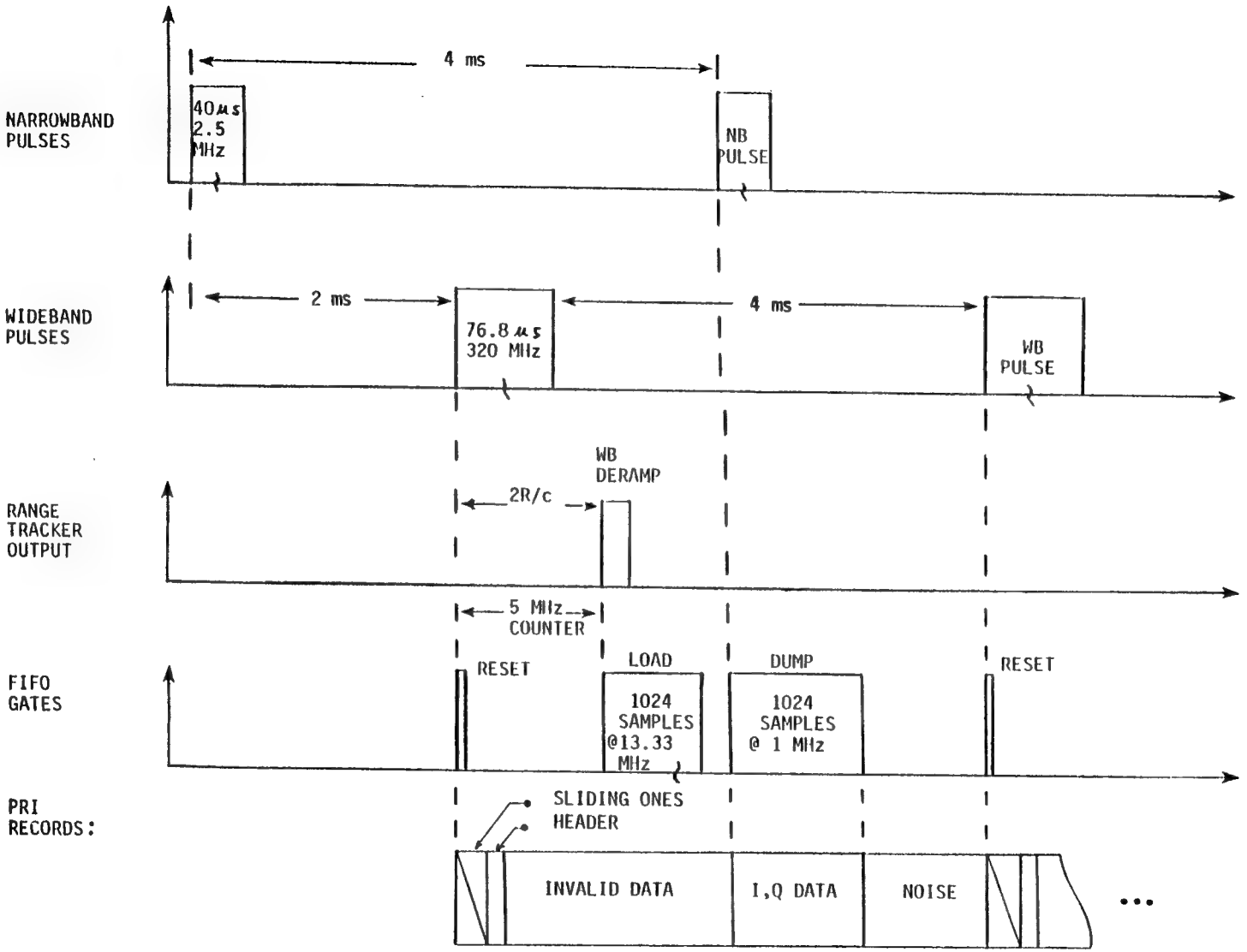

Figure 2.2.1-2 Interleaved Waveform Timing Diagram

2.2.2 Software Modifications

On this program, several modifications were made to the sophisticated STAR software code that reads and processes the WB radar data stored on HBR tape. Normally, only every 8th WB pulse record is processed to reduce the real-time delay. This decimation of pulses does not greatly affect the ISAR image quality because of the high SNR. It also permits a much smaller FFT size to be used for Doppler integration on the VAX computer. For UWB signature analysis, however, contiguous pulses had to be processed to observe the short-term temporal variations in the target return signal.

The second change to the STAR software involved acquiring only pulses where the range window remained constant. Ordinarily, whenever the track range gate changes because of target motion, the deramp signal for the WB pulse is moved accordingly. This keeps the target centered in the FIFO range acquisition window. However, the range samples are not contiguous if the track range is not properly updated in the header. In fact, there is a fixed, three pulse delay between the time at which the track range gate changes, and the time at which the corresponding header word is updated. Random data dropouts can also occur during recording and/or tape playback, leading to further misregistration of the pulse data and the range header. To circumvent this problem, dwells were acquired only when: 1) the track range gate did not change, and 2) no dropout errors were detected.

2.2.3 STRETCH Processing

For STRETCH processing, the WB pulse return is first mixed with a replica of the LFM transmit pulse at the deramp trigger. This produces a frequency-encoded signal that requires a FFT to reconstruct the range scattering profile of the target [5]. The STAR software code performs this PC step after first estimating and subtracting any ADC bias. Hamming weights are then applied to 949 of the

ADC samples and a zero-filled 2048-point FFT is performed. Note that the WB pulsewidth of 76.8 μsec and ADC rate of 13.33 MHz actually yield 1024 usable samples in the range window. However, certain STAR memory limits and fixed array sizes constrain the number of samples that can be processed to 949. This number could be expanded in future software revisions to process up to 2000 wideband samples. The present use of 949 samples reduces the 320 MHz waveform resolution of 0.47m by approximately 7% to 0.5m. (Hanning weighting further degrades the resolution to 0.65m.)

Following PC, the target returns are rotated so that the peak signal is centered in the range window. These are uploaded on a dwell-by-dwell basis to the VAX computer for storage in a standard SRC imaging (SRCIM) file format. This format, which is described in Table 2.2.3-1, includes a header that contains all relevant measurement parameters. Note that only the 512 range cells centered around the peak return are written to this SRCIM file. This number is sufficient to capture the entire moving target length. Furthermore, the zero-filling by a factor of roughly 2:1 prior to FFT integration effectively interpolates the data. This produces range sample cells that are spaced by one-half of the waveform resolution, or 0.25m.

2.3 Selected Target Dwells

The modified STAR software was applied to the recorded HBR tapes from the February 1990 data collection to obtain representative target dwells. The large 1.4 Gbyte IBIS disk that is attached to the STAR was employed for temporary file storage during this data selection task. The final 14 selected dwells are listed in Table 2.3-1 including target type, track range angles, and estimated velocity. Other information such as the original SRCIM file name and signal strength are also listed here for reference.

The first and last pulse return for one of the DC-10 dwells are plotted

TABLE 2.2.3-1 SRCIM DATA FILE FORMAT

1 Header Record: 150 words (not all used)

#3	=	Encoded Bandwidth: 320 MHz
#11	=	Radar Frequency: 3.408 GHz
#12	=	Range Resolution: 0.23498 m
#14	=	Number of Samples: 512
#17	=	Waveform PRF: 250 Hz
#19	=	Collection Type: 0
#20-21	=	Amplitude, Phase Types: 0,1
#27-28	=	Transmit, Receive Polarization: 0,0
#52-53	=	Data Types: 0,1
#58-59	=	First Cell, Number Unpacked: 1,512
#61	=	Range Sweeps Skipped: 7

256 Data Records: 1046 word (direct access)

Double Accuracy

#1	=	Pulse time in seconds
#2	=	Range in seconds
#3	=	Azimuth in radians
#4	=	Elevation in radians

Single Accuracy

#5	=	Max amplitude in volts
#6-16	=	Dummy array (not used)
#17-528	=	Negative phase angle
#529-1041	=	Magnitude in voltage with peak at #785

TABLE 2.3-1 SELECTED TARGET DWELLS

NO.	AIRCRAFT TYPE	HBR TAPE POS. (ft)	S-BAND TRACK			ORIGINAL			TARGET RANGE BINS	CELLS PER PULSE	RADIAL VELOCITY (m/s)
			RANGE (km)	AZIMUTH (deg)	ELEVATION (deg)	PEAK AMPL. (dBx)	SRCM FILE	CONTIGUOUS PULSES			
1.	BE-1900	2340	43	149	2	78	DE2	40-64	288-416	-1.4	-82.2
2.	BE-1900	2470	38	155	7.4	79	DE3	9-64	256-416	-1.18	-69.2
3.	BE-99	7000	28	309	2.1	81	DH0	1-50	224-416	-1.8	-105.8
4.	BE-99	6320	58	326	1.4	77	DH2	36-64	384-416	-2	-117.5
5.	BE-99	6750	38	320	2	81	DH6	11-60	256-448	-1.52	-89.3
6.	C-402	5820	46	23.2	2.6	71	DG1	1-37	256-384	1.6	79.4
7.	C-402	5950	52	22.6	2.2	70	DG4	17-41	256-352	1.35	94
8.	DC-10	1940	130.5	165	1.5	64	DCO	1-18	142-384	.88	140.3
9.	DC-10	1106	97.7	134.6	3.5	82	DC3	1-64	192-448	1.89	51.4
10.	DC-10	1249	99.8	139.8	3.4	82	DC6	1-84	64-352	2.39	73.4
11.	DC-10	1586	112.9	154	2.4	85	DC8	16-50	192-416	1.25	110.8
12.	DC-9	3192	42.5	297	12.1	82	THR	4-51	192-384	1.06	62.4
13.	DC-9	3197	42.6	297	12.1	84	NIN	1-64	192-448	1.03	60.6
14.	L-1011	5000	81	139	7	78	DF4	26-50	128-416	2.9	171.6

in Figure 2.3-1 on the same range axis. The noise was suppressed at the edges of these range sweeps for display purposes. The range shift of the target return signal, with only minor changes in its overall shape, is immediately apparent in this figure.

Figure 2.3-2 presents the first and last pulse returns for one of the BE-1900 radar dwells. Although the basic range scattering profile remains constant, the peak amplitude increases by some 5 dB over 92 seconds. Some of the individual scattering centers are also seen to merge, separate and/or change in relative strength in these two range sweeps.

The radial velocity of every aircraft target was estimated by the distance that nulls, rather than peak locations, moved between the first and last pulse of each dwell. Two of these nulls are indicated in Figure 2.3-1. This was done because the null locations are more easily defined, and because different nulls give better consistency than different peaks in estimating target velocity.

The target dwells listed in Table 2.3-1 form the basis of the UWB database. One of the C-402 aircraft dwells also contained a small amount of clutter interference. Eight pulse returns from this dwell are plotted in Figure 2.3-3. Note that the clutter scattering peak remains stationary in range, whereas the target peaks move a significant distance. This single instance of measured clutter interference was too weak to be used extensively for MTI performance evaluation.

2.4 Database Management Software

TSC developed several DBMS tools to synthesize test cases for algorithm evaluation. The overall DBMS configuration is shown in Figure 2.4-1. The selected target dwells are stored as SRCIM format files that contain up to 64 pulse records. These are input to the main DBMS utility, and then combined with simulated noise and clutter data to produce output files for evaluation testing.

Besides the SRCIM format, database files are stored in two other

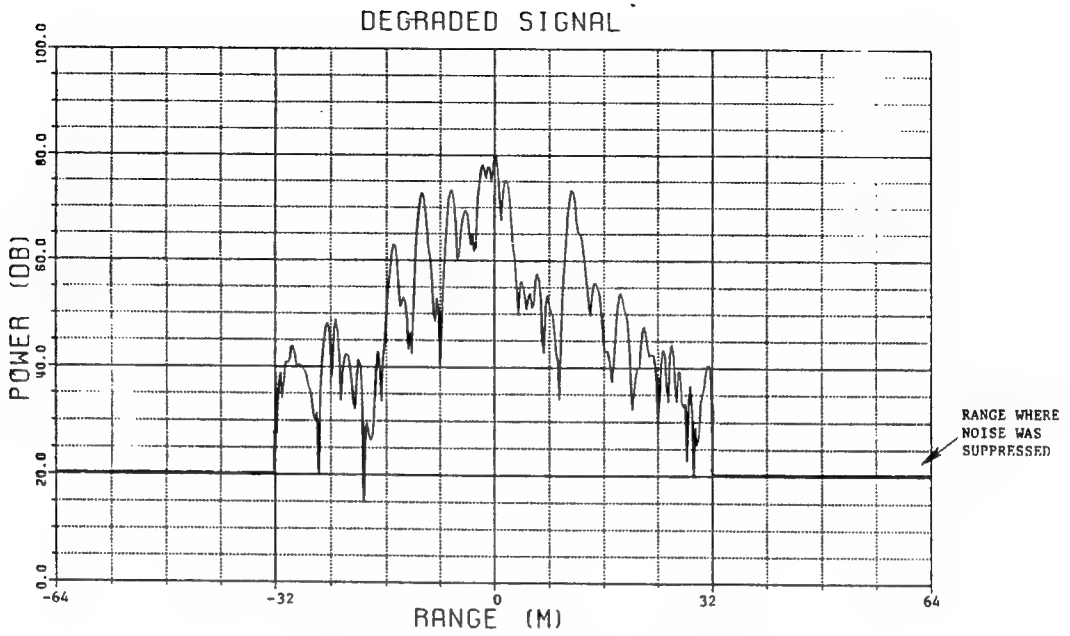

a) Range Sweep for Pulse Number 2
(Centered and Normalized to 80 dB)

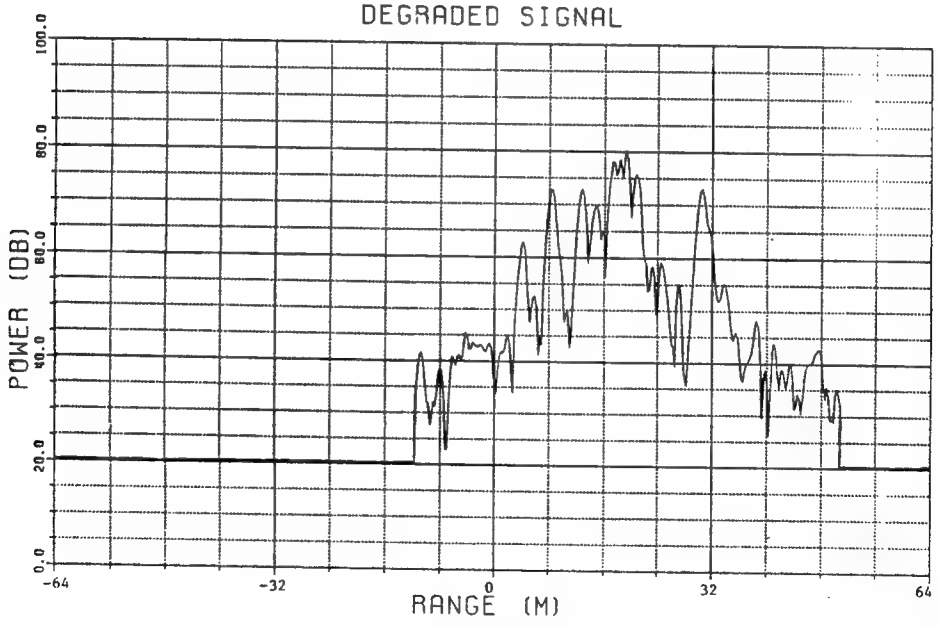

b) Range Sweep for Pulse Number 64
(252 ms Later)

Figure 2.3-1 HRR Returns for DC-10

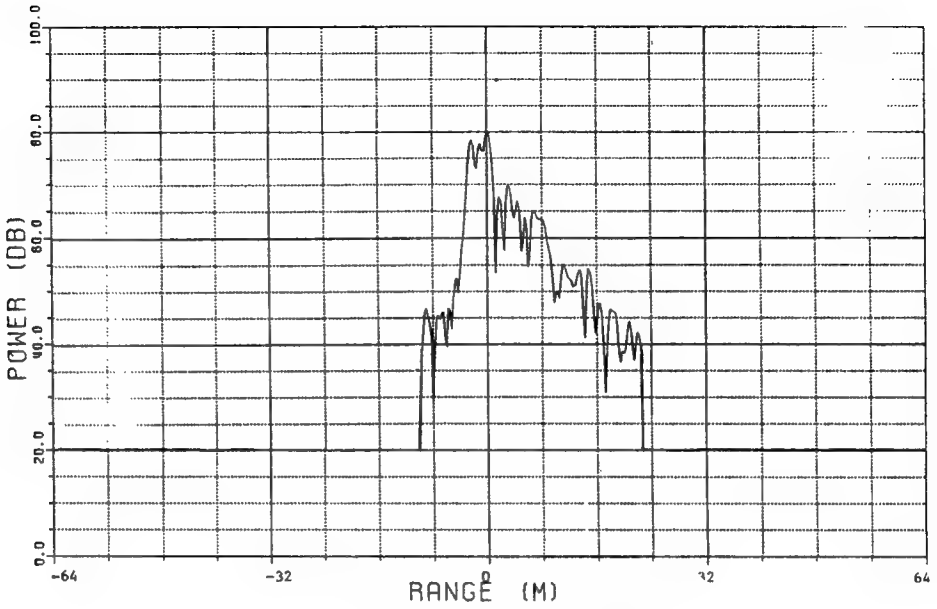

a) Range Sweep for Pulse Number 1
(Centered and Normalized to 80 dB)

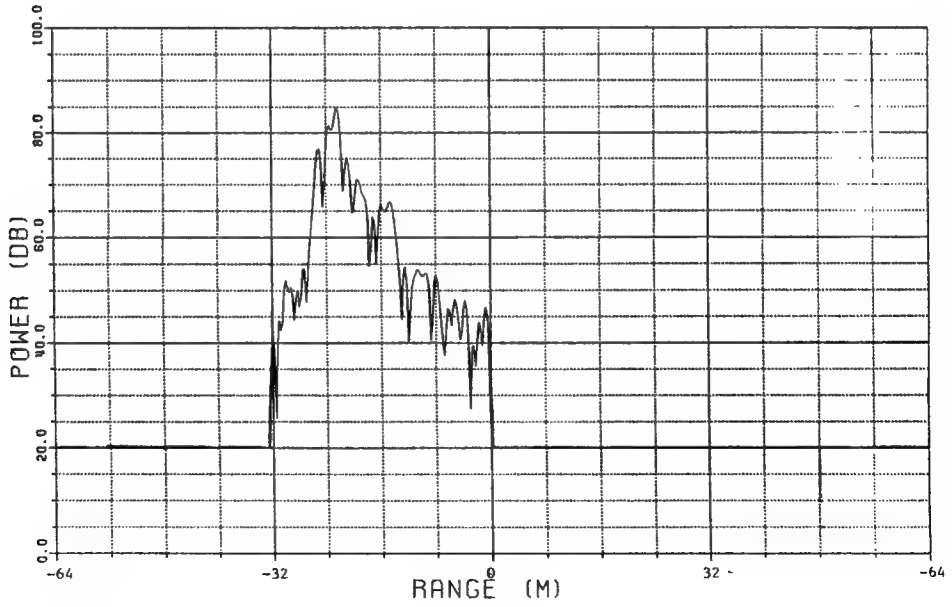

b) Range Sweep for Pulse Number 50
(196 ms Later)

Figure 2.3-2 HRR Returns for BE-1900

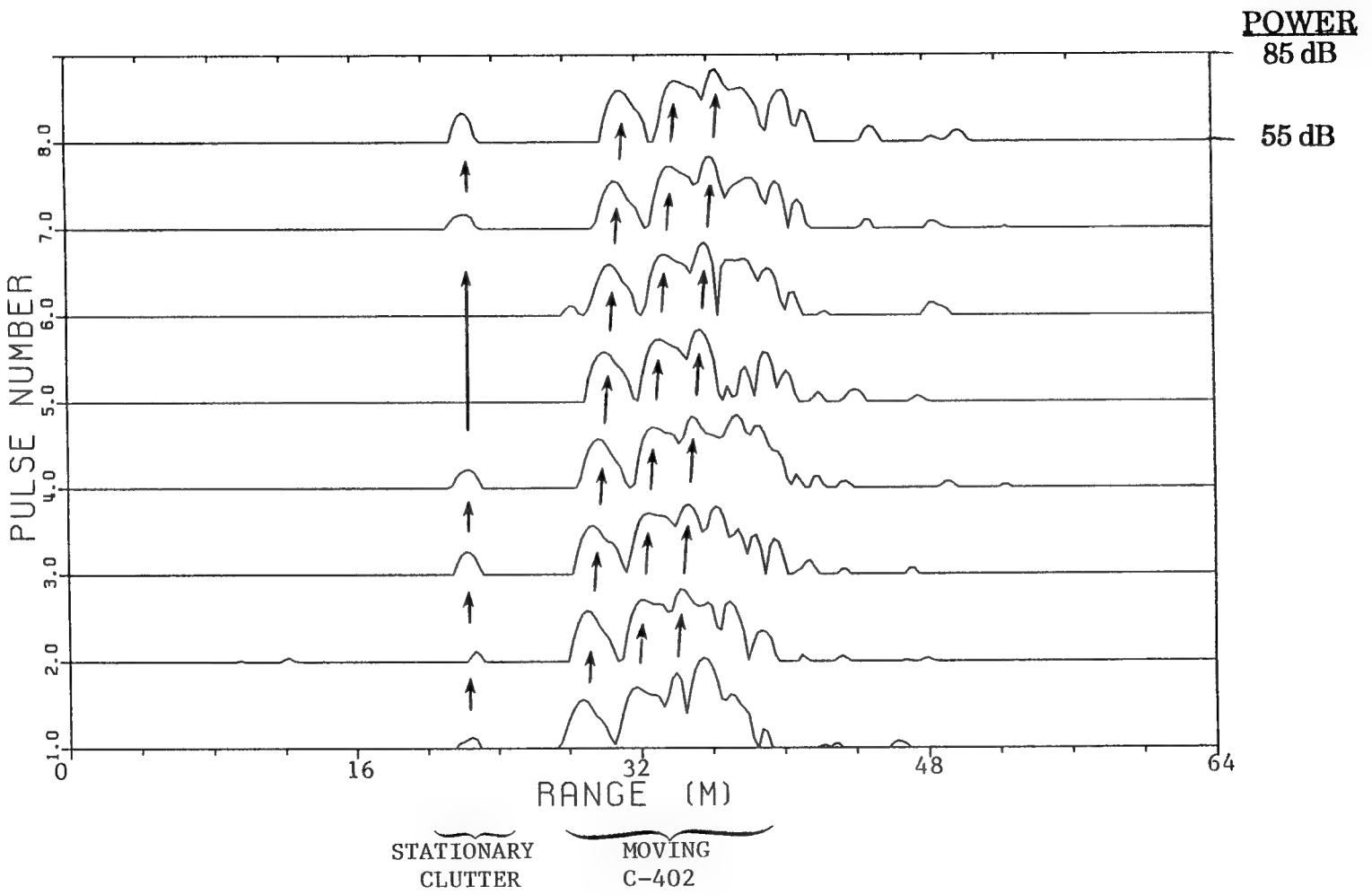

Figure 2.3-3 Measured Target and Clutter Returns

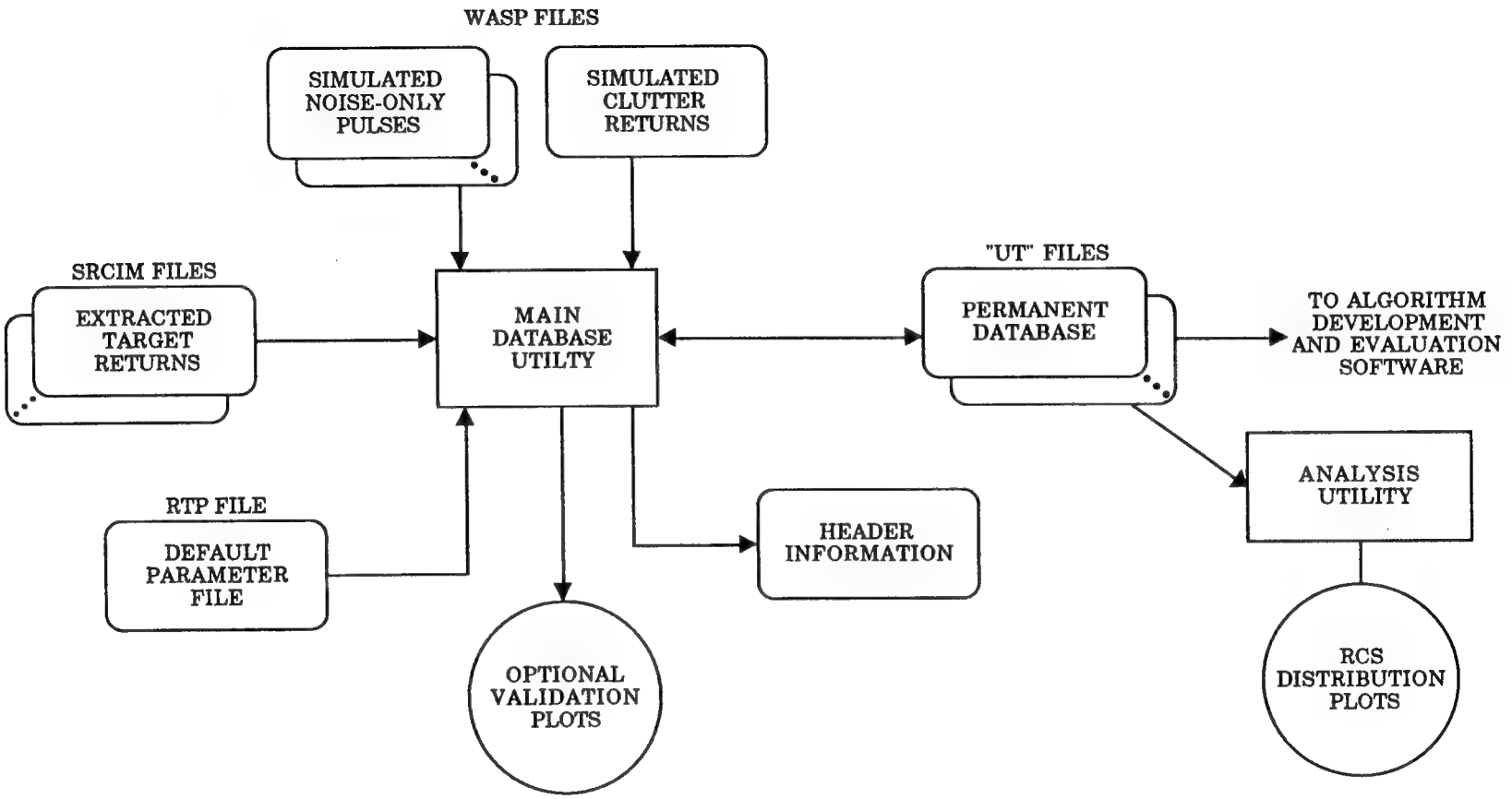

Figure 2.4-1 UWB Database Generation and Management Software

formats. The first is a binary format to increase I/O throughput for lengthy Monte Carlo simulations. The second is a more convenient, readable ASCII format associated with TSC's WASP software package.

The main DBMS tool is a menu-based program that permits step-by-step construction of virtually any test case. First, one of the 14 target dwells is selected for input, and can be optionally plotted. Target signatures are then automatically normalized to a convenient peak power of 80 dB, and recentered in range so that the peak return on the first pulse occurs in range cell number 257. Pregenerated noise and clutter signals are next input, and are scaled to yield a specified SNR and CNR. Finally, the complex I/Q samples are added together for each range cell and pulse number. These may be replotted in several ways using the DBMS utility to verify the generated test data.

Any test case can also be permanently saved in a UWB target database or "UT" file. The DMBS uses the following filename template:

UTabcd_E#N##L###C##L###D#.DAT

The alphanumeric field, abcd, corresponds to the aircraft type with trailing underscore "_" characters. The remaining numeric fields, marked #, specify the example number (E), noise case (N) and mean power level (L), clutter case (C) and peak power level (L), and number of discretes (D). One example might be a DC-9 target return with a simulated noise level of 70 dB, and two clutter discretes at 77 dB. This would be stored in the file:

UTDC9_ _ E1N1L70C01L077D2.DAT.

For each such permanent database file created, a variety of information about the original target measurement is stored in a separate database directory

file. (The user can later edit this information if a typographical error is made.) Database files can also be deleted or modified via various DBMS software menus. For convenience, default menu parameters for the DBMS tool are stored in a run-time parameter (RTP) file that can be edited by the user. The RTP file format is described in the RTMSAE Software User's Manual.

The generation of an example test case is illustrated in Figure 2.4-2a through 2.4-2d. Figure 2.4-2a shows the original high SNR DC-9 target signature. Figure 2.4-2b illustrates the simulated receiver noise which is effectively correlated in range by STRETCH processing. Figure 2.4-2c then shows the simulated returns from 2 clutter discretes displaced in range slightly from the target returns. These are finally added together in Figure 2.4-2d to produce a composite UWB test case with a peak SNR of 10 dB and an SCR of 3 dB.

A time history of this composite UWB return over eight pulses is illustrated in Figure 2.4-3. Here, only the portion of the signal above a threshold level of 75 dB is shown. Note that the target returns move together in range at the same radial velocity, whereas the two clutter discretes remain stationary. This is the basis of TSC's regression algorithms which detect moving targets, but reject stationary clutter discretes.

2.5 Simulation of Noise and Clutter

TSC employed the WASP software package exclusively to simulate receiver noise and clutter interference. Thus WASP output files are directly input to the DBMS tools as indicated in Figure 2.4-1. WASP is an interactive, menu-driven software tool that was developed in-house at TSC to analyze unique radar waveforms and signal processing algorithms. It includes basic signal generation, processing, and display functions, as well as file output (export) capabilities. These features of WASP were employed to simulate: 1) the UWB returns from stationary clutter discretes, and 2) the range-correlation effect of STRETCH processing on random

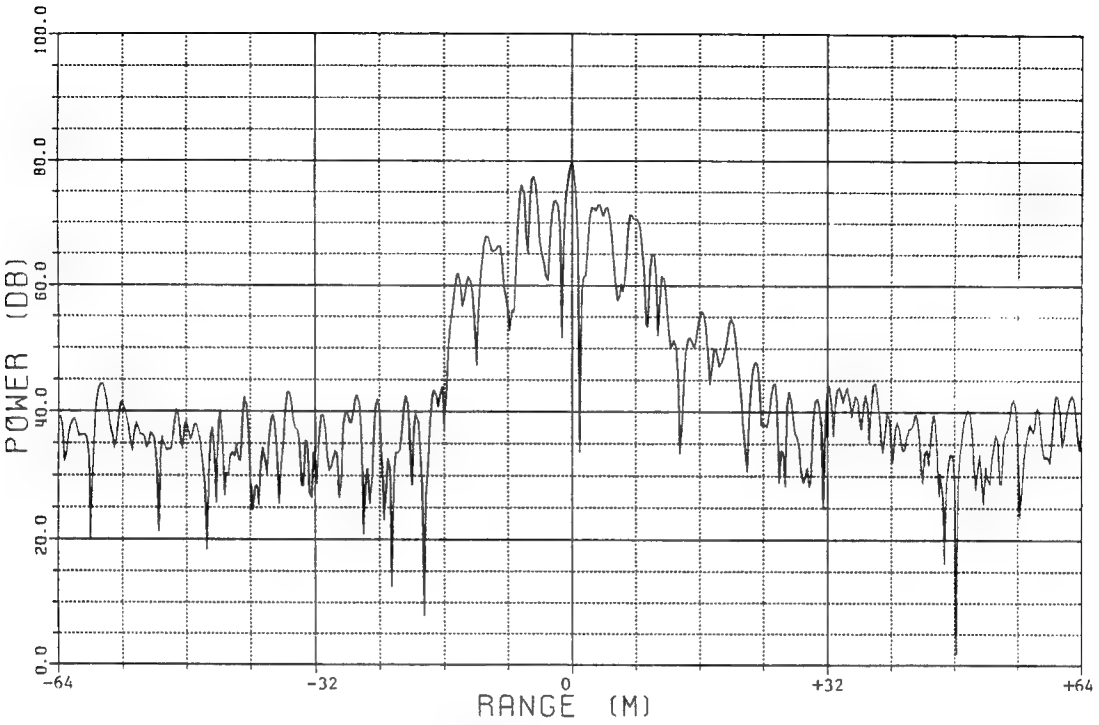

a) Measured Target Signature (DC-9 at SNR = 43 dB)

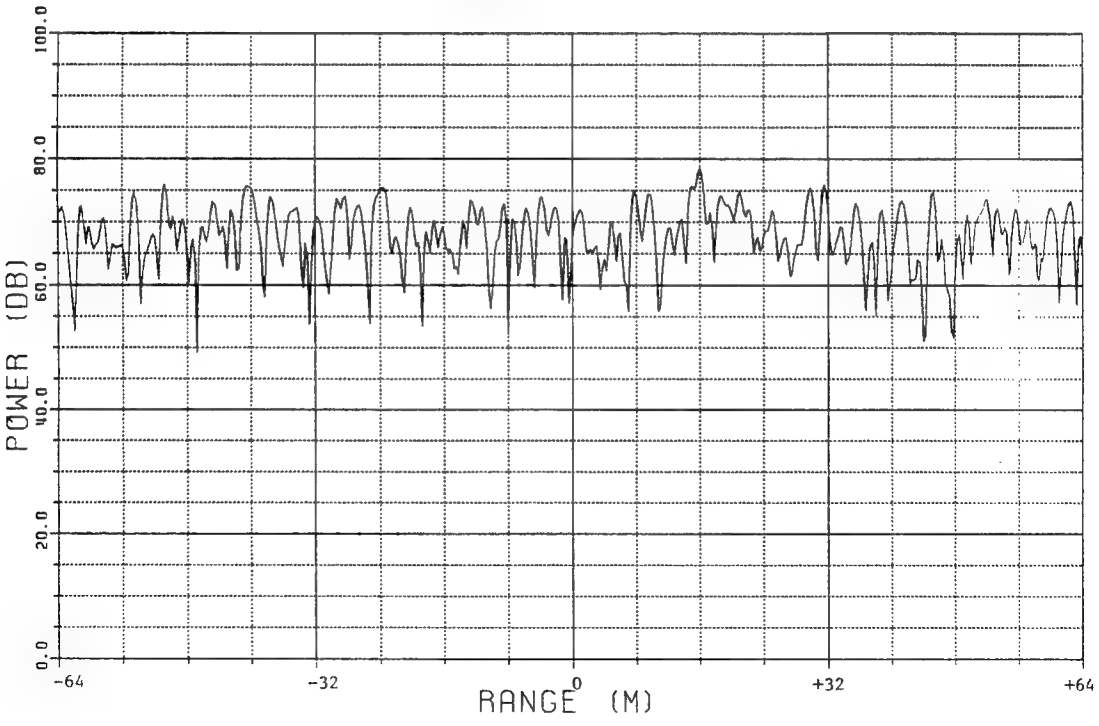

b) Simulated Receiver Noise (Mean Power = 70 dB)

Figure 2.4-2 Database Generation Example

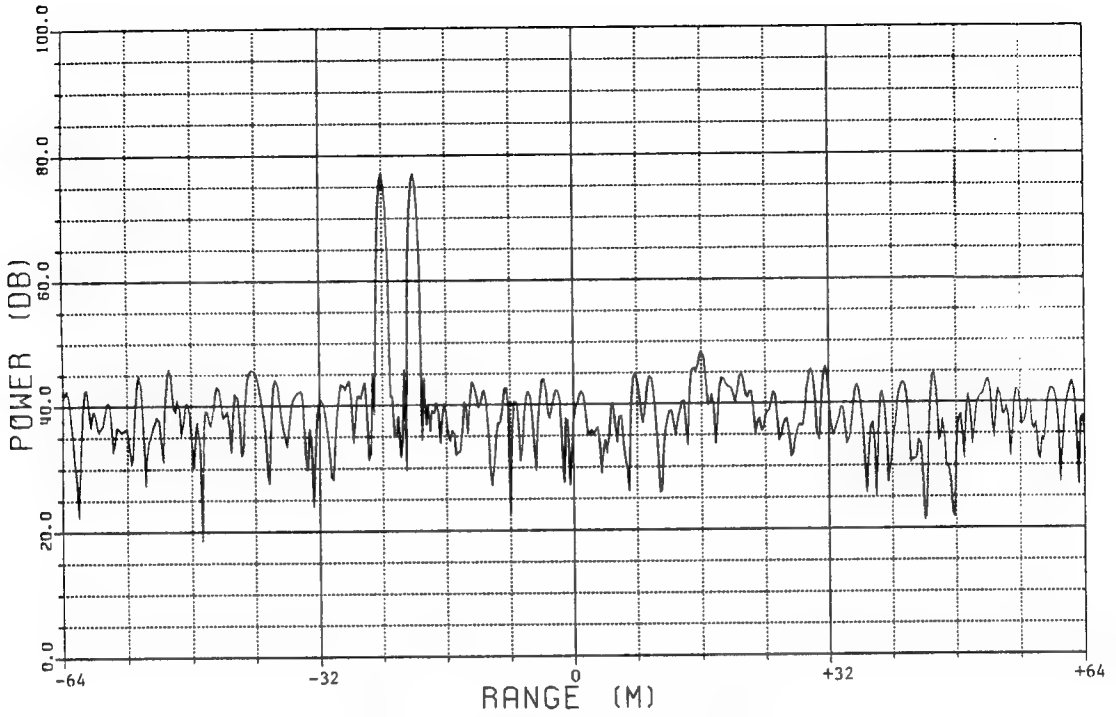

c) Simulated Clutter Discretes (Spaced by 4 m)

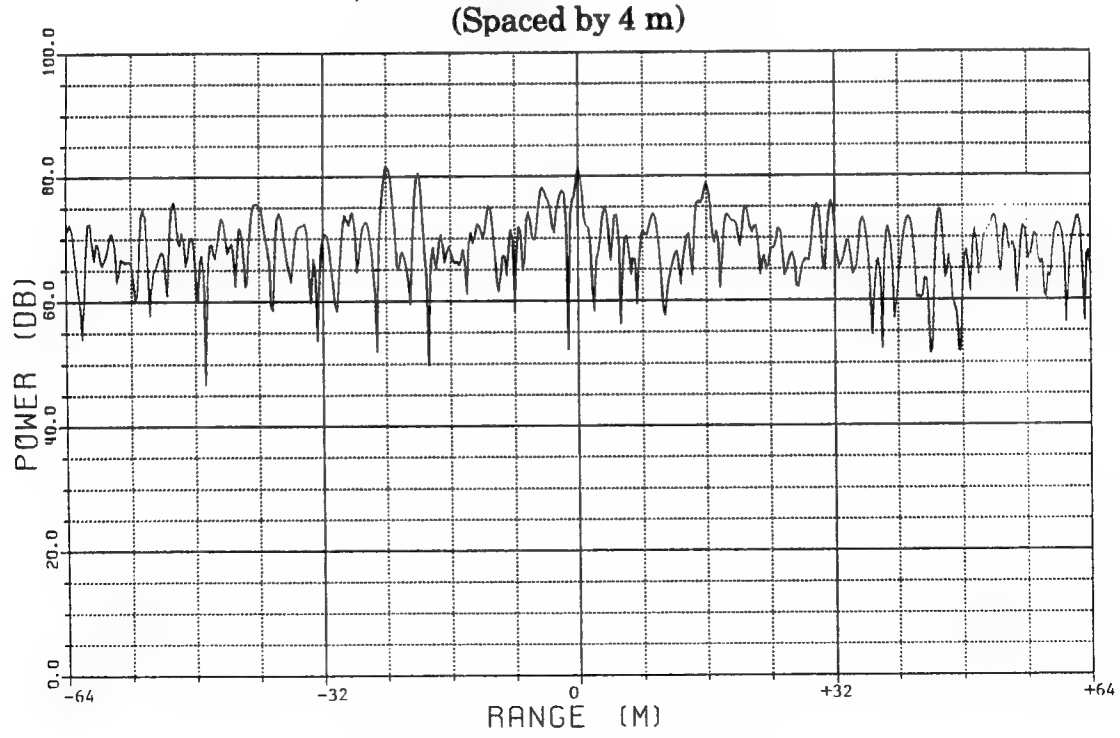

d) Composite UWB Return (SNR = 10 dB, SCR = 3 dB, CNR = 7 dB)

Figure 2.4-2 Database Generation Example (Continued)

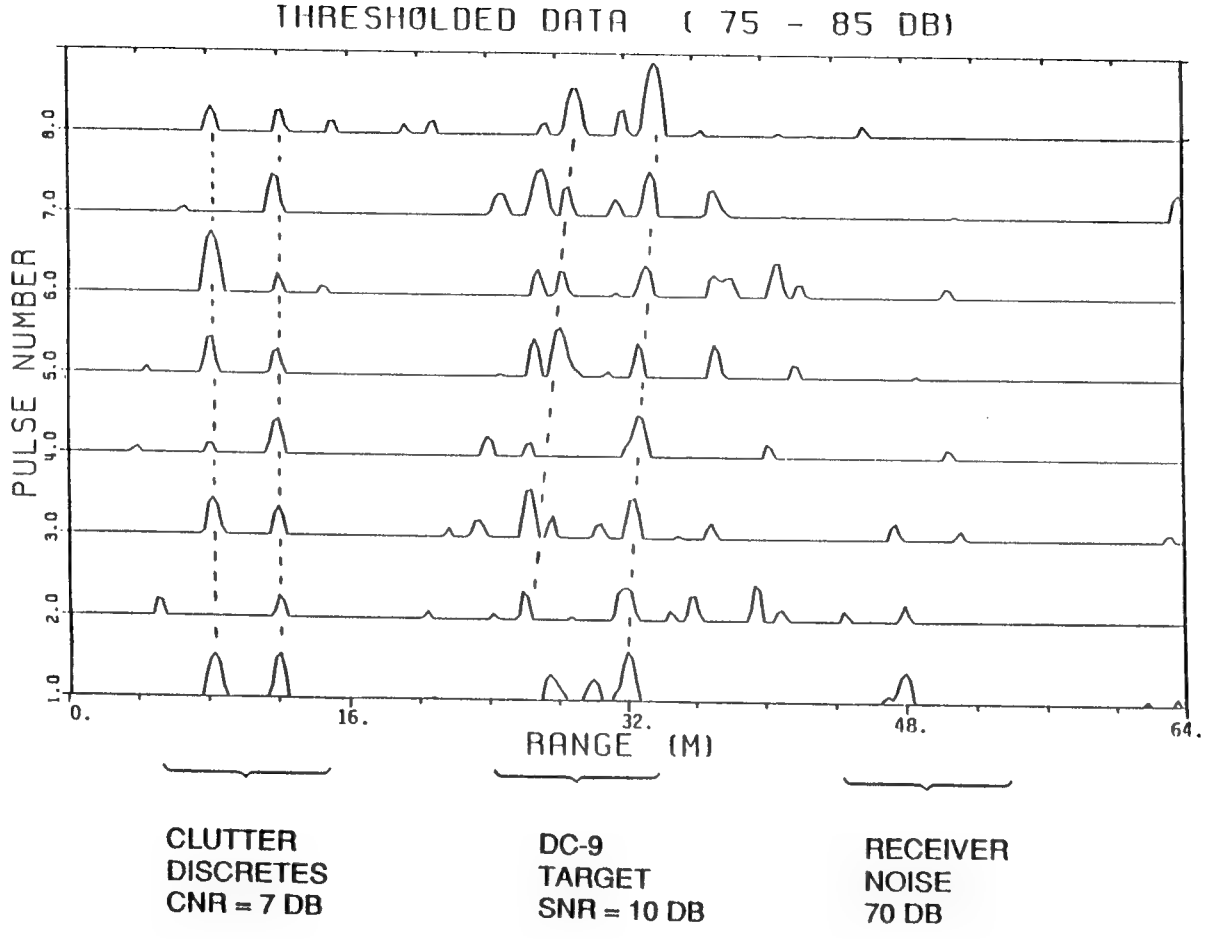

Figure 2.4-3 Time History of Composite Returns

receiver noise. The simulated data was then written to disk files on TSC's VAX computer for access by the DBMS tools and the automated MTD algorithm evaluation software.

In the S-band WB mode, a clutter discrete at some range shows up as a single frequency tone in the ADC output samples. STRETCH processing converts this tone to an isolated signal peak with 40 dB Hanning sidelobes. The WASP software performed the same STRETCH processing sequence as the real-time STAR code by defining an automated command file. For convenience, a single discrete was simulated at the center of the range acquisition window, corresponding to a zero-frequency (DC) tone. Returns from multiple discretes or a single discrete at another range location are generated by appropriately shifting and combining the WASP output data from this one simulation.

Radar receiver noise in the I and Q channels has a Gaussian amplitude distribution and a white frequency spectrum. Noise is thus independent between ADC samples. However, the receiver noise samples undergo the same STRETCH PC as target signals. This causes a correlation between the adjacent, interpolated range samples which can be seen simply because the 949 noise samples are converted to 2048 FFT outputs. A WASP command file was therefore defined to generate such processed noise outputs. Each random set of input noise samples produces a unique output signal. Ideally, noise data should be independently generated on a pulse-by-pulse basis in this manner and added to the measured target returns. However, it is impractical to generate or store a sufficient number of such noise-only pulses to conduct the extensive Monte Carlo simulations required. Therefore TSC adopted a more efficient approach.

First, a large set (N=256) of noise-only pulses is generated. STRETCH processing is then applied to each pulse to create an output file of processed, noise-only pulse records. To create a particular test case, as in Figure 2.4-2b, random draws (without replacement) are made from these processed noise pulses.

This provides a substantial savings in computer processing and disk file storage since a total of N!/N-8! unique sets of eight noise-only pulses can be chosen in this way.

The above procedure makes it feasible to conduct the millions of trials necessary to accurately establish the Probability of False Alarm (P_{FA}) for an algorithm. The situation is much more difficult than it is for conventional radar algorithm simulations. This is because each Monte Carlo experiment would require a 2048-point FFT just to generate the raw noise data for each pulse return.

It should be noted that this method does not perfectly model the processed noise distribution, and can therefore under or overestimate actual MTD performance levels. However, it is useful for comparing candidate techniques during initial development, for roughly setting algorithm parameters, and for noting certain performance trends.

Finally, note that simulated clutter and noise is generated for one output power level only. Therefore, the WASP outputs are scaled by appropriate factors to obtain the desired SCR and SNR for a particular experiment. This was done, for example, to produce the mean noise power level of 70 dB in Figure 2.4-2b.

3.0 SIGNATURE ANALYSIS

This section presents the results of TSC's analysis of UWB target signatures. These results are based on a limited number of aircraft target measurements, all collected at S-band with a 0.5 m processed range resolution. , The analysis conclusions are not expected to change significantly for higher waveform bandwidths, however. Nonetheless, a second, more thorough radar data collection effort at 640 MHz is strongly recommended. This collection effort would involve a greater variety of aircraft types and aspect angles, and would include an extensive clutter characterization study.

Measured target returns were found to extend over from 30 to 150 range sample cells, often with many large gaps. This extent is obviously dependent on aircraft size and waveform resolution. Of more importance, 60 to 80% of the target RCS is found to originate from 2 to 4 dominant scattering peaks; each of these scattering peaks being spread over from 3 to 6 range samples. This suggests that the principal scatterers at S-band wavelengths (0.09m) are not point objects such as rivets or extremities. The individual scatterers are more likely larger structures such as whole wing sections, window cutouts and engine components or supports.

The target return signals are primarily nonfluctuating (Swerling Case 0) as if from a single scatterer, with some evidence of Swerling Case 3 scattering having been observed. This is evident from temporal variations such as those shown earlier in Figure 2.3-1 and 2.3-2. Case 3 scattering arises from a single dominant scatterer plus several smaller, independent scatterers. Case 3 scattering causes the return to vary slightly from pulse-to-pulse, as the dominant and secondary scatterers sum together in different ways.

The existence of a few dominant scatterers of similar strength is reasonable form a physical point of view. At conventional radar resolutions, these

roughly equal and independent scatterers add together to produce the significant pulse-to-pulse fluctuations associated with a Swerling Case 1 target. At higher resolution, however, there is only a single dominant scatterer remaining within any one range cell, and so the fluctuations disappear.

Figure 3-1 presents the RCS distribution for one DC-10 aircraft measurement at S-band. A rank ordering of the RCS contributions from each scattering peak is shown in Figure 3-2, illustrating that most of the received power comes from the largest few scatterers. In this case, some 56% of the energy is returned by the two largest scatterers.

Typical S-band signatures for large and small commercial aircraft are shown in Figures 3-3 and 3-4, respectively. The percentages listed on these figures show the return power from each scattering peak, and thus their individual RCS contributions. Note that these are only typical signatures, and that the actual range return is highly dependent on the particular radar viewing geometry. The azimuth aspect angle relative to a nose-on view of the aircraft are given for each target in these figures. The length (nose-to-tail) and width (wing-tip-to-tip) are also listed for each aircraft. In all cases, the range extent roughly agrees with a projection of one of these dimensions onto the radar Line-Of-Sight (LOS).

Figure 3-5 shows the measured signature variation over 84 msec for the Cessna 402, the smallest aircraft for which data was collected. Four scatterers are evident, which are labelled A through D, with B and C being the strongest. Due to a slight LOS aspect and/or altitude change, the scattering peak D separates from C, and A grows substantially weaker during this period.

What is most significant is that small aircraft returns are composed of a distribution of several scattering peaks, each with an RCS on the order of 10-40% of the total. Scaling this to a total 0.1 m^2 RCS for a LO target means that such targets would be detectable as a set of 0.01 to 0.04 m^2 RCS scatterers. This may or may not be true of LO aircraft or missiles, however, because these have

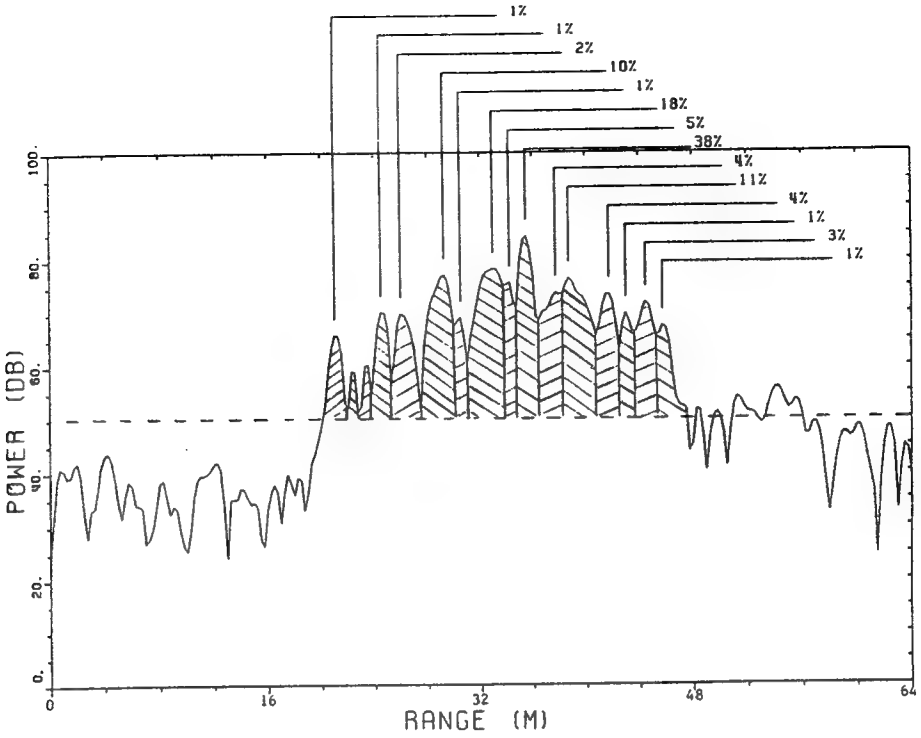

Figure 3-1 RCS Distribution for Scattering Peaks in DC-10 Return

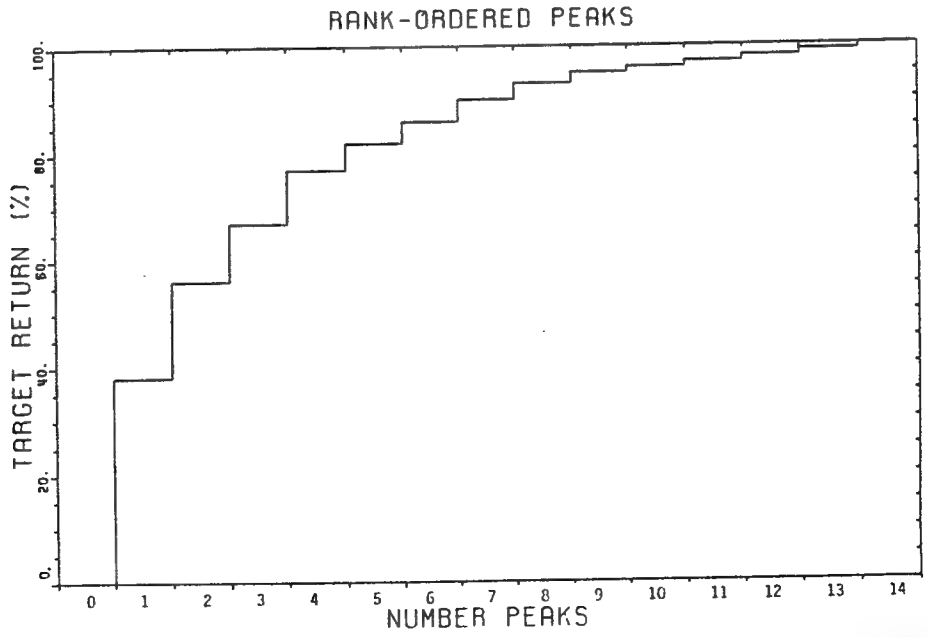

Figure 3-2 Rank Order of Scattering Peaks in DC-10 Return

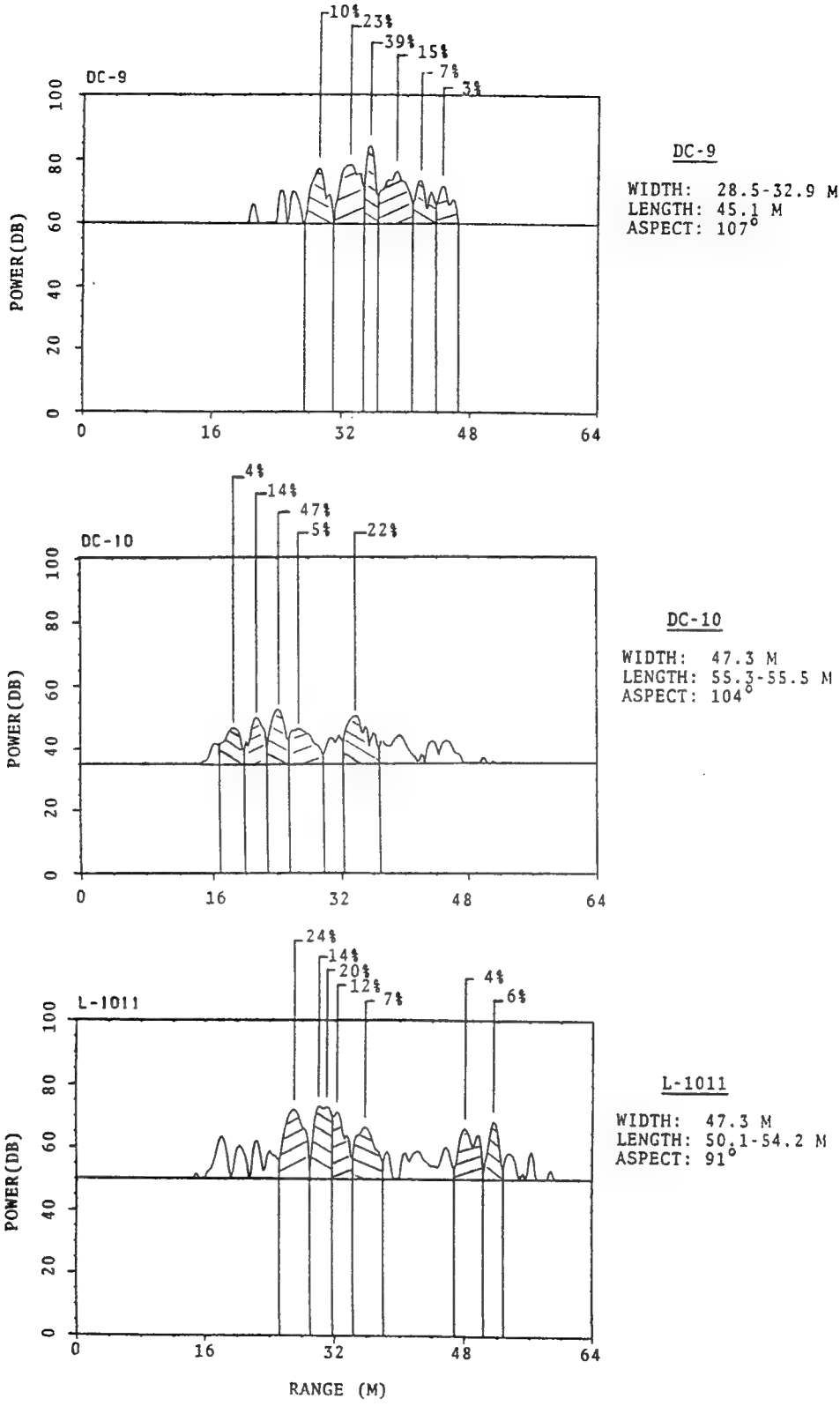

Figure 3-3 Large Aircraft Signatures

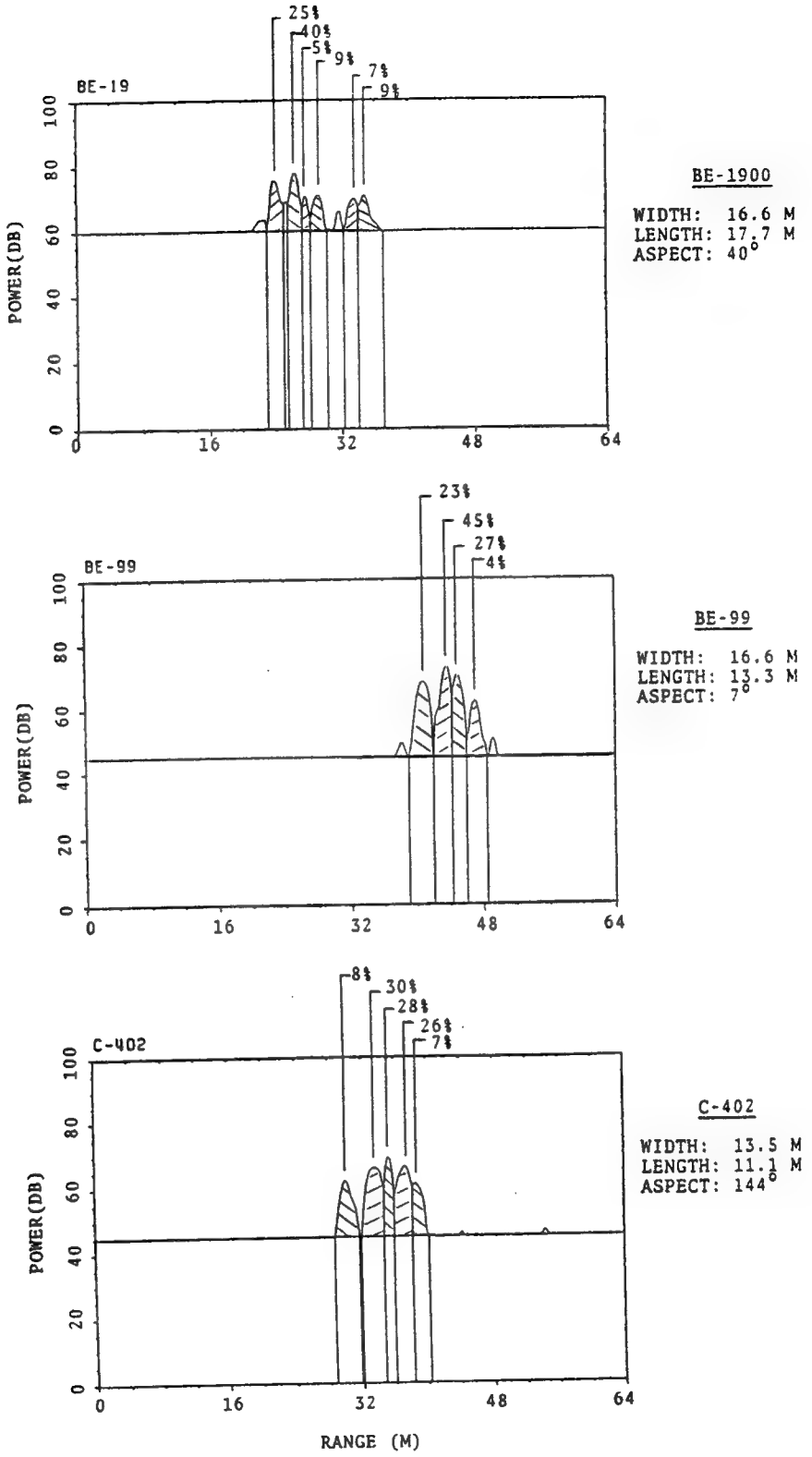

Figure 3-4 Small Aircraft Signatures

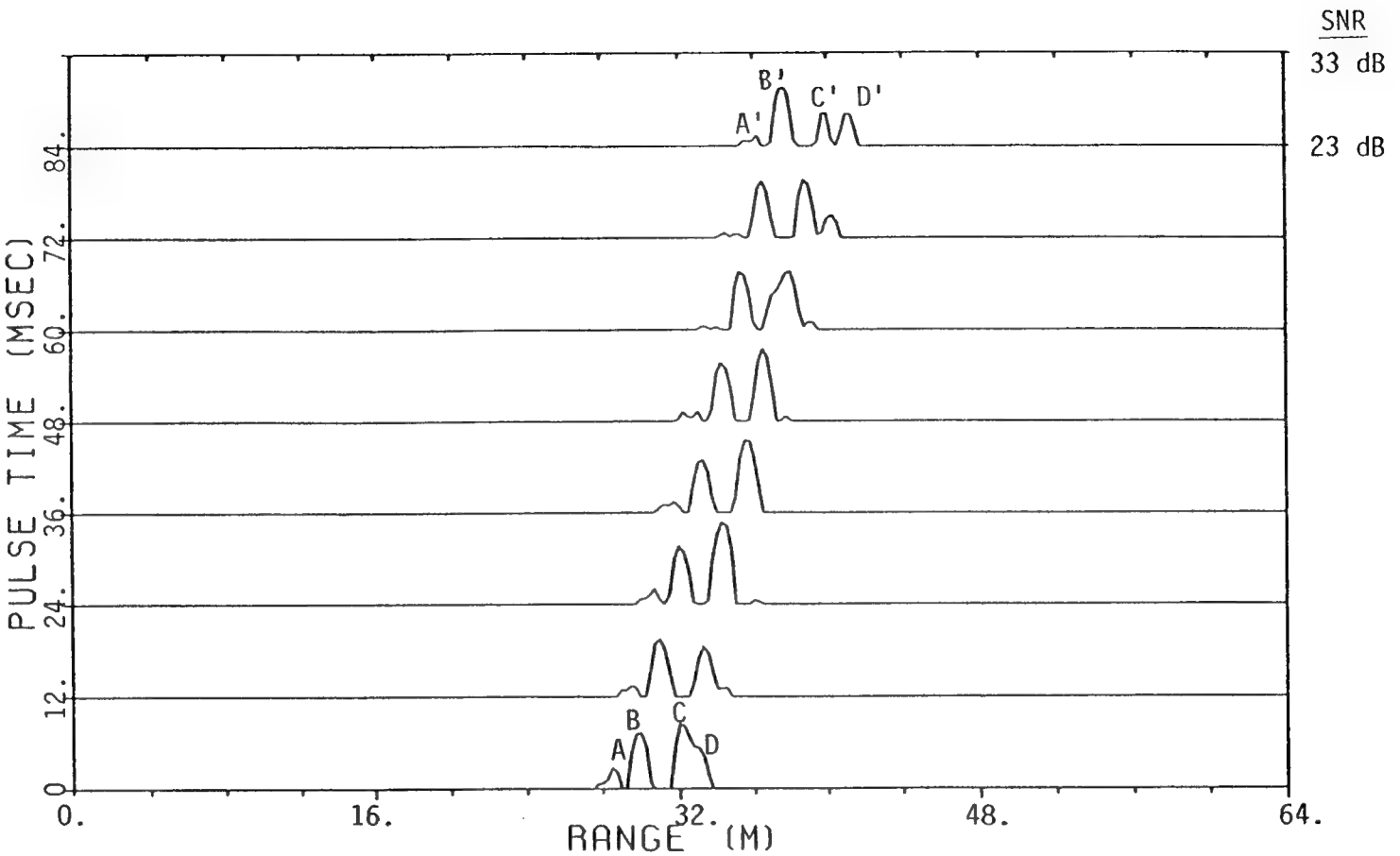

TARGET = CESSNA 402
PEAK SNR = 31 dB
TRACK RANGE = 52 km
RADIAL VELOCITY = 94 m/s

Figure 3-5 Measured C-402 Signature

limited wing surface areas, internal engines and few or no windows.

These observations have important implications for UWB radar design. A certain bandwidth will be sufficient to resolve the dominant scattering peaks. If a MTD algorithm exploits only these scattering peaks, the performance has therefore been maximized. Higher resolution probably will not result in any greater detection performance.

The relatively constant nature of the target return also benefits MTD algorithm processing. The scattering peak amplitudes, widths, spacings and phase relationships remain constant, and therefore predictable, from pulse-to-pulse. This permits peak association algorithms to identify the same scatterer in several pulses and to perform regression analysis more accurately.

Targets exhibit nearly perfect linear motion over the short dwell times investigated by TSC. Thus all of the observed scatterers move together as the aircraft traverses its line of motion. An analysis of the small rotational effects and/or acceleration components caused by up to a 6 g maneuver shows that such motion effects are negligible over a CPI as long as 32 msec. Therefore, strictly linear regression analysis is sufficient for detecting almost all aircraft targets, except perhaps fighters performing severe maneuvers or rocket-powered missiles. Furthermore, the same regression fit applies to all of the individual target scatterers. This fact was exploited in the PAC algorithm described in Section 5.

In summary, the analysis of UWB target signatures at S-band reveals several exploitable features for MTD processing. First, most of the RCS is contained in a few dominant scattering peaks that are each spread over several range cells. Second, the returns do not tend to fluctuate, leading to constant peak amplitudes and other parameters. Finally, all scattering peaks on the target move together with the same range shift per pulse. These key features of UWB target returns are not expected to significantly vary at greater bandwidths and/or other radar operating frequencies.

4.0 UWB PROCESSING TECHNIQUES

TSC investigated a number of potential UWB processing techniques to develop a practical and reliable MTD algorithm. These techniques included both single and multiple-pulse processing methods. Multiple-pulse processing has an advantage for detecting targets at low SNRs, and in rejecting clutter interference. Both coherent and noncoherent signal processing were also considered in this study to address diverse system implementations. The only restriction was that the algorithms be compatible with advanced signal processing hardware.

Processing methods that were analyzed are briefly described here include running-sum range integration, cross-correlation of consecutive pulse returns, and signal thresholding to isolate dominant scatterers. Multiple-pulse processing techniques that were considered included optimal coherent integration, noncoherent integration, and linear regression analysis. Hybrid methods that combine these traditionally distinct forms of processing were also considered. Prefiltering algorithms to reject clutter interference are covered separately in Section 6.

4.1 Range Integration

A single-pulse processing technique for over-resolved radar measurements is to integrate the detected returns over a sliding range window. This provides a noncoherent integration gain for the target signal; however, it has several drawbacks. First, the process is inefficient if the range integration window is made too small. This can be the case if the target aircraft size is unknown, or the surveillance viewing geometry is highly variable.

Similarly, there is a collapsing loss if the range integration window is made too large, and the target's range extent is actually small. A good approach

for handling all such cases is to form a bank of range integration windows, one for each possible target extent. The largest normalized output from this bank can then be selected for detection thresholding.

A second, more serious problem with range integration occurs at low SNR conditions. Based on the observed target signatures, there can be large gaps between the signal peaks that arise from the few dominant scatterers. At low SNR, these empty range regions contain primarily receiver noise that degrades the range integration. These gaps effectively reduce the sensitivity of range integration algorithms to weak target signals. One means of improving this sensitivity is to form a sum of the largest N signal peaks within a sliding range window. Some performance variation can be expected for different values of N as a function of target type and viewing geometry. Hence, a bank of range integration windows with values of N between 2 and 6 could be used to provide near optimum performance in all cases.

A third deficiency of the range integration approach is that it has no inherent clutter immunity. Clutter returns that are distributed in range are also integrated, and can result in numerous false alarms. With multiple pulses, clutter prefiltering could be performed prior to range integration to overcome this limitation. The range integration sums, with or without prefiltering, could also be utilized as input to the regression analysis algorithms described in Section 4.4.

4.2 Cross-Correlation of Pulse Returns

A straightforward method of detecting targets in over-resolved radar data is to perform a cross-correlation of consecutive pulse returns. Based on the collected UWB signatures, target returns remain relatively constant on a pulse-to-pulse basis, except for range shifts due to their motion. Thus a cross-correlation of two target returns should show a peak at a certain non-zero range shift. Cross-correlating multiple pulse returns would provide additional peaks at range shifts

that are proportional to the time separation of the individual pulses. This linear relationship could then be used as a target detection mechanism.

Cross-correlation processing offers a coherent integration gain for the target signal only when its noise-free signature is available. Low SNR target returns produce a noisy matched filter function, and as a result, cross-correlation detection performance will be poor. There is also a mismatch loss because the target location and extent are unknown relative to the size of the range correlation processing window. As with range integration, the solution is to form a bank of cross-correlation windows, one for each expected target range extent. However, this substantially increases the processing load.

With cross-correlation processing, stationary clutter returns will peak at a range shift of zero, and are thus readily discarded. However, clutter correlation sidelobes from strong, distributed clutter returns can easily obscure nearby target signals. Clutter rejection prefiltering is therefore required.

In conclusion, the cross-correlation of pulse returns would not provide a reliable detection mechanism if used alone. Regression analysis to detect a linear relationship between the cross-correlation peaks and the pulse time differences offers greater promise. The techniques discussed below in Section 4.3 and 4.4 could thus be combined with cross-correlation in a hybrid detection algorithm.

4.3 Thresholding and Association Processing

The most striking feature of UWB target signatures is the few dominant scattering peaks. The peaks move together in range on successive pulses at the target's radial velocity, and have relatively constant features and relationships that include amplitude, width, range spacing and phase difference. These constant characteristics can be exploited by thresholding and association algorithms which match unique scattering peaks from different pulses.

Note that multiple pulse returns are required to perform any peak-to-peak association because there is no special relationship between the scattering peaks of a single pulse return. After an interpulse peak association is made, however, intrapulse peak associations become possible. For example, the spacing of the peaks in one pulse return can be used to associate target scattering peaks in another pulse.

For maximum efficiency, only the largest N peaks and/or those above some threshold setting may be initially selected for association processing. This rank-ordering and thresholding effectively throws away part of the signal energy. Algorithms that include thresholding need not ignore all peaks smaller than the applied threshold setting or greater than a certain rank, however. This would be counterproductive for detecting weak target signals where a scattering peak may briefly fall below the defined threshold on several pulses, due either to corruption by noise to slight RCS fluctuations. Instead, the association process can compare the N largest peaks to the entire set of M signal peaks.

Clutter prefiltering is also needed to reduce the number of peaks examined during association processing. This can prevent the misassociation of target and clutter scatterers that happen to have similar features. It is particularly important when the clutter is intermixed in range with moving target returns.

Once thresholding and peak association is completed, regression analysis can be more easily performed on the reduced set of data. The same linear movement per pulse for one or more associated peaks is highly indicative of a moving target. Note that association and regression analysis processing need not be done in a serial fashion. For example, each time a peak association is made, a linear projection through the remaining pulses can be used to cue further associations. This more efficient approach is employed in the regression algorithms described in Section 5.

4.4 Regression Analysis

Standard regression analysis can be utilized in a rule-based MTD algorithm that checks scattering peaks or other signal patterns, such as cross-correlation outputs, for evidence of linear motion. A number of associated pulse peaks is generally required to perform such analysis efficiently, although regression analysis can be applied to the entire set of scattering peaks. Either processing technique offers reliable target detection at a modest SNR level.

Regression analysis is most efficiently implemented in combination with thresholding and association processing that first identifies a number of signal peaks tentatively belonging to the same target scatterer. The linear relationship between the range location and pulse number of these peaks can then be evaluated directly through standard regression formulas.

First, the linear slope (range change per pulse) and intercept (projected signal peak location on the first pulse) are computed from the range centroids and pulse numbers of the associated peaks. Figures of merit for the resulting linear fit, such as the mean square error or correlation coefficient, can then be calculated. These parameters can be immediately compared to some threshold setting to declare a target detection. Alternatively, the number of peaks lying within some distance of this line can be used as a target indicator.

Regression analysis best describes the way that humans recognize target returns in noisy UWB radar data. The signal pattern, including both peaks and nulls, appears shifted between pulses for targets, whereas noise looks completely random. This means of human recognition suggests that adaptive neural networks (ANN) could be used to detect moving target returns in UWB data. The tolerance of ANNs to noisy inputs should further benefit this approach. The UWB database created by TSC is ideal for providing the necessary training and evaluation data to develop such ANNs. The inputs to this regression analysis network could be the raw UWB radar data, associated peaks, or the outputs from

an initial range integration or cross-correlation processing stage. The ANN could also be trained to directly reject clutter interference, thereby eliminating the need for any prefiltering.

4.5 Two-Dimensional Coherent Integration

Optimal processing of the multiple range and pulse returns from over-resolved targets involves Two-Dimensional (2-D) coherent integration. In this technique, FFT Doppler filtering is performed for the range returns along every possible line of motion. These lines of motion are defined, for a given maximum target velocity, by the possible starting and ending range cells of a target scatterer on the first and last pulse returns. This operation optimally combines the target signal over N pulses, and produces a peak response in one of N velocity filters. A second integration of these filter outputs across range cells could also be performed to sum the returns from the entire target range extent. It is generally not possible to do this, however, because the matched filter function in range for an arbitrary target is unknown.

The main drawback to this optimal method is that it has extremely large processing requirements. This processing load increases rapidly with range resolution, coherent dwell time, and maximum target velocity. These quantities increase the integration window size, number of possible lines of motion, and total number of filter outputs that must be thresholded to declare a target detection. As a result of this rapid growth, 2-D coherent integration is presently not practical as a real-time MTD algorithm for most UWB radar surveillance applications.

4.6 Noncoherent Integration

Two-dimensional noncoherent integration, where the detected magnitudes of the range and pulse returns are summed over all possible lines of motions, can also be performed. This processing results in only a small loss in

performance with respect to the optimal 2-D coherent processing when a small number of pulses are integrated. However, the processing requirements are only reduced by roughly one order of magnitude. This reduction is due mainly to the change from complex to real computations, and the difference between calculating a FFT and a real sum. As a result, 2-D noncoherent integration is also not a very practical MTD technique.

4.7 Hybrid Techniques

Hybrid techniques to detect moving targets in UWB radar returns can take many forms. The most promising of these hybrid techniques involves some sort of screening to reduce the number of tentative target detections, so that more sophisticated processing methods can be applied. This screening process effectively lowers the net processing load, since the more complex operations which follow are performed much less frequently.

Many hybrid techniques are possible, and each of the methods reviewed in this report can be combined in novel ways. For example, range integration, interpulse cross-correlation, or the noncoherent integration of a few pulse returns could be used for initial preprocessing of the UWB radar returns. The resulting outputs can then be processed to find possible lines of motion via a regression analysis algorithm. The original returns could then be reprocessed, perhaps in several different ways, to yield a final detection decision.

Characteristics of UWB returns that are measured in real-time, including number of scattering peaks, mean amplitude, and/or estimated SNR, can also be employed to select among diverse processing techniques. This would permit the MTD algorithm offering the greatest performance benefit to be automatically chosen. Hybrid methods of this sort could provide optimal performance over a wide variety of surveillance conditions.

5.0 REGRESSION-BASED MTD ALGORITHMS

TSC concentrated its efforts on developing regression-based MTD algorithms. Such regression algorithms have the greatest potential for reliably detecting weak target returns that consist of only a few scattering peaks. Algorithms that incorporate thresholding, peak association and regression analysis also have modest processing requirements compared to optimal integration techniques. These regression algorithms generally require clutter prefiltering which is covered separately in Section 6. A hybrid regression/coherent processing method that combines the best features of both regression analysis and optimal coherent integration was also developed, and is described below.

5.1 Key Assumptions

The key assumptions made by TSC in developing regression-based MTD algorithms are summarized in this section. First, the performance loss due to noncoherent, rather than coherent, processing of the target returns will be small. This is true if only a small number of pulses (typically on the order of 8) are processed.

Second, the majority of clutter interference, including discretes and diffuse scattering, can be eliminated by coherent or noncoherent MTI prefiltering algorithms. This processing reduces the number of scattering peaks that cross the first threshold, and vastly simplifies the subsequent, peak-to-peak association and regression analysis steps.

Third, it is assumed that small targets are of most interest to UWB radar surveillance systems. Larger aircraft targets can be readily detected by a collocated, conventional radar, by a NB radar mode, or by the large signal return that is observed with the WB radar without using sophisticated processing.

Since small aircraft and missiles are of greatest interest, target returns

will contain very few (possibly only one or two) scattering peaks. Thus the regression algorithms can be restricted to searching for one or two lines of motion that are formed by scattering peaks above the applied signal threshold.

Finally, in a practical UWB surveillance system, processing might be implemented only over some range window, as a periodic mode, or as a trip-wire for other sensors. For example, a window could be placed at the maximum detection range for the expected target threat. This would require that detections be made primarily under low SNR conditions. These low SNR cases were thus heavily represented in the algorithm training and evaluation data.

5.2 Algorithm Training Procedure

A small training set that included low single-pulse SNR target returns of from 6 to 12 dB was employed to initially develop the regression-based MTD algorithms. This training set was used to initially establish the individual algorithm parameters, and to define the peak association and linear alignment checking rules. Extensive Monte Carlo computer simulations with noise-only pulses were then used to fine-tune the parameters and algorithm rules. In this way, a desired P_{FA} operating point of 10^{-6} was achieved.

Addition algorithm refinements were also made to recover missed target detections. This procedure was repeated until a satisfactory MTD performance level was reached. A full performance evaluation over a range of target SNR conditions was then conducted, as described in Section 7.

A limited number of clutter cases were also simulated and processed as part of the algorithm training procedure. This was done to determine the effect of clutter residue on algorithm performance. Modifications to the regression algorithms were then made in some cases to minimize the impact of clutter interference on target detections, and to reduce the number of clutter-induced false alarms.

The clutter conditions included in the training set involved either one or two discretes at a CNR between 6 and 12 dB, with a SCR of -6 to 6 dB. These discretes were displaced from the target by 5 to 20 m in range, as well as intermixed with the target returns. Note that these modest SCR and CNR conditions are measured at the output of the clutter rejection prefiltering.

5.3 Peak-Pair Matching (PPM) Algorithm

The first regression-based MTD algorithm developed by TSC employs an integrated peak-association and linear regression approach. The algorithm searches for pairs of intra-PRI scattering peaks on two pulse returns that move together with the same range shift. Such matched pairs are more reliable indicators of target presence than single, isolated peaks. The drawback of this approach is that a minimum of two scatterers must be present on the target, both of which must be above the applied signal threshold. A somewhat higher peak SNR is thus required to guarantee that the second peak is above the threshold. However, the PPM algorithm has the potential to out-perform single-peak regression algorithms in the presence of highly correlated receiver noise, severe clutter leakage, or ECM interference that includes deception pulse jamming.

5.3.1 PPM Algorithm Operation

The PPM algorithm is an efficient, rule-based technique, since it processes only pulse returns with at least two scattering peaks. Targets at positive and negative velocities are also handled separately, permitting a dual-processor implementation. The PPM algorithm consists of the following five basic processing steps:

1. Apply a threshold nominally 6 dB above the mean noise level.

2. Identify pulse returns having two or more threshold crossings.

3. Determine the peak amplitudes and centroids.

4. Compare peaks from different pulses to find matching pairs with the same intrapulse range spacing.

5. Declare a target detection if these pairs exhibit an interpulse range shift that is within the maximum target velocity.

For Step 1, the threshold setting of 6 dB was selected to detect small target scatterers while keeping the number of noise crossings low. The threshold could also be adaptively lowered so as to obtain the requisite minimum number of peaks for processing. Alternatively in Step 2, single peaks can be retained and the algorithm modified so that pairs of matched peaks need not originate from the same two pulses.

For Step 3, a variety of additional features besides amplitude were investigated for matching pairs of peaks from different pulses. For example, TSC investigated using the phase angle difference of scattering peaks as a matching criterion. However, it was found that phase information was unreliable and difficult to extract from range-spread target returns at low SNR. The phase information was also found to be extraneous if other signal features such as relative peak amplitude and width were used at moderate-to-high SNRs.

A range motion constraint is employed during Step 4. This constraint defines a range window for comparing peaks for different pulses. First, only peaks that are within a distance that the target could have moved at maximum velocity are considered. Second, to avoid associating clutter residue that might be shifted slightly in range on consecutive pulses, peaks within a certain guard region in adjacent pulses are ignored. This guard region, which is several range cells in width, yields a minimum detectable velocity (MDV) on the order of 25 m/s.

An example of PPM processing is illustrated in Figure 5.3-1 for the DC-9 target and clutter example presented in Section 2. In this figure, a high confidence peak-pair match, A-B and D-C, has been identified for pulses 3 and 7.

The simple detection logic of Step 5 can be modified in several ways to make the algorithm less susceptible to random noise and interference signals. For example, a target detection can be declared only if additional supporting peak alignments occur. Two specific examples are shown in Figure 5.3-2a and b.

Figure 5.3-2a shows a common case, where a strong scattering peak is a member of two separate matched pairs. Figure 5.3-2b illustrates a case where a high confidence target detection can be declared. There are two sets of matched peak pairs: A-B, C-D and A'-B', C'-D'. Both of these exhibit the same linear range shift per pulse. They also have only one scattering center in common, indicating three distinct target scatterers. Efficient rules to recognize such arrangements of peaks were developed by TSC to declare high confidence detections.

Besides peak amplitude features, other radar observables, including polarization angle, could readily be incorporated into the PPM algorithm matching rules. However, it becomes increasingly difficult to optimize the various error bounds and detection rules over all target types, viewing geometries, and interference conditions.

5.3.2 PPM Algorithm Processing

PPM and other regression-based MTD algorithms developed by TSC are composed of both logical (IF/THEN) rules and numeric computations. Therefore, a processor that has both high MIPS and MFLOPS performance is required for real-time implementation. The large number of range cells that would typically exist in a UWB surveillance radar leads to a processing load that is somewhat beyond present general-purpose computer capabilities; hence a custom, high performance processor will probably be needed. A number of

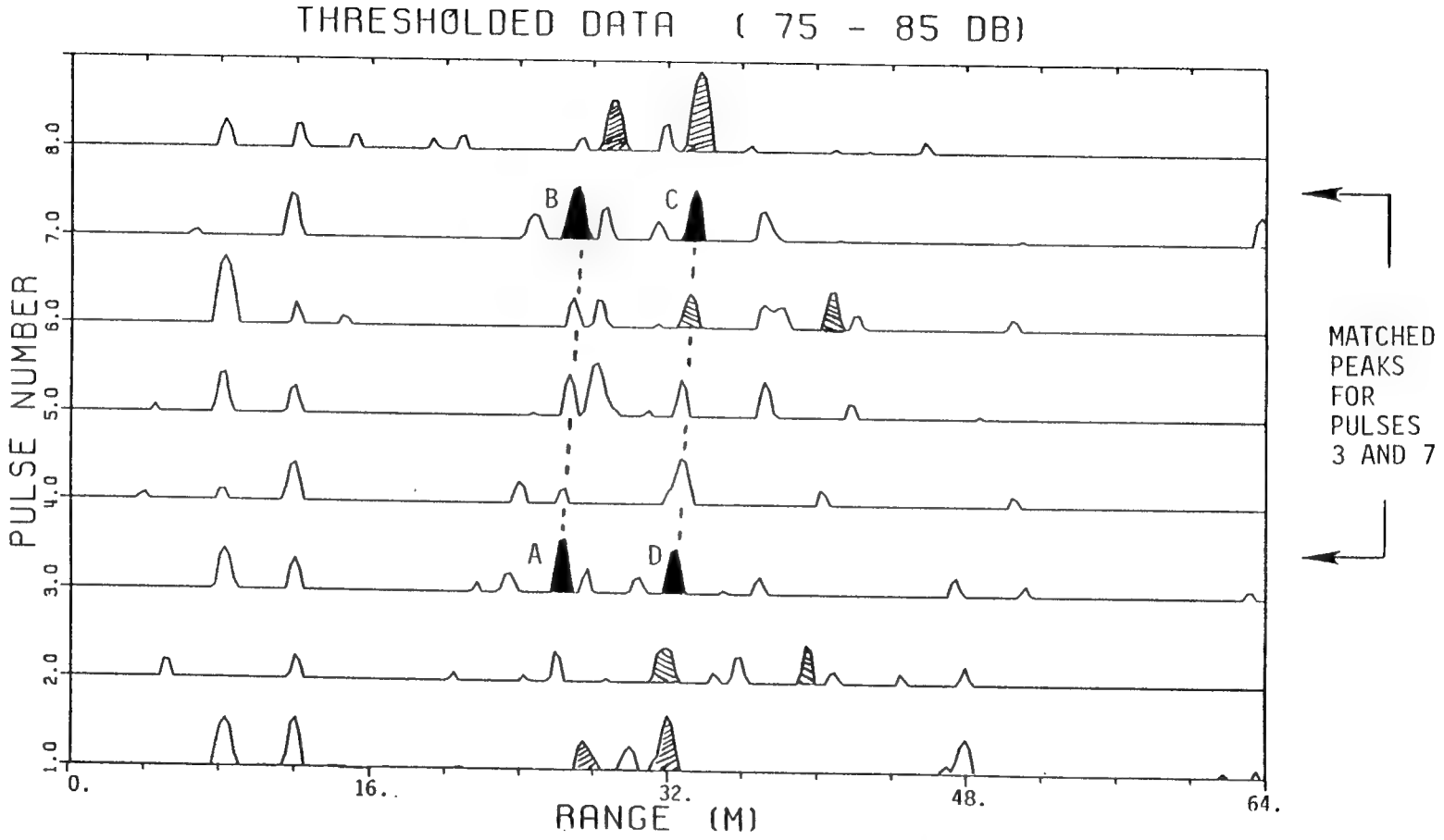

Figure 5.3-1 Peak Pair Matching Example for DC-9 Target in Clutter (Darkened Peaks are Discussed in Text, Left and Right Cross-Hatched Peaks Show Additional Matches)

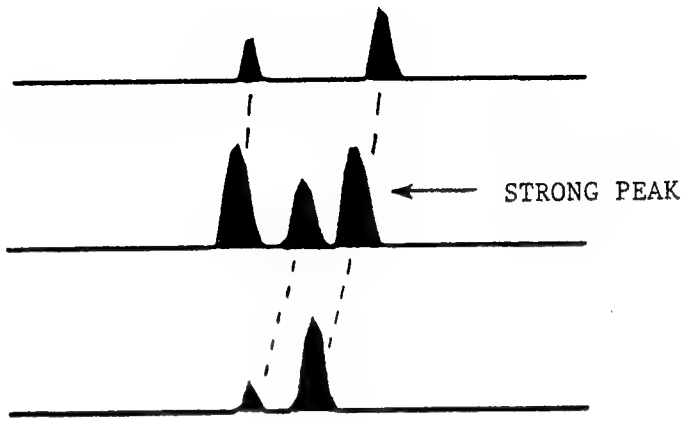

a) One Strong Peak is a Member of two Separate Matches

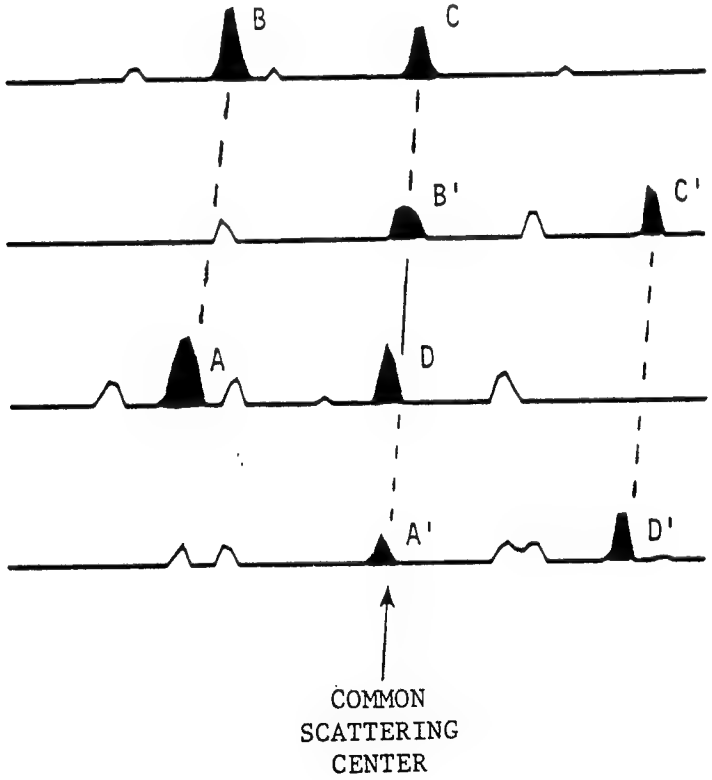

b) Two Independent Matches Have a Common Scattering Center

Figure 5.3-2 Examples of High Confidence Peak Pair Matches

processing shortcuts were therefore investigated by TSC to reduce the complexity of regression algorithm without greatly impacting its performance. However, a thorough, quantitative trade-off study could not be performed within the limited program resources.

To reduce the PPM processing load, several simplifications can be made. First, only the largest N peaks in each pulse can be processed by the algorithm, where N=2 to 4 is found to be practical. This substantially reduces the processing load, particularly in dense clutter regions. Second, the search for matching peaks can be made hierarchical in order of peak size. In this case, the largest peaks are sequentially compared to peaks from other pulses in order of their size. The search for a matching pair is then terminated at the Mth largest peak. This procedure shortens the PPM search time, but neglects smaller peaks from secondary target scatterers.

Another, more efficient PPM search procedure was developed by TSC. As soon as a match is found between scattering peaks in any two pulses, the next largest peak from each of these same two pulses are compared. Thus for a match between the two largest peaks from pulse 3 and 5, i.e., the second largest peaks of these same two pulses, are compared. This procedure quickly identifies most matching pairs of scattering peaks.

5.4 Peak Alignment Counting (PAC) Algorithm

Based on processing considerations, a second, regression-based MTD algorithm was developed by TSC. This method also involves matching peaks from different pulses using a set of association rules. However, as soon as any acceptable match is found, the linear range shift per pulse is determined. Scattering peak locations are then predicted for all other pulses. The number of peaks that align with this projected line of motion (within certain range error bounds) are then counted. If this number, n, exceeds a threshold, N, a target detection is declared.

A second line of motion is also formed by linearly projecting the next largest scattering peak from the original two pulses. The number of additional peaks m that align with these predicted locations is similarly counted, and target detection is declared if n+m exceeds a second threshold M.

The PAC algorithm is designed to detect target returns with only one or two dominant scattering peaks. Such returns correspond to the small targets that will be of primary interest to advanced UWB surveillance radars. The present PAC algorithm effectively neglects the received energy from a third or fourth scatterer on a larger target. Integrating this energy would be important for detecting large targets at extremeley long ranges. For a slight increase in processing load, the present method could readily be extended for the long range application.

The PAC algorithm consists of the following processing steps:

1. Apply a threshold nominally 6 dB above the mean noise level.
2. Combine contiguous groups of threshold crossings into a single range centroid and peak amplitude.
3. Form all possible peak-to-peak associations for the largest P=2 peaks from different pulses.
4. Determine the range shift per pulse and excise any zero velocity lines as clutter residue.
5. Project the remaining lines of motion into all other pulse returns.
6. Count the number of peaks, n, that closely align with the predicted scatterer locations.
7. Form parallel lines of motion through the next largest peaks of the two original pulses.

8. Count the number of additional peaks, m, that align with the predicted scatterer locations.

9. Declare a target detection if $n \geq N$ or $n+m \geq M$.

10. Derive a more accurate velocity estimate from a linear fit through all of the aligned peaks.

The last processing step provides an improved radial velocity estimate, and is performed only when a target detection is declared.

The quantity n or n+m provides a confidence measure for each target report sent to the radar operator or automatic tracking algorithm. If n+m is considered too low, the estimated velocity and range centroid can be sent to a knowledge-based Track-Before-Detect (TBD) algorithm [6]. This technique was originally developed by TSC under contract to AFRL to detect LO targets. For conventional radar applications, TBD employs a reduced detection threshold and performs scan-to-scan integration to sort random false alarms from valid target tracks. With slight modifications, it is ideal for this UWB application as well.

Several refinements to the basic PAC algorithm were explored by TSC. For example, in Step 3, the largest P=4 peaks of each pulse were considered rather than P=2. This increased the processing load substantially, since many more associations are possible in Step 3. However, somewhat better detection performance was obtained at low SNR. The related increase in misassociations and clutter false alarms was counteracted by considering only the largest two peaks in Steps 6 and 8.

Another improvement to the PAC algorithm was to not consider peaks from adjacent pulses during association processing if the range shift was small. This prevented clutter residue that occurs on consecutive pulses from causing excessive false alarms. Many of the processing shortcuts discussed in Section 5.3.2 for the PPM algorithm are applicable to the PAC technique as well.

TSC developed an algorithm with satisfactory detection and false alarm performance by using detection thresholds of N=5 and M=7, and counting only the two largest peaks from each pulse. The smaller scattering peaks in each pulse are considered only during the initial association processing of Step 3. Here, they must match up with a larger peak from another pulse to define a candidate line of motion.

Examples of PAC processing are illustrated in Figures 5.4-1 and 5.4-2. In Figure 5.4-1, the target is detected as a single line of scattering peaks with n=6. The matched peaks originated on pulses 3 and 5, and form a line of motion with radial velocity of -90 m/s, as indicated. The darkened peaks are considered aligned because they are within range error bounds of the projected scatterer locations on these pulses.

Figure 5.4-2 shows an example where a second, parallel line of motion was formed. A target detection was declared in this case because seven peaks aligned along the two lines. The original two matched peaks occurred on pulses 2 and 6. The next largest peak of pulse 6 was then linearly projected using the same slope, yielding the additional peak alignments.

5.5 Hybrid Regression/Coherent Doppler Filtering

The ability of the regression algorithms to accurately estimate radial target velocity led to a successful, hybrid processing concept [7]. Here, the estimated radial velocity (expressed as a range shift per pulse) is used to realign the range returns on each pulse so that the returns from individual scatterers on the target become registered. Once this alignment is accomplished, the target returns can be coherently integrated via an FFT, or other Doppler filtering technique.

Both block range shifts, where the UWB data is shifted to the nearest range cell, and range interpolation schemes were investigated for alignment purposes. Even if the range shift estimate is relatively coarse, the FFT output will

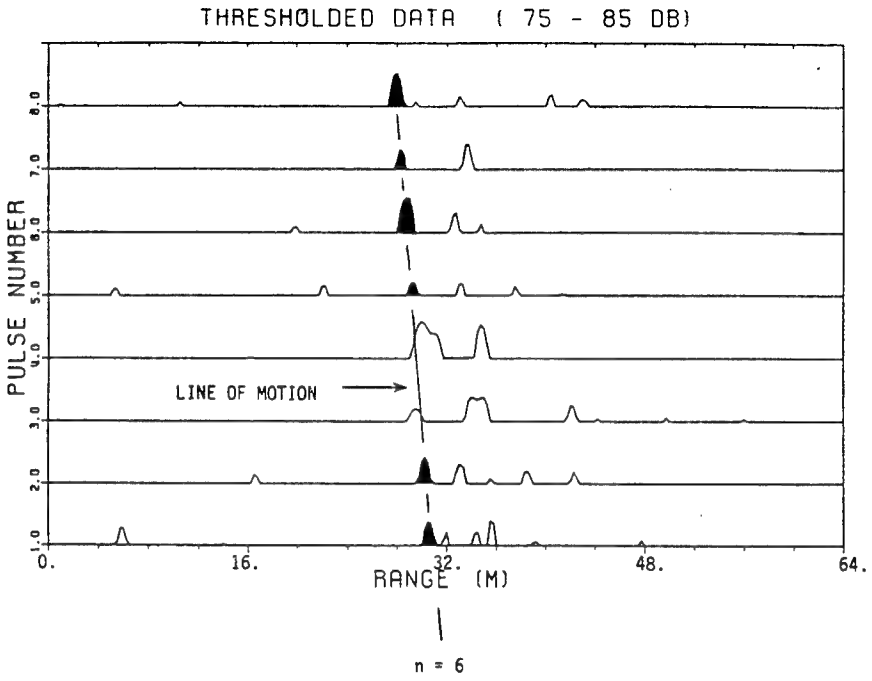

Figure 5.4-1 Peak Alignment Example #1

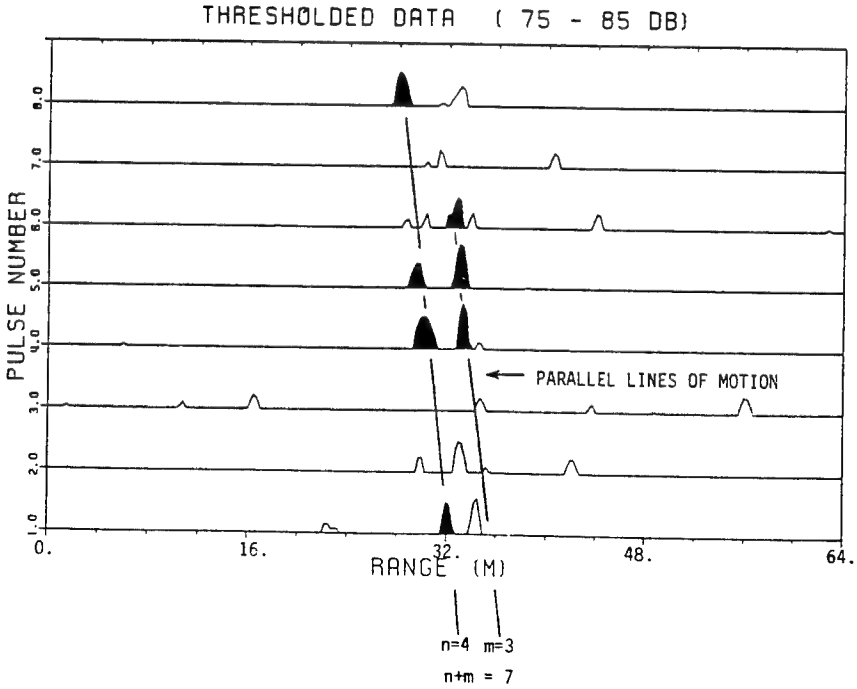

Figure 5.4-2 Peak Alignment Example #2

peak in a Doppler filter bin which corresponds closely to the target's radial velocity. This occurs because the range spread of the individual scatterers makes the Doppler response relatively insensitive to small range registration errors. More importantly, the filter bin of maximum response is nominally the same for all scatterers associated the moving target. The resulting "ridge" in range-Doppler space provides a convenient means of target detection.

The hybrid MTD algorithm developed by TSC consists of the following six basic steps:

1. Apply the PAC regression algorithm to find one or more candidate target lines of motion.
2. Realign the UWB range returns, based on the estimated target radial velocity.
3. Perform FFT Doppler filtering on the pulse returns for each registered range cell.
4. Determine the Doppler filter bin having maximum response over the most range cells.
5. Refine the radial velocity estimate using this Doppler frequency and repeat Steps 2 through 4.
6. Declare a target detection if the resulting range-Doppler ridge exceeds a threshold T.

Clutter prefiltering should preceed the PAC regression algorithm in Step 1. If this prefiltering involves only noncoherent processing, the raw, unfiltered UWB data must still be input to Step 2. The stationary clutter will then cause random FFT output peaks, as well as an increase in the mean FFT output level. To compensate for this effect, Step 6 might include the computation of an FFT for the unaligned radar data. This can serve as a normalized reference level to guard against excessive false alarms in the presence of severe clutter interference.

In Step 1, one or more candidate lines of motion are identified by the

PAC regression algorithm. Coherent processing is then performed before making a final detection decision. A reduced signal threshold or lower values of M and N in this first step will therefore permit weak target returns to obtain a coherent integration gain. Clutter or noise signals along lines of motion corresponding to false alarm events do not receive this coherent gain because of their radar phases. For most clear or clutter-contaminated regions, no lines of motion will even be identified by the PAC algorithm. This is the basis for the algorithm's reduced average processing load. Only a few radar resolution cells must undergo the range alignment and FFT computation steps which follow.

For Step 2, both block shifts and range interpolation techniques were investigated. An example of the more successful range interpolation method is illustrated here. The original UWB radar data is shown in Figure 5.5-1, together with the single line of motion identified by the PAC regression algorithm. Note that the estimated range shift per pulse is 1.52 cells, a non-integer value corresponding to a radial velocity of 95 m/s. Thus block shifting would have moved each UWB range return by a full two cells per pulse, rsulting in improper scatterer registration.

Figure 5.5-2 presents the results of the range alignment and FFT Doppler filtering steps for this example. Peaks in the aligned and interpolated data of Figure 5.5-2a have been darkened so as to show the correspondence with the original UWB range returns of Figure 5.5-1. The three-dimensional view also demonstrates the proper alignment of target scatterers. The registered returns are then Doppler filtered to produce the FFT output response plotted in Figure 5.5-2b. Note the elevated ridge that is formed in range-Doppler space with peaks at each of the scatterer locations. A few other, random peaks also occur above the noise floor, but only at isolated range-Doppler locations.

The FFT of Step 3 is an efficient means of performing coherent integration, since all velocity filters are formed simultaneously. However, the

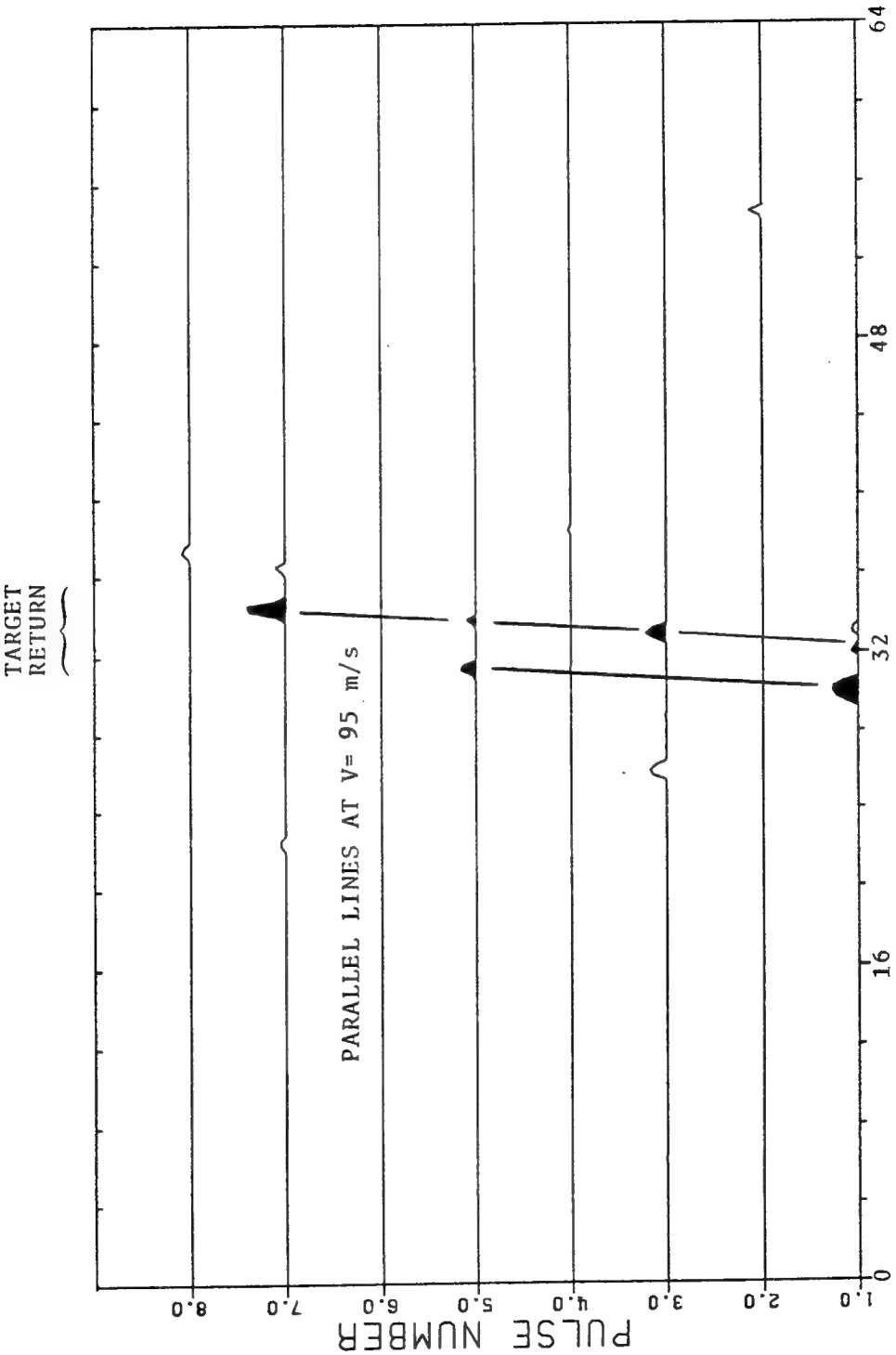

Figure 5.5-1 Initial Regression Stage

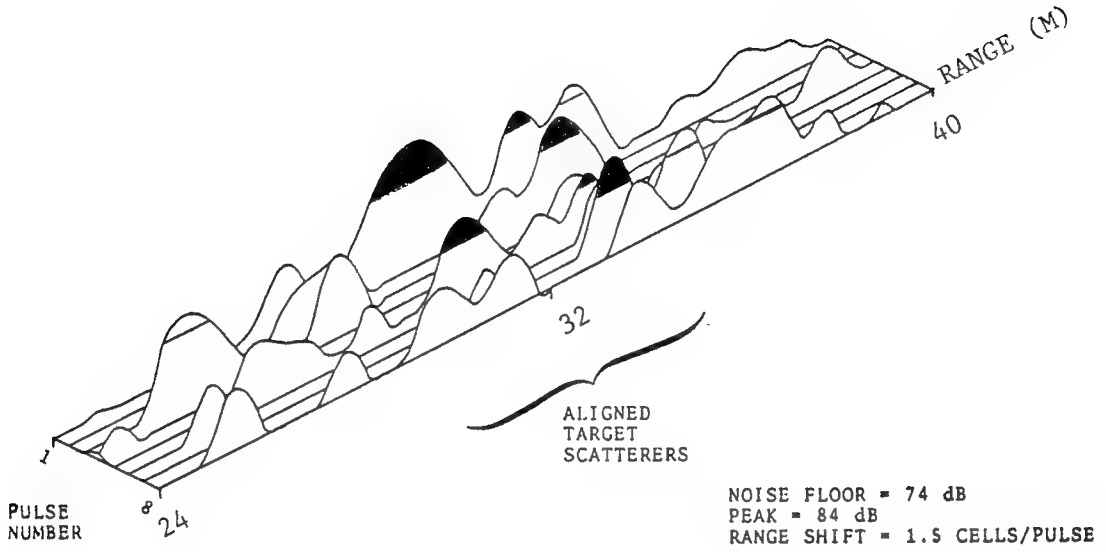

a) Aligned Range Data

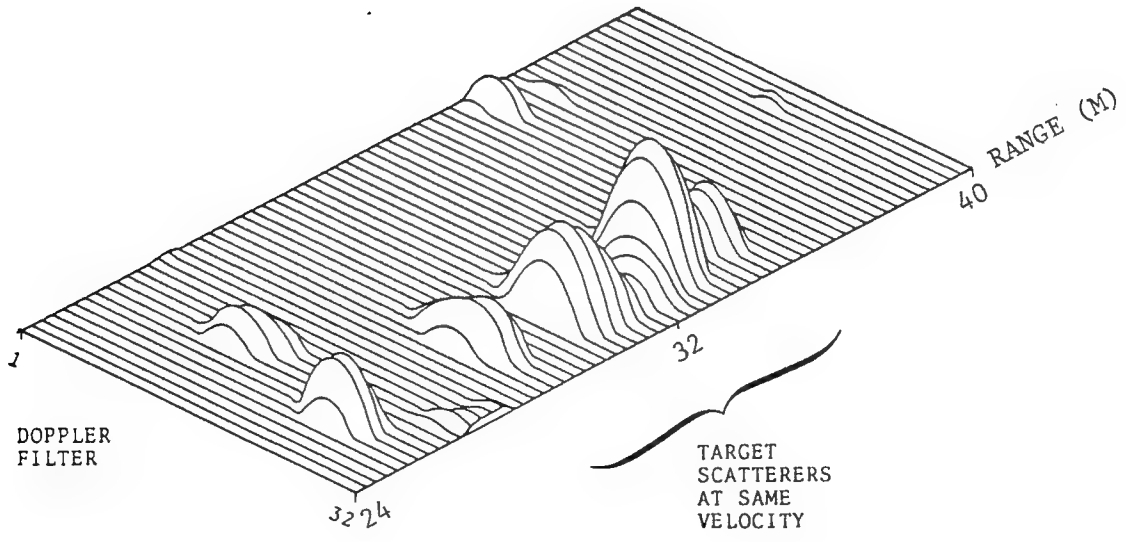

b) FFT Output Power

Figure 5.5-2 Coherent Doppler Filtering Stage

unambiguous velocity at S-band for a 250 Hz PRF is only ±5.5 m/s. Since the velocity estimation accuracy of the regression analysis is much poorer than this, the correct target velocity must be unfolded. Several means of accomplishing this were investigated by TSC.

It is obviously beneficial to know the estimation accuracy of the linear regression slope. Knowing this parameter minimizes the number of separate FFTs that must be performed to unfold the correct target velocity. An initial goodness-of-fit can be obtained from a standard RMS error analysis as part of Step 10 in the PAC regression algorithm. On subsequent iterations of the hybrid algorithm, the maximum Doppler response can be isolated in a single FFT, and the correct target velocity will be resolved.

Besides the FFT, TSC explored several other means of velocity filtering. These included Maximum Entropy Method (MEM) and autoregressive (AR) spectral estimation techniques. These methods further improve the velocity estimate by combining iterative range alignment and MEM or AR spectral estimation of the radial velocity.

Step 6 involves making a final target detection decision. Rules to recognize range-Doppler ridges that are characteristic of a moving target return need to be further developed. To be effective, these rules must examine both the peak amplitude and range-Doppler extent of ridges such as the one shown in Figure 5.5-2. The integrated Doppler energy in the ridge can then be compared to a threshold T to declare a target detection.

To reduce the processing requirements of the hybrid algorithm, several simplifications can be made. For example, only range cells near scattering peaks that were identified by regression analysis need to be processed. This will discard some of the smaller target scatterers, but should not significantly affect detection performance. It will, however, substantially reduce both the number of FFTs and magnitude detection and thresholding operations that must be performed. Clutter

residue typically will not fall along the lines of motion associated with these scattering peaks and will thus be rejected.

In summary, hybrid regression/CDF processing is a very promising MTD algorithm. It combines the best features of both regression analysis and Doppler filtering to detect and then coherently integrate the peak scatterers which contain most of the target's RCS. The only remaining work is to optimize the detection rules and thresholds for this algorithm. This can be done most effectively by implementing the algorithm on a high speed processor, and then conducting extensive performance trade-offs.

6.0 CLUTTER REJECTION

Clutter rejection filtering is an important requirement for regression-based MTD algorithms. The presence of uncancelled clutter residue can degrade MTD algorithm performance by: 1) increasing the overall data processing load, 2) causing target peak misassociations and, 3) producing false alarms. As in a conventional radar, it is very important to achieve a constant false alarm rate (CFAR) under all clutter interference conditions with minimal impact on target detection probability.

There are many techniques available for rejecting clutter interference at conventional radar resolution. Many of these can be adapted for application to UWB radars once the nature of target and clutter returns are better understood.

6.1 Clutter Model

UWB clutter returns from clutter discretes can be extremely large, particularly those from man-made structures such as buildings, automobiles, and utility networks. The specular returns from sea spray, tree trunks and branches, and rock formations can also be large relative to the surrounding diffuse clutter background. Once individual scatterers are resolved in this manner, the clutter can no longer be described as a homogeneous distribution. Instead, the clutter returns become "spiky" in nature, and must be modelled as a collection of discretes with independent amplitudes.

A fundamental question is whether all diffuse clutter returns, including scattering from essentially uniform terrain, becomes discrete-like at sufficiently high resolution. This phenomenological issue can only be addressed in a clutter measurement program that quantifies clutter statistics including small-scale range and temporal correlations. For the present study, the clutter model will consist of a small number of isolated discretes, each having an

independent CNR. Because of antenna sidelobes, these discretes may be near to, or intermixed with, the target range returns. The clutter measurement presented in Figure 2.3-2 supports this clutter model.

6.2 Temporal Filtering

Temporal filtering in the form of a fixed coefficient Delay Line Canceller (DLC) is a very efficient means of clutter rejection. A DLC can be applied to either the coherent radar returns or to the detected magnitudes. In the second case, the technique, which is called Area MTI filtering, can be further combined with noncoherent integration of the UWB pulse returns. The cancelling can then be performed on a dwell-by-dwell or a scan-by-scan basis.

The DLC is most suitable for rejecting large, stationary clutter discretes that are relatively stable. Under these conditions there is little clutter decorrelation over the two to three pulse returns used in the DLC, and near-perfect cancellation can be achieved. To avoid the SNR loss associated with such DLC processing, the canceller can be bypassed when the measured CNR falls below 0 dB.

A comparison of target and clutter returns at conventional and UWB resolution reveals a number of subtle differences. Figures 6.2-1 and 6.2-2 show stationary clutter (C) and moving target (T) returns on consecutive pulses for these two cases, respectively. For simplicity, the UWB return is made up of only two target scatterers (S1,S2) and two clutter discretes (D1,D2). The vectors at each range indicate the received signal strength and its phase angle.

The pulse returns in Part a and b of these figures are subtracted to produce the difference signal in Part c. In both cases, the stationary clutter is completely cancelled. At conventional radar resolution, the target signal remains in the same range cell, and undergoes a phase change due to its Doppler frequency shift. The difference signal then appears in the same range cell. However, in the UWB case, the target return signal moves in range and two "doublets" are formed.

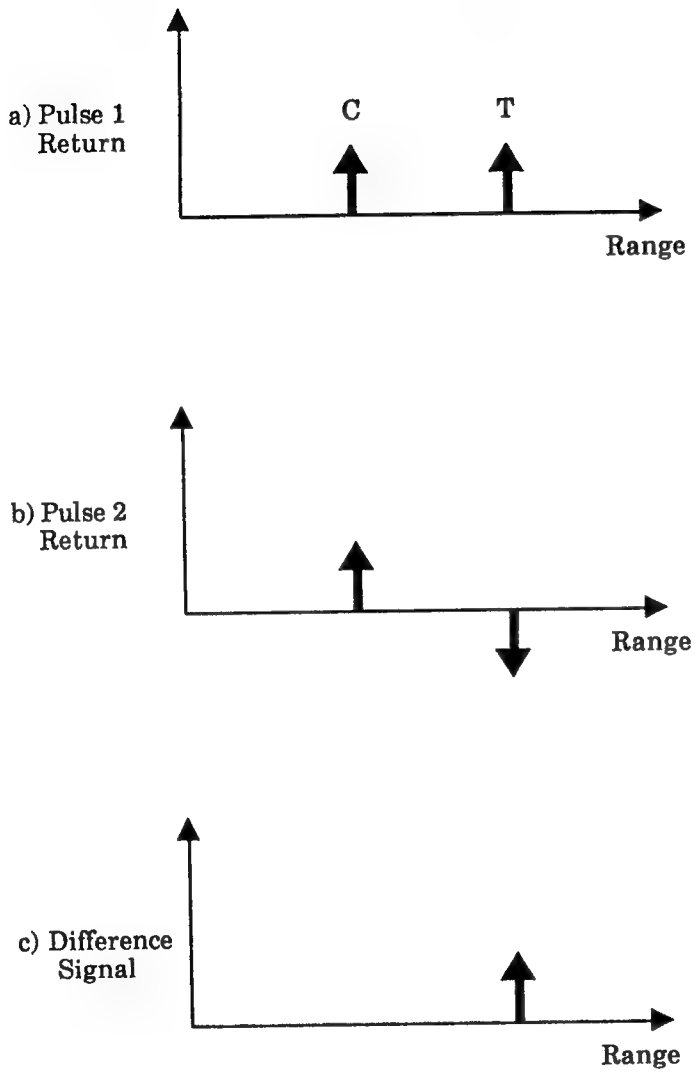

Figure 6.2-1 Conventional Radar Returns

(T = Target, C = Extended Clutter)

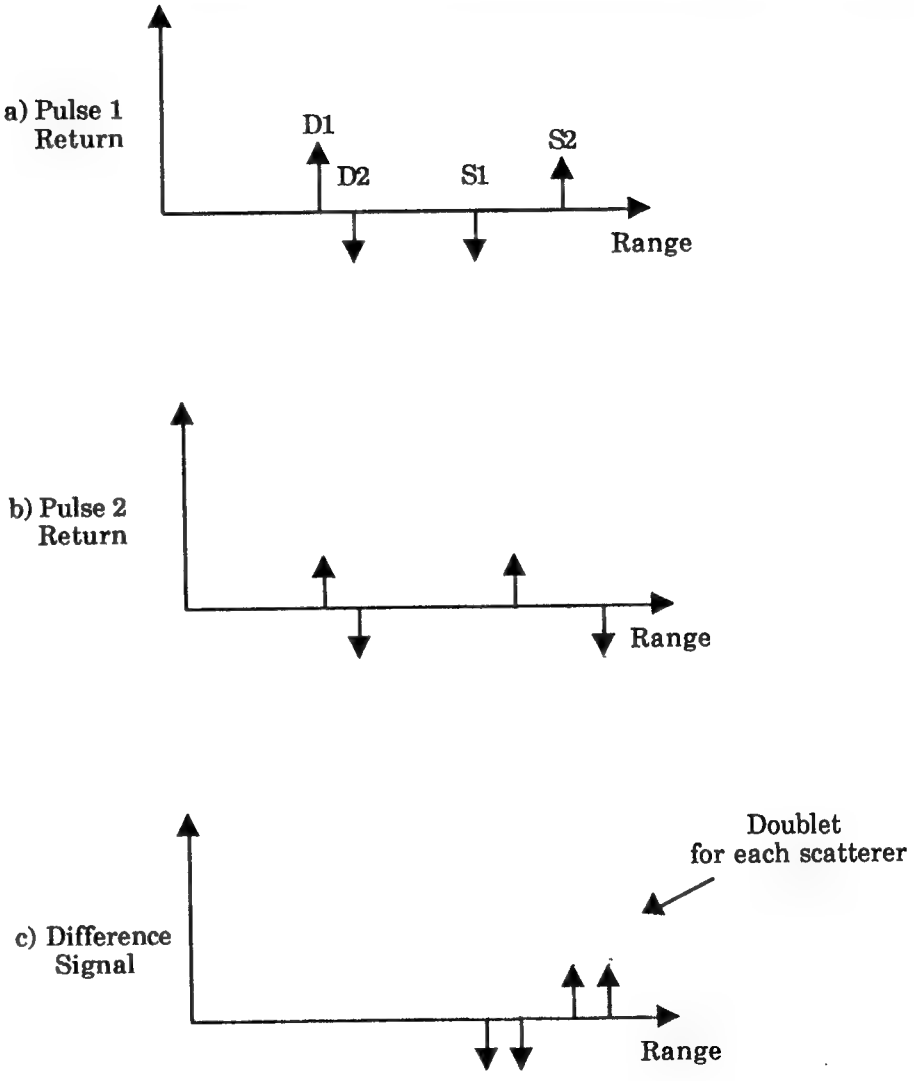

Figure 6.2-2 UWB Radar Returns

(S1, S2 = Target Scatterers, D1, D2 = Clutter Discretes)

Each doublet is spaced by the distance travelled by the target between pulses.

At some radial velocities (Dopplers) the net phase change will be 0° and no target difference signal is produced by the DLC at conventional resolution. These are the radar MTI "blind speeds." However, no blind speeds exist at UWB resolution. The only possibility is a partial signal cancellation, which occurs for unique scatterer distributions with certain amplitude and phase relationships.

Next, consider a small shift in the location of one of the clutter scatterers depicted in Figure 6.2-2. This shift may be due to instabilities in the UWB radar system, small clutter discretes such as tree branches swaying back and forth in the wind, or both. These slight motions are readily visible at UWB resolution and can cause the clutter return to shift between different range cells on different pulses. This will result in imperfect clutter cancellation that depends heavily on the clutter's range correlation and its pulse-to-pulse range motion. The residue is a dual-peaked signal, which is not unlike two nearby scattering peaks. These peaks are very difficult to discriminate from target returns during regression analysis.

In summary, a simple DLC produces a very different clutter residue and target response for UWB and conventional radar resolutions. The principal effect is a replication of all moving target range-shifted clutter scatterers in the DLC output signal. For range-spread target returns, the doublets of Figure 6.2.2c become dual peaks. Such DLC outputs cannot be sent directly to the regression-based MTD algorithms developed by TSC. For example, the dual peaks would greatly complicate the peak centroiding, pair matching, and alignment checking steps of the regression algorithms described in Section 5. Thus, the conventional DLC must be modified so as to eliminate these doublets.

6.3 Modified DLC Bank

A novel prefiltering algorithm was developed by TSC to cancel

stationary clutter, and to provide a single-peaked output response for moving target scatterers. The technique employs a bank of modified DLC filters (MDLC), where each filter is designed to pass a selected target velocity. For improved processing efficiency, each MDLC operates on the detected signal magnitudes of a short range window by N-pulse dwell. Stationary clutter is cancelled roughly equally in all of the MDLC filters. However, target returns moving at the filter velocity v_i are passed, and produce an output response that has a strong peak centered at each scatterer's range. Two secondary range peaks are also produced, but this resulting shape is much preferred to a dual-peaked signal for subsequent regression analysis.

The individual MDLC filter outputs are peak-detected over the entire range window and N pulses to determine the filter with greatest response. This filter's output signal is then used for regression processing. The filter bank implementation also provides a crude velocity estimate which offers the possibility of a hybrid MDLC/CDF technique that avoids regression analysis altogether.

Each MDLC filter operates by first subtracting pulse returns to eliminate clutter. It then adds back the difference signal at the presumed target range shift to produce a single output peak. The difference equation is:

$$D_i(R,t) = | A(R,t) - A(R,t') + A(R+v_i\Delta t,t') - A(R+v_t\Delta t,t)| \qquad (6.3\text{–}1)$$

where t and t' are pulse times, $\Delta t = t\text{-}t'$ is the time difference, and R is the range. The absolute value is taken to avoid negative quantities in the output.

A critical refinement to the MDLC involved subtracting range returns with greater mean time separation, rather than simply adjacent pulses. This permits greater target motion between the subtracted pulses, and reduces self-cancelling of range-spread target returns. It implicitly assumes that the clutter remains stable over short radar dwells.

Since only a fixed number of pulses are available for processing, some of the subtractions must be between pulses with different time separations. For example, to achieve a mean time separation of 3.5 PRIs, the following pulses are subtracted: 8-5, 7-4, 6-3, 5-2, 4-1, 7-3 and 6-2. Other pulse combinations are also possible. Because the pulse indices are not uniformly spaced as in consecutive pulse differencing, however, extra care must be taken when implementing the MDLC algorithm in software.

An example of MDLC processing is presented in Figure 6.3-1. The input data is illustrated in Part a and the output response is shown in Part b. The target in this case was a C-402 with a velocity of 1.6 cells per pulse, and a simulated peak SNR of 7 dB. The mean noise level here is 73 dB. Because of the low SNR, it is very difficult to make out the target signal at all. Two clutter discretes with a CNR of 9 dB are also present.

The MDLC filter bank velocities were spaced by 0.5 range cells per pulse. The filter at +1.5 cells per pulse produced the peak output response shown in Part b. To reduce sensitivity to noise and the production of secondary peaks, this MDLC filter only operates on detected magnitudes above a threshold setting of 79 dB. The mean time separation between subtracted pulses here was 4.5 PRIs, and the output data was realigned for display.

Figure 6.3-1c illustrates the results of averaging the MDLC filter's output response after realigning the data in range. The two dominant target scatterers are readily apparent, and the clutter discretes have been suppressed. This crude integrated clutter rejection/MTD techique provides a rough velocity estimate and could thus provide inputs for TBD processing and further scan-to-scan integration.

Additional refinements to the MDLC algorithm are certainly possible. These include a coherent processing version that accounts for the Doppler phase shift of the target signal between pulses. The filter outputs for these pulse differences

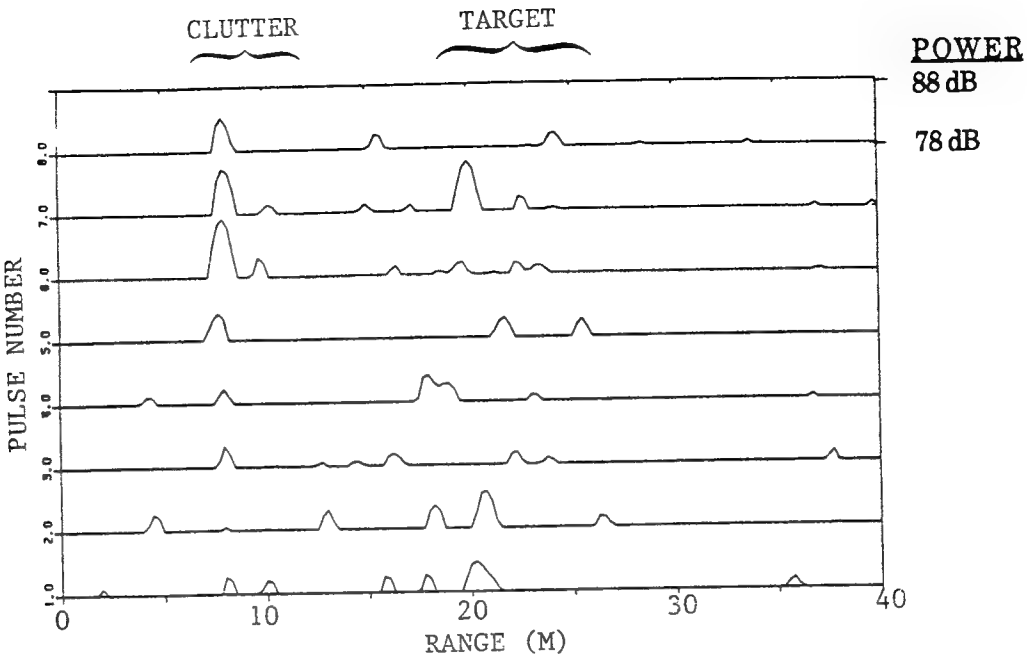

a) Original UWB Data

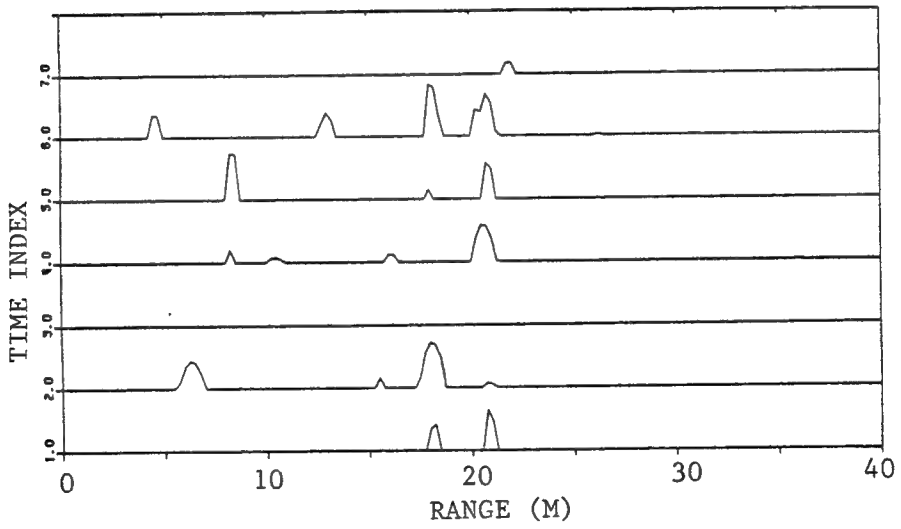

b) MDLC Filter Outputs

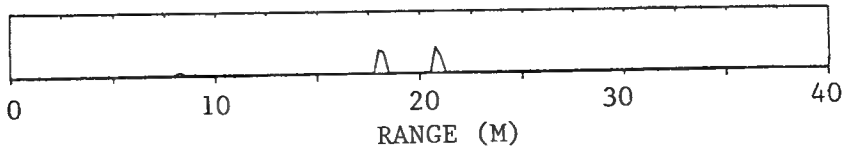

c) Aligned and Averaged Filter Outputs

Figure 6.3-1 MDLC Processing Example

could then be coherently integrated at each range cell much as in Figure 6.3-1c. This processing would be done after realigning the range data, just as in the hybrid algorithm described in Section 5.5. The resulting output signal can then be peak detected and thresholded to declare a target.

7.0 PERFORMANCE EVALUATION

This section presents performance results for the PAC regression algorithm of Section 5.4. The proper procedure for evaluating each MTD algorithm is to run a large number of Monte Carlo trials under variable signal-to-noise and clutter conditions. The input data for each trial can be generated, as described in Section 2, from the UWB target measurements at S-band, and the clutter or noise-only pulses simulated using WASP. The results of these computer experiments are then combined to obtain a receiver operating curve (ROC).

7.1 Evaluation Software

To conduct lengthy computer experiments, efficient VAX FORTRAN software routines were developed to: 1) generate M range cell by N pulse dwells for each test case, 2) execute the PAC regression algorithm, and 3) plot the detection probability and the root-mean-square (RMS) velocity error versus SNR. The relationship between this evaluation software and the other DBMS files described in Section 2 is illustrated in Figure 7.1-1.

The software routines depicted in this figure are internally documented and have an entirely modular structure. This allows portability to other computers such as the Sun workstations at AFRL. It also supports direct comparisons of other MTD algorithms and the inclusion of clutter rejection algorithms to evaluate combined algorithm performance.

The GETDAT subroutine shown in Figure 7.1-1 has several input parameters. These are used to select among noise-only, clutter-only, or target plus noise and/or clutter cases. For targets, any one of the seven small aircraft from Table 2.3-4 may be chosen. The desired signal, noise and clutter power are also specified as input parameters, as well as the distribution of simulated clutter discretes. For target cases, the actual target velocity is returned by the GETDAT

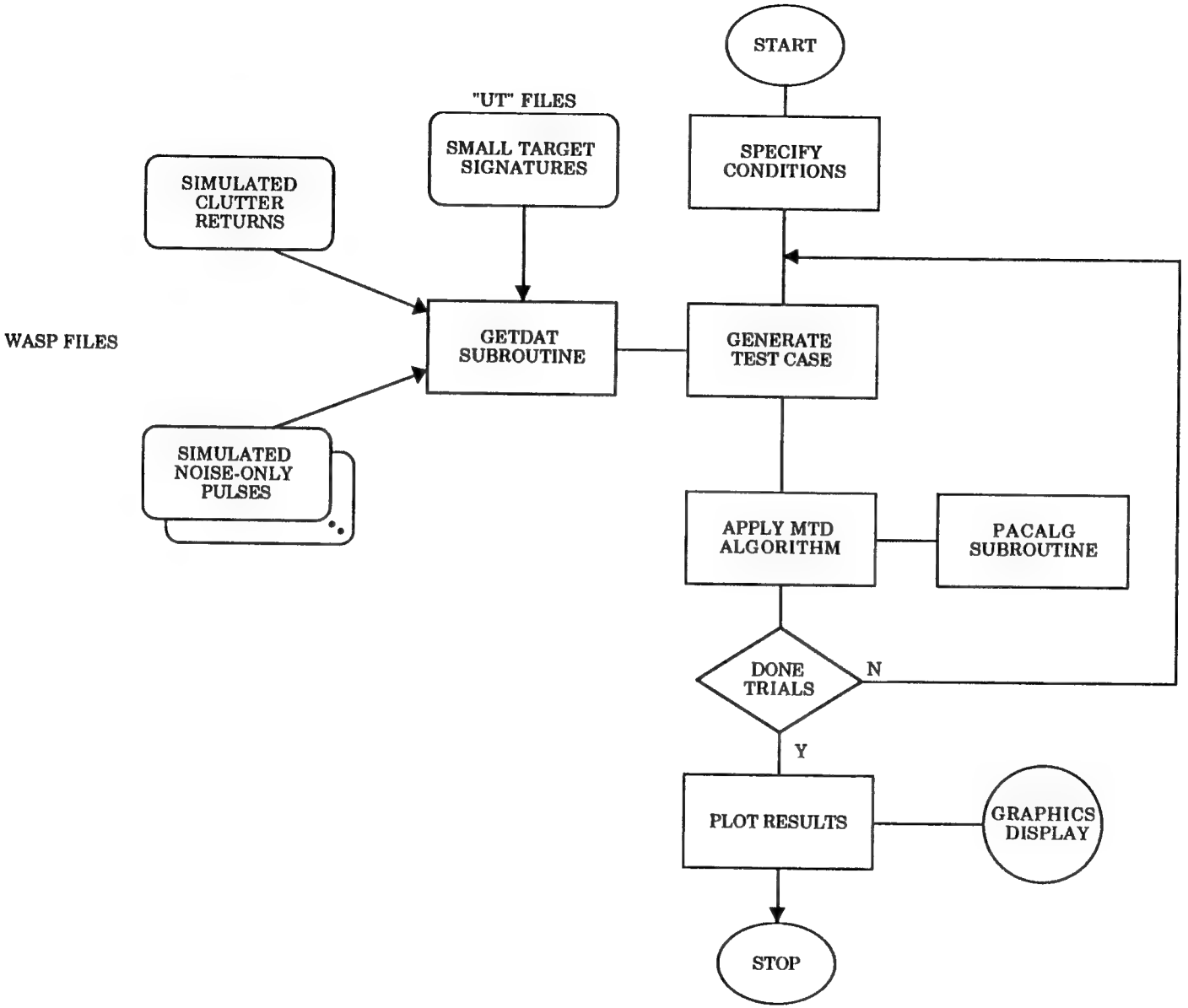

Figure 7.1-1 Performance Evaluation Software

routine to support algorithm error analysis.

The PACALG subroutine performs the PAC regression analysis and returns a target detection flag, confidence level and estimated radial velocity. If a detection is declared, the range centroid of the largest scattering peak (projected into pulse 1) is returned. The range of any secondary scatterer identified by the algorithm is also returned when a parallel line of motion is found.

The main program includes a user input sequence, logic to loop through specified SNR values, and data plotting and graphics control. Presently, both the probability of detection and RMS velocity error are plotted as a function of target SNR for a fixed number of Monte Carlo trials. All of the software, which runs under the VAX/VMS operating system, is extremely easy to use.

7.2 Performance Results

Figures 7.2-1 through 7.2-3 present the performance results for the PAC regression algorithm against the seven small aircraft examples that were evaluated. Slight differences in the scatterer amplitudes, their range distributions, and the target radial velocities lead to minor performance variations for each aircraft. Several trends are apparent, however. First, there is a sharp increase in P_D with SNR in these ROC curves. This is a direct result of the target scatterers demonstrating nonfluctuating, Case 0 statistics. These statistics lead to a 3 to 4 dB loss compared to a Case 1 target at low single-pulse SNR. However, the P_D increases rapidly at moderate SNR. This effect is compounded by the presence of multiple target scatterers with roughly equal RCS. These multiple scatterers, in fact, compensate for much of the SNR loss.

Next, the RMS velocity error is found to decrease with increasing SNR, but in an extremely irregular fashion. This occurred independently of the number of Monte Carlo trials that were conducted. The cause of this velocity error is that the range accuracy of the individual peak centroids remains poor at

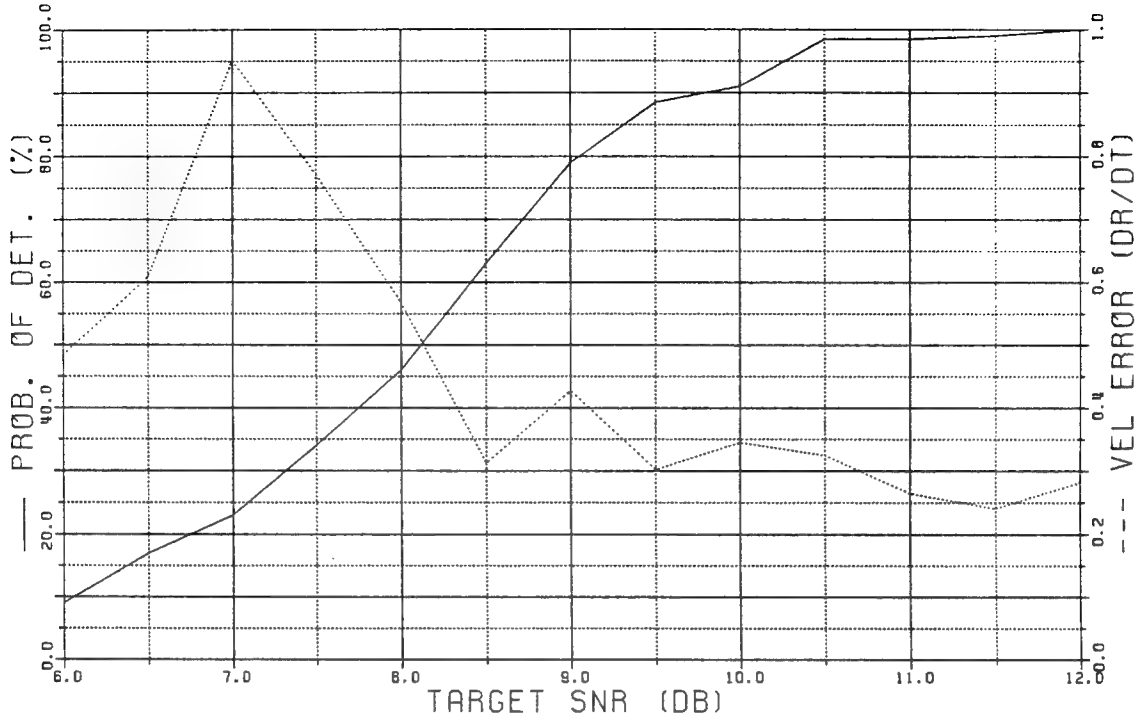

Figure 7.2-1a Detection Performance Against C-402 (Example #1)

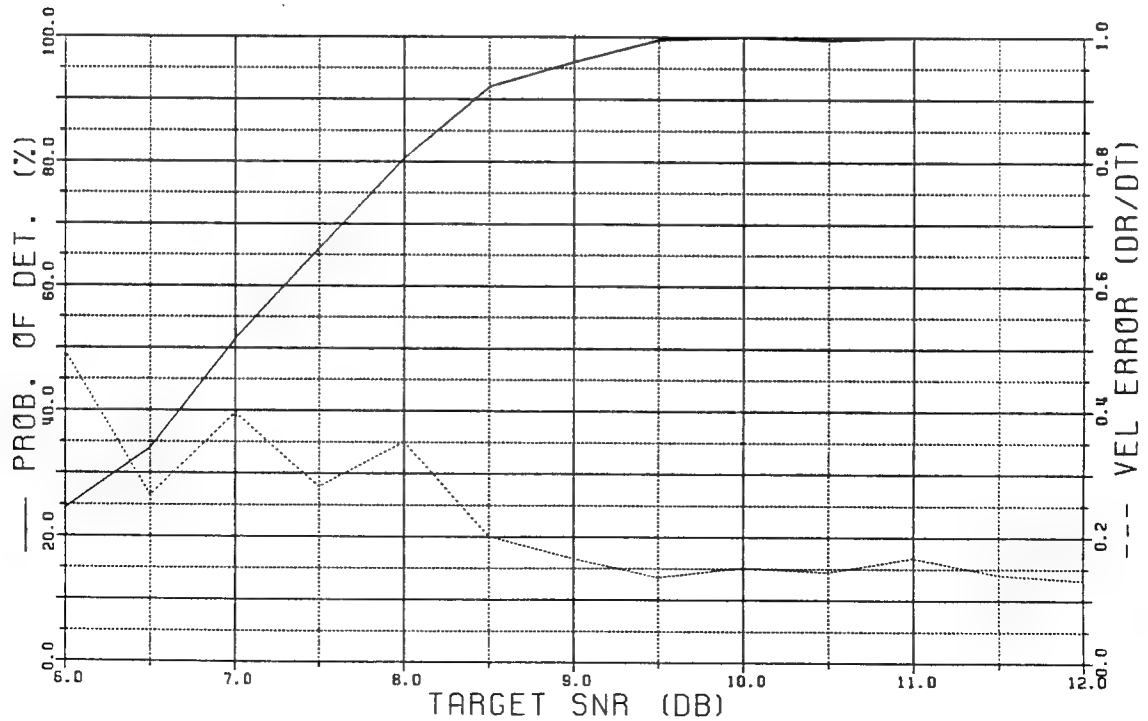

Figure 7.2-1b Detection Performance Against C-402 (Example #2)

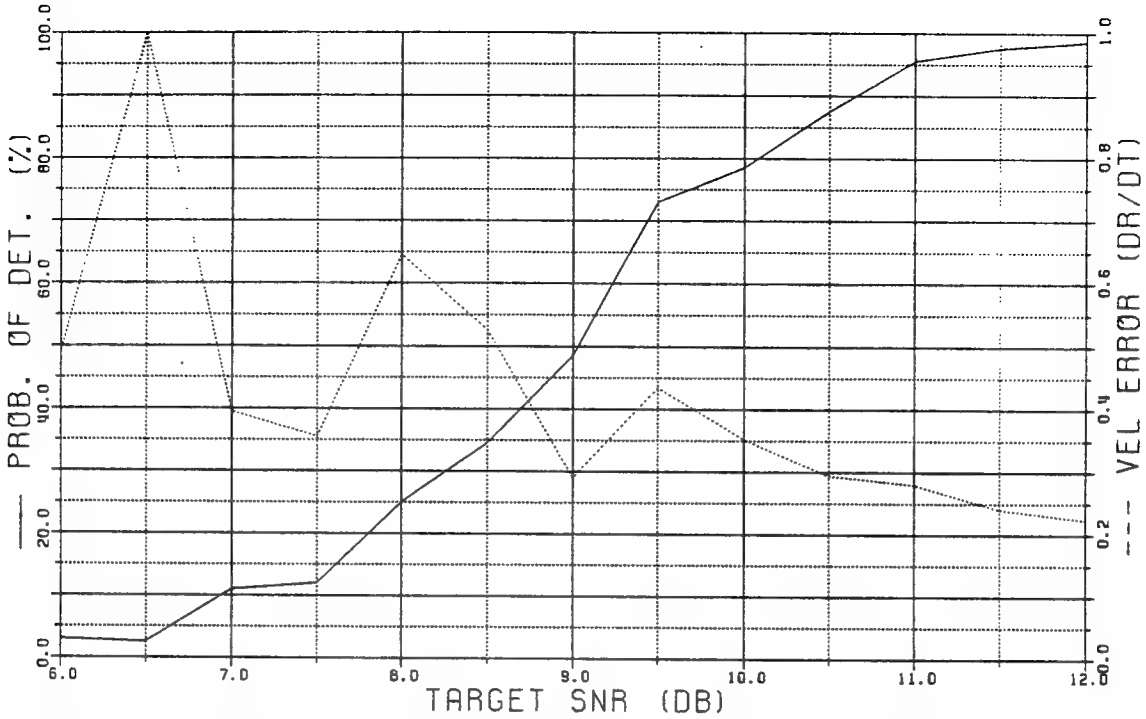

Figure 7.2-2a Detection Performance Against BE-1900 (Example #1)

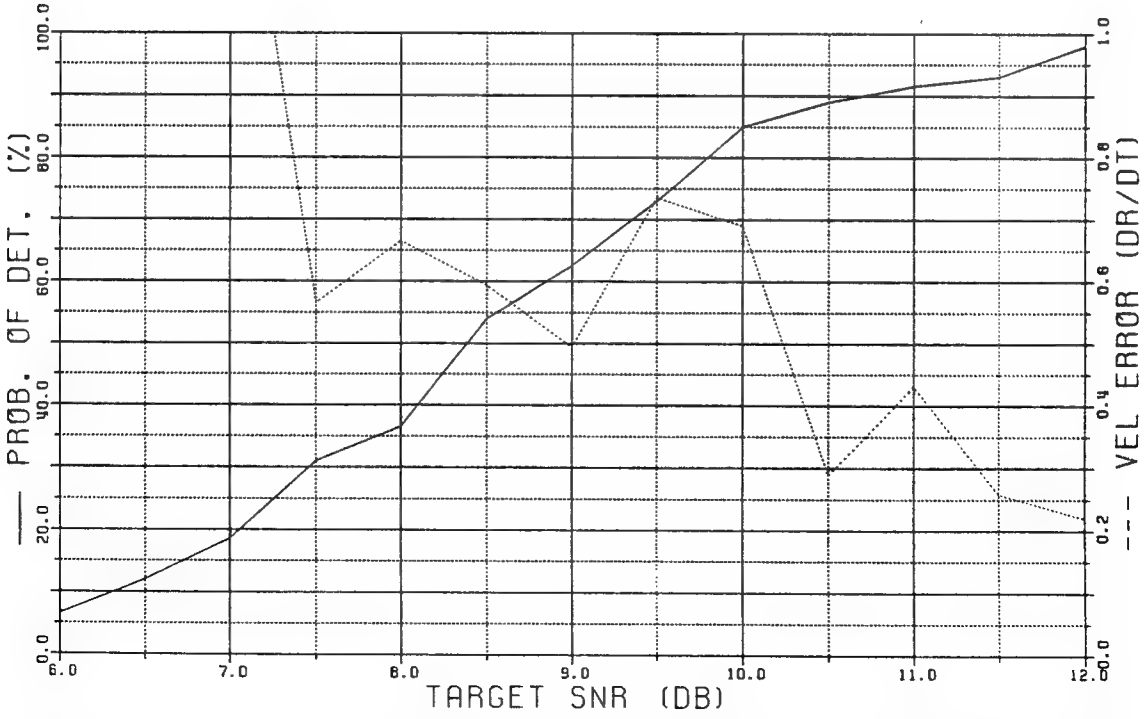

Figure 7.2-2b Detection Performance Against BE-1900 (Example #2)

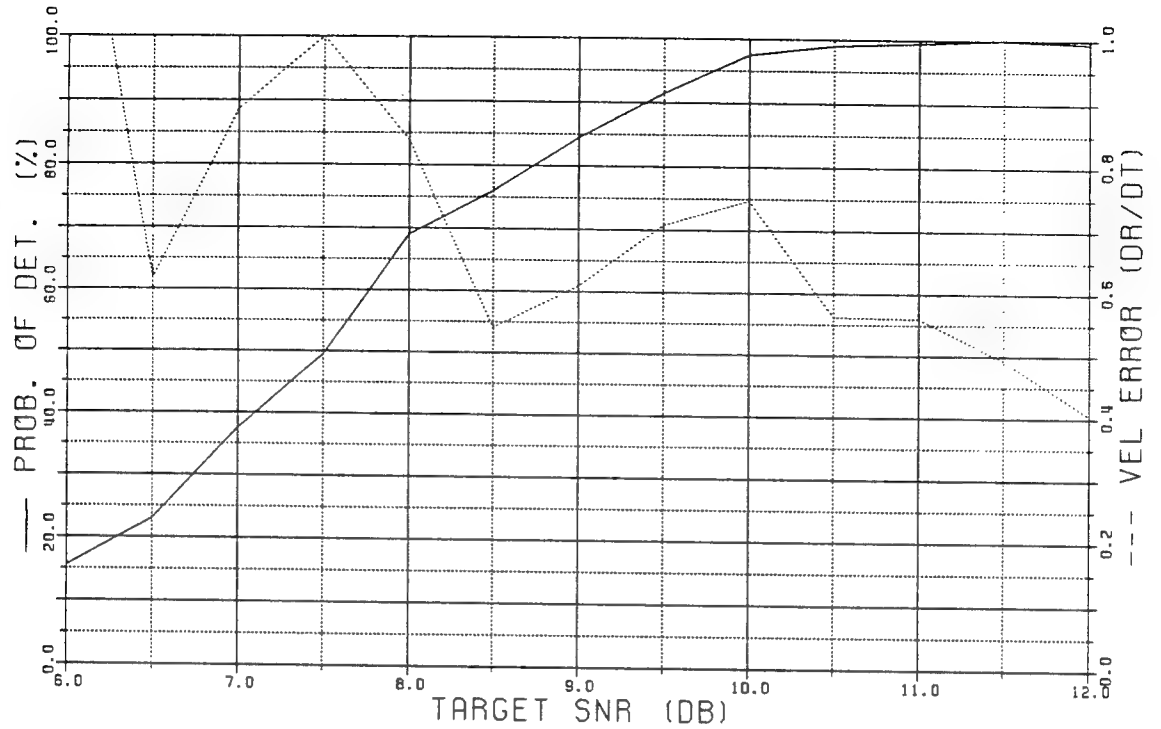

Figure 7.2-3a Detection Performance Against BE-99 (Example #1)

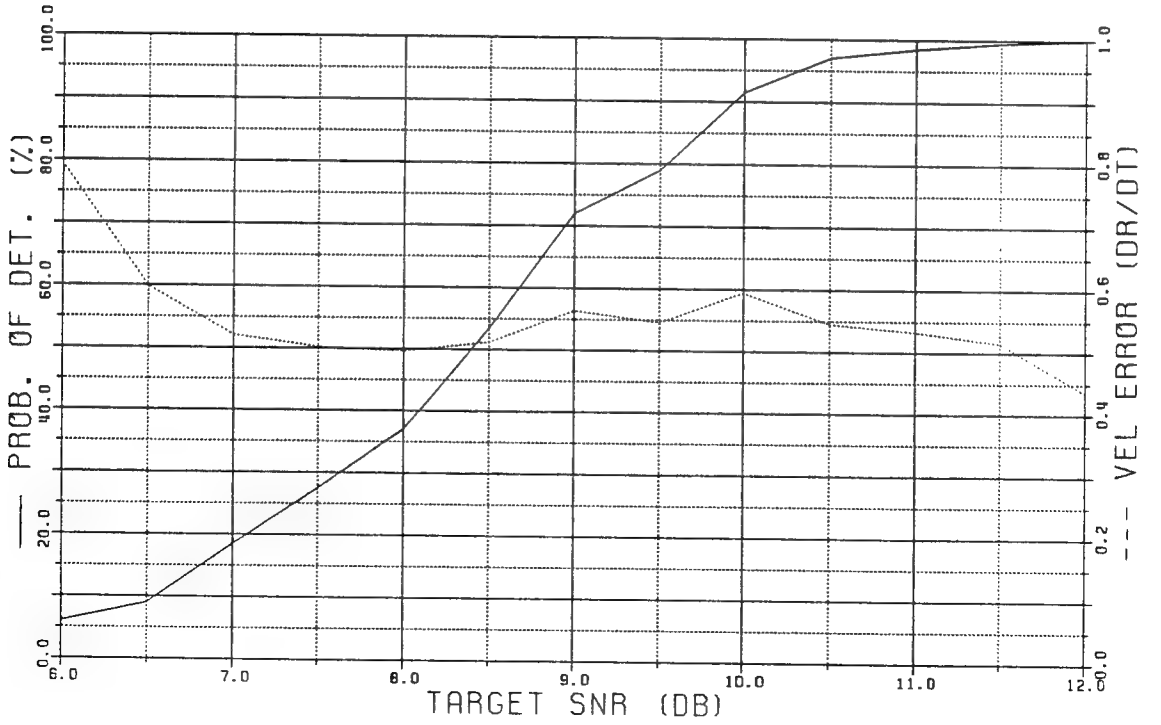

Figure 7.2-3b Detection Performance Against BE-99 (Example #2)

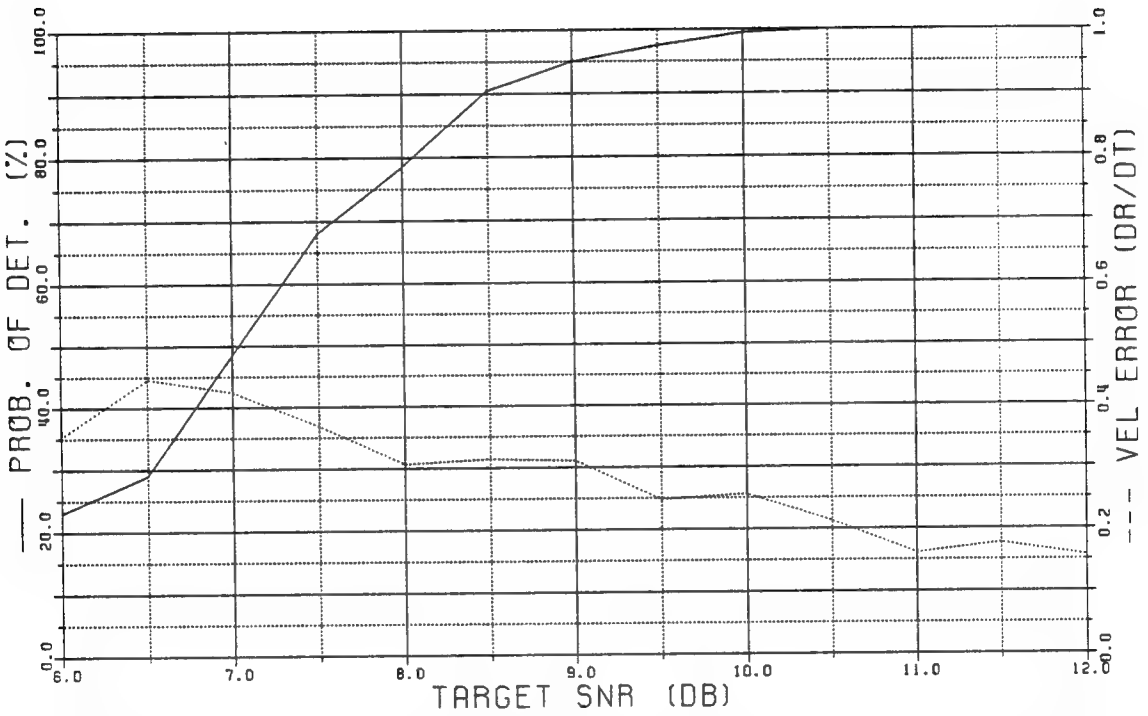

Figure 7.2-3c Detection Performance Against BE-99 (Example #3)

low-to-moderate SNR. For small targets with several nonfluctuating scatterers of similar RCS, the detection probability increases rapidly with SNR. However, since none of the individual peak locations is known very well, the velocity error remains high. In addition, if two scatterers are located very close together, the line of motion identified by the M-of-N coincidence logic can pass through either one.

Note that the BE-1900 exhibits somewhat wider swings in the RMS velocity error at different SNRs. This occurs because it has many more small scattering peaks, and thus there are more opportunities for peak misassociations during PAC regression algorithm processing. The large variations at low P_D for the BE-1900 and the C-402 example of Figure 7.2-1a can be discounted because of the small number of trials represented.

Third, it can be seen that a peak SNR of roughly 8 to 9 dB is required to achieve a P_D of 80% for most of these small aircraft target examples. This may seem large, but is comparable with conventional radar detection performance against a Swerling Case 1 target when noncoherent pulse integration is used.

The detection performance against the BE-1900 aircraft was found to be somewhat worse, requiring a SNR near 10 dB to achieve a P_D of 80%. This case requires additional analysis. Referring to the measured signature presented in Figure 3-4, the BE-1900 signature is composed of more small scatterers than either the BE-99 or C-402. In fact, the BE-1900 has only two major scatterers containing more than 20% of the RCS, whereas the C-402 and BE-22 have three. In this respect, the BE-1900 is more like the large aircraft signatures of Figure 3-3.

The target SNR for all of these examples was measured as the peak power to mean noise level, regardless of the number of individual scatterers present. Because the BE-1900 has two, rather than three, major scatters, there is actually one-third less total signal energy being processed than for the C-402 or BE-99 returns. Taking this fact into account, the detection performance as a function of total processed signal energy is roughly equal for all of these aircraft.

8.0 UWB SURVEILLANCE APPLICATION

This section presents an example UWB surveillance system to investigate typical detection performance levels and algorithm processing requirements. The example system is loosely based on the parameters of the S-band tracking radar at AFRL, which is not entirely ideal for this application. A bandwidth of 600 MHz (18%) is assumed, with an LFM waveform and real-time STRETCH processing similar to what was employed to measure UWB target signatures. The specific surveillance mission for purposes of this example is to detect low-flying penetrators that are below the conventional radar elevation coverage. The main L-band surveillance radar at AFRL has a wide, cosecant-squared elevation beam, with a gain that falls off near the horizon to reduce mainlobe clutter interference. The postulated UWB S-band system can fill in this gap in low elevation angle coverage.

8.1 System Parameters

The postulated S-band radar parameters are listed in Table 8.1-1. The elevation beamwidth of 0.8° is assumed to cover a sufficient elevation extent at the detection ranges of interest. If not, a wider beam or elevation scanning could be employed. The total number of azimuth beam positions over the full 360° azimuth coverage is 450. Thus the total scan period to acquire 8 pulses per beam at a nominal 250 Hz PRF is 450x8x4 ms or 14.4 sec.

It will be assumed for this application that STRETCH processing must be performed in real-time. Thus, a 2048 point FFT is performed once every 76.8 μsec in a front-end signal processor. These individual pulse-compressed (PC) outputs are then concatenated to cover the entire 100 km range swath of interest. This implies a processing rate of 1.5 GFLOPS, which is within the capability of some advanced processors. Note that a 2K FFT is required even

TABLE 8.1-1 POSTULATED UWB SURVEILLANCE SYSTEM PARAMETERS

S-Band Frequency	3.35 GHz
Azimuth Beamwidth	0.8°
Scan Period	14.4 sec
PRF	250 Hz (4 ms PRI)
Pulses Per Beam	8 (450 beams)
Waveform Modulation	LFM Stretch
Pulse Width	76.8 μsec
Bandwidth	600 MHz
Range Resolution	0.25 m
Range Swath	100 km
Transmit Power	100 KW
Antenna Gain	41 dB
System Loss	5 dB
Noise Figure	5 dB
Antenna Loss	2 dB

though only 1K complex data samples are acquired over the WB pulse length of 76.8 μsec at the 13.33 MHz ADC sampling rate. This is because 2:1 zero-filling is employed to smooth the range returns and thereby improve the peak centroiding and regression algorithm performance. Hanning weights are also applied to the received data in this processor and magnitude detection and thresholding could be performed here as well. These miscellaneous operations only slightly impact the signal processor requirements.

A more general purpose MTD processor is needed to perform multiple-pulse processing, including any clutter rejection prefiltering. For this purpose, the PC outputs from the front-end signal processor would be accumulated over eight pulses in a large memory buffer. Several parallel MTD processors could access this buffer to cover separate range regions. To guarantee that the entire target return falls within a single range region, the regions must be overlapped by one-half of the maximum target extent. The regression-based MTD algorithms would process an entire range region to declare a target detection. A convenient size for range might be 160m. Allowing for a 20m maximum target length, the spacing of these regions is then 150m.

Note that a target detection is declared for the entire 160m range region. However, the target range accuracy is almost always much better than this, because individual scatterers are resolved. More careful analysis can yield raid count information such as the number and spacing of aircraft flying in close formation.

8.2 Radar Detection Range

The radar range equation is next employed to predict the distance at which a small aircraft can be reliably detected with this system. The PAC regression algorithm requires roughly a 9 dB SNR for an 80% P_D. This produces a per-dwell P_{FA} of 10^{-6} for each range region where MTD takes place. For discussion purposes,

the clutter rejection prefiltering will be assumed adequate to provide this same level of CFAR performance.

A total of 450 azimuth beams and 667 overlapping range regions of 160m each are need to cover a 100 km range swath. Thus the P_{FA} of 10^{-6} results in 1.25 false alarms per minute. This is an acceptable rate for most applications. If not, additional coincidence detection and/or TBD algorithm processing can be applied.

A convenient form of the radar-range equation for UWB performance prediction is:

$$R_D = \left(\frac{P_T \tau G^2 \lambda^2 \sigma}{(4\pi)^3 SNR_1 \, kT_o \, NF \, L_S \, L_A} \right)^{1/4} \qquad (8.2\text{-}1)$$

where

P_T	=	Transmit Power	=	100 kw
τ	=	Waveform Pulsewidth	=	76.8 μsec
G	=	Antenna Gain	=	41 dB
λ	=	Radar Wavelength	=	.09 m
σ	=	Target RCS	=	1 m^2
SNR_1	=	Required Single-Pulse SNR	=	9 dB
kT_o	=	Noise Power Spectral Density	=	204 dB
NF	=	Noise Figure	=	5 dB
L_S	=	System Loss	=	5 dB
L_A	=	Antenna Loss	=	2 dB

The values to the right are estimated or measured quantities for the S-band tracking radar at AFRL. Note that the target RCS in this equation corresponds to that of the largest scatterer, because of the way SNR has been defined. The resulting detection range is 314 km (170 nmi) for a peak scatterer RCS of 1 m^2. However, the

RCS will be much smaller for LO aircraft and missiles. For a 0.01 m^2 RCS, the detection range is approximately 100 km. A surveillance sector of 100 km radius could thus be covered by this postulated UWB system.

For comparison with conventional radar performance, this is roughly the same detection range that can be achieved by a NB LFM waveform with the same uncompressed pulsewidth of 76.8 μsec, when 8 pulse noncoherent integration is employed. This can be seen by first replacing the required single-pulse SNR above with 12 dB to detect a Swerling Case 1 target. The RCS can then be roughly doubled to account for the vector summation of individual scatterers.

The advantage of UWB radar operation is that extended clutter is now resolved, and can thus be more readily rejected. The added system complexity and much greater processing requirements of a UWB radar may only be justified to detect stealth targets in a clutter-limited radar environment. Interestingly, AFRL is located in a valley where near-in (<30 km) conventional radar detection of conventional targets is presently difficult because of strong ground clutter returns. Finally, as there are no Doppler ambiguities, targets at all velocities can be detected by this UWB system.

8.3 Processing Requirements

This section compares the processing load for full-scale coherent and noncoherent integration, the PAC regression algorithm, and the hybrid regression/CDF technique. Only the MTD algorithm processing requirements are considered here. All of the algorithms have the same front-end STRETCH PC requirements and similar clutter rejection prefiltering needs.

On each dwell, detection processing must be performed for a total of 800K range sample cells, which are spaced by one-half of the 0.25 m range resolution due to interpolation. If a maximum, subsonic target velocity of ±300 m/s (Mach 0.9) is assumed, an individual scatterer could migrate over a total of:

$$300 \text{ m/s} \times N\text{-}1 \times PRI/\Delta R/2 = 67 \qquad (8.3\text{-}1)$$

range cells per dwell in either direction. Therefore some 800K x 67 x 2 individual lines of motion must be evaluated for full-scale coherent or noncoherent integration. Figure 8.3-1 illustrates one integration path over an 8 pulse CPI, and indicates the interpolated range sample cells.

For the regression processing estimate, most range cells are assumed to contain only receiver noise with a threshold setting of 6 dB relative to the mean noise level. The average number of isolated false alarm peaks per pulse is 7.3K. However, as receiver noise can be highly correlated between adjacent, interpolated range cells, centroiding is performed on any adjacent noise crossings. Thus the number of independent false alarm peaks per pulse is computed from the number of individual range resolution cells to be 400K. The average number of false alarm peaks within each of the overlapping range regions where detection takes place is then 93.8 or F=11.7 per pulse.

This quantity provides a means of estimating the number of candidate lines of motion that must be examined by the regression-based MTD algorithm. The total number of times, T, that a second noise peak will occur within the maximum target range migration window for the remaining pulses of a dwell can be computed to be T = 106.2K. This calculation involves the range window growth as a function of time, and the average density of noise peaks per range sample cell. These 106.2K events are divided among the R = 667 overlapping range regions to yield an average of A = 170 successful associations. Only a very small subset of these peak-to-peak associations will result in any additional peak alignments that might cause a false alarm output event. Furthermore, rank-ordering to use only the largest P = 4 peaks per pulse for association processing substantially reduces the number of successful associations. The reduction factor is P/F, if the P largest peaks in each pulse are compared against all other F peaks per pulse.

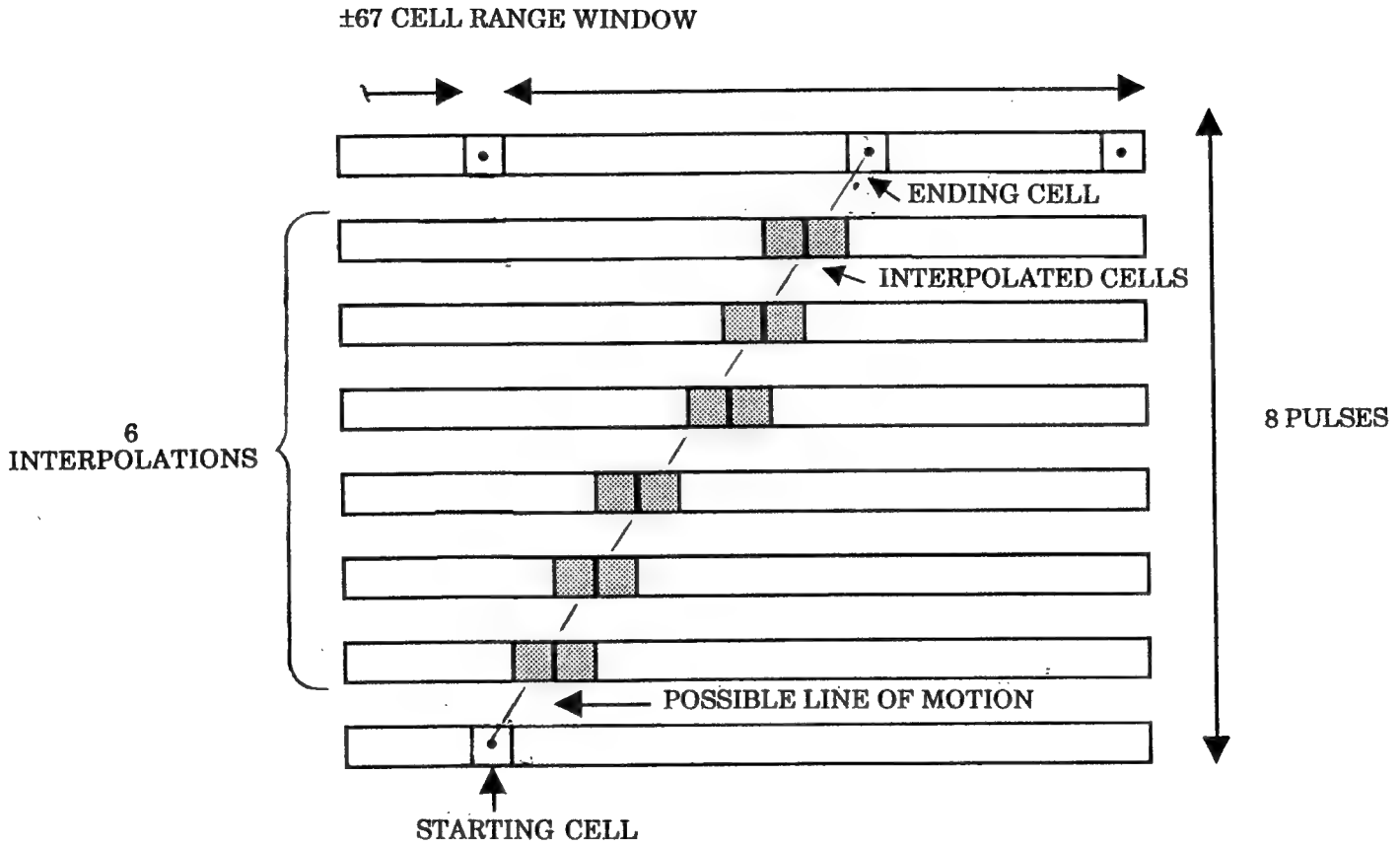

Figure 8.3-1 Coherent Integration Path

Thus, an average of only L = 58 lines of motion will be identified for the peak projection and alignment stages.

To quantitatively compare algorithms, several basic operation counts are listed in Table 8.3-1. Counts for regression algorithm functions, such as association and alignment tests, are estimates. In practice, these functions are highly dependent on the details of the algorithm implementation, e.g., whether it is programmed efficiently in machine language. It is also difficult to determine an exact operation count since the algorithm flow is highly dependent on the input radar data. For example, the shape and amount of clutter residue that leaks into the regression algorithm will effect the number of threshold crossings, and how many peaks per pulse must be compared. A detailed Monte Carlo simulation with a mix of clutter and clear conditions is required to obtain an accurate average operation count. The maximum operation count is also of interest, since without sufficient buffering capacity, the processor could not keep up with the real-time input data rate.

Table 8.3-1 contains notes explaining the regression operations, and how the counts depend on the false alarm statistics discussed above. Note that a linear regression is performed only for moving targets and false alarms that pass the detection logic.

8.4 Algorithm Comparison

Full-scale coherent processing first requires six complex interpolations for every possible line of motion, as indicated previously in Figure 8.3-1. This aligns the range returns in pulses 2 through 7 prior to 8-point FFT processing. The data on pulse 1 and 8 does not need to be interpolated since these range cells define the endpoints for each line of motion.

A total of 800K range cell starting points then exist on pulse 1 for the coherent FFT integration. Following the FFT, magnitude detection and threshold-

TABLE 8.3-1 BASIC OPERATION COUNTS

FUNCTION	OPERATIONS
Compare	1
Real Add or Multiply	1
Complex Add	2
Complex Multiply	6
Magnitude Detect	5
Thresholding	1
8-Point FFT (Including Hanning Weighting)	136
2-Point Real Interpolation	3
2-Point Complex Interpolation	6
8-Point Noncoherent Sum	7
Centroiding[1]	12 T
Rank Ordering[2]	P*(F-(P-1)*(P-2))*N*R
Association Tests[3]	P*F*P N*(N-1)/2*R
Projections[4]	2*(N-2)*L*R
Alignment Tests[5]	P*(N-2)*L*R
Linear Fit[6]	100

NOTES:

1. Compute centroid and average amplitude for T=58.6K total false peaks.
2. Find largest P=4 of F=11.7 false alarms per pulse in R=667 range regions.
3. Test P=4 largest peaks against F peaks from N-1 other pulses.
4. Project L=58 lines of motions into remaining N-2 pulses.
5. Perform alignment tests on P=4 largest peaks.
6. Regression analysis for detected lines of motion.

ing must be performed on each range-velocity filter output. For simplicity, integration of the distributed target scatterers is not considered. This yields a total of 23.6 billion operations per second, which represents a formidable processing requirement.

Noncoherent integration involves similar operations except that: 1) the interpolation is performed on magnitude detected data and, 2) the FFT is replaced by a sum. The number of thresholding operation is also reduced, since there are no separate Doppler filters to consider. The net number of operations is 2.8 billion, which is still a large processing requirement.

Unlike integration, where all of the range data must be processed, the PAC regression and hybrid algorithms operate only on threshold crossings. Magnitude detection and thresholding are first performed on the 800K range sample cells for a combined operation count of 38.4 MOPs. These highly parallel operations could be implemented in the high speed front-end processor at the same time as STRETCH PC.

The expressions in Table 8.3-1 are employed to estimate the processing load for the remaining regression algorithm stepswill require 3.1 MOPs. This represents a small fraction of the front-end processing load, but involves data dependent operations rather than parallel processing. Thus it must be implemented in a more general-purpose, high MIPS computer processor. The total processing count for the PAC regression algorithm is 41.5 MOPs, and considerably less than either coherent or noncoherent integration.

The slightly more sophisticated hybrid MTD algorithm employs the PAC algorithm as its first stage. A substantial increase in false alarm peaks will occur if a reduced threshold is applied so as to detect weak target returns. Alternatively, the detection threshold may be lowered so that a greater number of candidate lines of motions are output from the PAC regression stage to the CDF stage. A worst-case estimate of 100 such false alarm lines of motion per beam position is

assumed. Each of these will required linear regression analysis to find the best fitting line of motion. All 640 range sample cells of the 160m region are processed coherently for the identified line of motion. In this case, range interpolation must be performed for 7 of the 8 pulse returns. Finally, magnitude detection and thresholding are performed to test for the presence of a target. The additional number of operations for this CDF processing stage is 29 MOPs, for a combined total of 70.5 MOPs. Thus hybrid MTD processing involves only a modest increase from straightforward regression analysis.

In conclusion, the PAC regression and hybrid algorithms yield much lower processing requirements than either coherent or noncoherent integration for this example system. A 32 ms period is available in which to complete the entire MTD processing sequence. Table 8.4-1 contains a summary of the required processing rates for the various algorithms, and regression-based processing is most practical. The PAC and hybrid algorithm requirements of 1.3 and 2.2 GFLOPS are comparable to the front-end PC processing requirement of 1.5 GFLOPS. These front-end PC and MTD processing requirements pose a relatively small challenge to near-term UWB surveillance radar development.

TABLE 8.4-1 ALGORITHM PROCESSING REQUIREMENTS

PULSE COMPRESSION	1.5 GFLOPS
COHERENT FILTERING	737 GFLOPS
NONCOHERENT FILTERING	87.5 GFLOPS
PAC REGRESSION	1.3 GFLOPS
HYBRID PAC/CDF	2.2 GFLOPS

9.0 STUDY CONCLUSIONS

The achievements of this study include creating a UWB radar database, obtaining a better understanding of UWB target signatures, developing new MTD algorithms, and building advanced software tools to support further performance evaluations. This section briefly summarizes the conclusions reached by TSC in several areas during the course of this program. It also presents suggestions for further work in UWB data collection, algorithm development and real-time MTD processing experiments.

9.1 Target Signatures

The analysis of measured UWB radar signatures at S-band for small and large aircraft revealed a number of exploitable features for target detection. First, the overresolved target returns are composed of a few dominant scatterers that exhibit slow temporal fluctuations. The signal parameters associated with these returns remain relatively constant, and therefore predictable, on a pulse-to-pulse basis.

Second, the individual scattering peaks are spread over several range cells at the processed S-band waveform resolution of 0.5 m. There are also large gaps in the range returns between these peaks that contribute little to the RCS. The most efficient means of range integration is therefore to extract and sum only these scattering peaks.

Third, nearly all aircraft targets follow straight-line trajectories over short radar dwell periods. The scattering peaks associated with a moving target thus exhibit a linear range shift per pulse that is proportional to radial velocity. Multiple scatterers from the same target can therefore be readily identified.

9.2 Algorithm Investigation

A number of signal processing techniques have been investigated by TSC for detecting moving targets in UWB radar returns. The most promising of these involved regression analysis and hybrid methods.

Regression algorithms were found to reliably detect small targets at a SNR of 8 to 9 dB for modest, 8-pulse processing. A performance reduction of 3 to 4 dB from conventional radar target detection occurs because the resolved scatterers exhibit a lower RCS than the aggregate value. This is somewhat compensated for by their Swerling Case 0 statistics. However, it is extremely difficult to detect moving targets much below a single scatterer SNR of 6 dB. It is assumed that MTI prefiltering has reduced the clutter to an acceptable level.

The hybrid regression/CDF algorithm developed by TSC offers the best performance for a marginal increase in processing. In this approach, the regression algorithm first identifies candidate lines of motion among the scattering peaks so that weaker target returns can be coherently integrated. A further performance gain is achieved with hybrid processing by reducing the first signal threshold so that weaker target returns are found in the first regression stage. The coherent processing gain, which does not apply to noise or clutter, can then boost the weak target signal to a point sufficient for reliable detection. Furthermore, the alignment of all scatterers in a single Doppler bin provides a means of integrating the entire range-spread target return.

Clutter interference is effectively reduced at high resolution because extended clutter returns break up into a distribution of discretes. These discretes can cause a significant number of false alarms unless eliminated early in the processing sequence. MTD algorithms, particularly those based on regression analysis, must therefore be preceded by some form of clutter rejection prefiltering.

The MDLC algorithm developed by TSC exploits the pulse-to-pulse range shift of moving target returns to suppress such clutter. Clutter measurements are now needed to validate this technique.

The clutter residue from periodic distributions of discretes such as man-made objects, e.g., fences, railways, parked cars, etc., presents the greatest challenge to regression-based algorithms. Such clutter could cause frequent false alarms, particularly at low CNR, since they result in signal patterns not unlike a weak, moving target return. Knowledge-based techniques to eliminate such instances of clutter should thus be investigated.

9.3 Recommendations for Further Work

Additional work in several areas is recommended by TSC. First, additional Monte Carlo computer simulations are needed to quantify detection and false alarm performance in the presence of clutter interference. If valid results are to be obtained, this will require additional UWB clutter measurements to refine the present clutter models. A parametric characterization of clutter rejection and MTD algorithm performance can then be completed. Performance sensitivities to radar parameters including transmit frequency, PRF, and CPI under various clutter conditions also need to be established. Most of these sensitivity studies will require additional radar measurements or and/or much more detailed simulation models.

The second major area of work involves a real-time implementation of the most promising MTD algorithms developed to date. This would support the experimental validation of the new techniques, as well as direct performance comparisons with conventional radar waveforms and processing. Such comparisons are best conducted by using an interleaved WB/NB waveform, much like the AFRL S-band radar now employs. In this way, the same target signal and interference conditions are present in both detection channels. This interleaved approach

also permits ideal waveforms to be used in each case, rather than artificially reducing the bandwidth through post-processing. Any difference in the transmitted energy for the two waveforms must, of course, be considered for performance analysis.

Besides experimental testing, real-time implementation offers high speed processing for more efficient algorithm evaluations against simulated and/or already recorded UWB data. The algorithms can be implemented on either the STAR-100 array processor or the new SKYbolt processor that is attached to the SUN SPARCserver 470 at AFRL. The hybrid regression/CDF algorithm, which includes both rule-based and numeric processing, is ideal for such real-time implementation since it runs relatively slowly on the general-purpose VAX computer. Many aspects of this hybrid processing method could then be more efficiently investigated. These include MEM Doppler filtering, the integration of range-distributed target scatterers, and iterative velocity unfolding methods.

Hybrid MDLC/CDF methods that avoid regression-analysis altogether should also be pursued. Because artifacts are introduced by prefiltering, integrated clutter rejection and MTD algorithms are preferred. Several novel processing techniques that could not be pursued during the course of this brief study may offer suitable integrated algorithms. These include ANNs and morphological filtering (MF).

MF is an image processing technique that has been applied to detect target tracks in conventional radar data under AFRL sponsorship [8]. The method uses simple neighborhood operations to enhance certain patterns in the raw or thresholded range-azimuth returns versus scan time. Target tracks show up as linear traces in the resulting 3-D data. Knowledge of aircraft kinematics is then exploited for detection. Similar 2-D traces can be observed when UWB range returns are plotted as a function of pulse time.

9.4 Data Collection

A comprehensive UWB data collection effort is recommended. This effort would extend the present UWB database that is now limited to a few commercial aircraft targets of opportunity. To support this experimental work, the S-band tracking radar at AFRL has recently been upgraded to 640 MHz. This represents a 20% bandwidth, which is reasonable for a near-term UWB surveillance radar. As discussed above, the first collection priority should go to clutter measurements of urban areas and man-made objects that present the greatest challenge to clutter rejection algorithms. Dual polarization signatures should also be collected, since polarization offers one potential means of discriminating target returns from clutter.

Radar signatures of additional military and commercial aircraft targets of opportunity should also be collected at 640 MHz. For example, the helicopter squadron assigned to Griffiss AFB offers a target class of particular interest to some UWB surveillance applications. It could easily be arranged for one or more of these helicopters to fly at low speed just above the trees. This would provide valuable data for evaluating combined clutter rejection and MTD algorithms under realistic operating conditions.

More carefully planned flight tests with military and/or rented private aircraft could also contribute to a better understanding of UWB scattering phenomonology. In such tests, ground truth is available so that exact range, aspect angle and ground speed are known. This would permit calibrated RCS measurement of the individual target scatterers.

Finally, the question of what minimum bandwidth is sufficient to achieve a desired performance level must be addressed. To answer this question, data at several different bandwidths can be collected using the AFRL S-band radar. Post-processing, in the form of low pass filtering, to reduce the effective bandwidth can then be used to roughly interpolate between the different measurements. Once

a satisfactory operating bandwidth is defined, predictive algorithms involving AR modelling can be explored to compensate for further reductions in the transmitted waveform bandwidth. In this way, the absolute minimum UWB requirement can be defined.

10.0 REFERENCES

1. Ultrawide Bandwidth Linear FM Waveform Analysis Final Report, TSC, AFRL Contract No. F30602-88-R-0066, August 1990.

2. Real-Time Multisensor Algorithm Experiment Final Report, TSC, RL-TR-91-76, August 1991.

3. Adaptive Multiband and Ultra Wide Band Polarization Canceller Research Proposal for Ph.D. Dissertation, Mr. C.J. Lee, Syracuse University, August 1991.

4. Radar Siting System Functional Description, TSC, B52-0634, May 1991.

5. High Resolution Radar, Donald Wehner, Artech House, 1987.

6. Ultra Wideband Techniques Final Report, TSC, Subcontract No. P44549 to Kaman Science Corporation, November 1991.

7. Track-Before-Detect Development and Demonstration Program Phase II Final Report, TSC, AFRL Contract No. F30602-84-C-003, November 1985.

8. Knowledge-Based Target Tracking Final Report, Atlantic Aerospace Electronics Corporation, AFRL Contract No. F30602-87-D-0153, December 1989.

PHASE II, VOLUME II

TECHNOLOGY SERVICE CORPORATION

FINAL TECHNICAL REPORT

AIR FORCE ROME LABORATORY
CONTRACT NO. F30602-91-C-0035
SYRACUSE UNIVERSITY
SUBCONTRACT NO. 352-1272

Abstract

A unique concept for UWB radar operation is presented. Advantages of the postulated concept are described. An innovative, computationally efficient signal processing technique utilizing wavelet transforms that has been developed by TSC is discussed. An example is presented in which actual UWB data that has been interpolated to simulate a high-PRF waveform is processed to validate the concept. A demonstration concept for the postulated UWB modulation is proposed.

AN ULTRAWIDE BANDWIDTH (UWB) HIGH-PRF RADAR CONCEPT

1.0 Introduction

The use of a high-PRF waveform is very desirable for both airborne and ground-based radars. Because the high-PRF has no blind velocities and few ambiguous velocities, it is possible for the radar to readily discriminate between low-observable (LO) targets and returns from such things as birds, insect swarms, and ground moving targets, based on their Doppler frequency. Also, a radar using a high-PRF waveform can achieve an adequate average power level without utilizing an extremely long transmit pulse, and hence not have an unacceptably long minimum detection range.

Although the E-3 AWACS radar has successfully used a high-PRF waveform, neither ground-based radars nor the sensors being considered for ADI applications favor this concept. In the case of the ground-based radar, a low-PRF waveform is most commonly used. This is because the high-PRF causes the return from the near-in clutter to be very large, which in turn both requires a very large dynamic range and masks LO targets.

The ADI radar concepts, on the other hand, are favoring active array designs and medium-PRF waveforms. Such active arrays have significantly higher antenna sidelobes than the E-3, due to the module-to-module amplitude and phase variations, and must resort to adaptive space-time processing to suppress the sidelobe clutter. This processing requires a large number of accurately balanced receiver channels and the use of powerful signal processors to form and invert the covariance matrices necessary to cancel the clutter return. The increased clutter return for a high-PRF waveform, coupled with the computational difficulties that result from the reduced number of range gates, make a high-PRF waveform impractical for detecting low velocity targets that compete with the sidelobe clutter returns.

2.0 The UWB High-PRF (UWB/HPRF) Waveform Concept

The high-PRF waveform limitations described above are predicated on the use of conventional surveillance radar bandwidths (e.g. 1 to 10 MHz). Suppose, however, that the waveform had a bandwidth on the order of 500 to 1000 MHz. Because of the very high range resolution, from 20 to 30 dB of clutter rejection could be achieved as a result of the reduced clutter cell area. This should be sufficient to allow the high-PRF waveform to be used in ground-based surveillance radar applications, and also to detect LO targets from an airborne platform, either with a much reduced or possibly without any adaptive array processing requirement. The high-PRF waveform could serve as the primary modulation for the radar, as a war-reserve mode, as a waveform that is interleaved with a conventional pulse (i.e. a combination analogous to the AWACS pulse-Doppler and beyond-the-horizon waveforms), or as a waveform to be used in sectors for which severe clutter and/or jamming might exist.

An advantage of the UWB modulation is that the radar should be readily able to resolve range ambiguities with only two unique PRFs, due to the large number of range gates that will be formed. Additionally, the UWB modulation could minimize the range eclipsing loss that exists for high-PRF waveforms if impulse-like pulses are transmitted. Other advantages of this waveform are that: 1) it will reject multipath returns for most geometries through time-gating, 2) it can provide immediate NCTI data through both radar signal modulation (RSM), possibly even range-resolving the individual compressor blade lines of an engine, and high range resolution (HRR) target profiling techniques, and 3) it should have an LPI/ECCM advantage, due to its wide bandwidth.

The parameters of the UWB/HPRF waveform envisioned by TSC for a UWB/HPRF waveform are as follows:

Bandwidth	0.25 to 1.00 GHz
Range Resolution	0.15 to 0.60 m
PRF	

L-Band	8 to 12 kHz
S-Band	25 to 30 kHz
X-Band	70 to 100 kHz
Pulse Length	
Pulse Compression	0.5 to 1.5 μsec
No Pulse Compression	1.0 to 4.0 nsec
Coherent Processing Interval	5.0 to 20.0 msec

As will be explained in the following section, it is desirable to ensure that from 2 to 5 pulses are obtained within a range gate at the highest target velocity to provide the ability to reject mainlobe clutter by MTI and/or Doppler filtering.

3.0 UWB/HPRF Waveform Signal Processing

The classic signal processing problem for UWB waveforms is that the target can traverse many range gates during a dwell time. As a consequence, rejecting clutter without degrading the signal-to-noise ratio (SNR) becomes a very difficult task. For example, if N-pulse MTI filtering is performed and the target is only present in the range gate for one of the N pulses, N-1 noise samples are added to the single target pulse, and the SNR will be degraded. If, however, the Doppler filter is matched to the target's velocity, matching its return as it traverses range gates, the clutter from a single range gate becomes impulse-like and is not rejected.

Recognizing this problem, TSC has developed a computationally-efficient technique that both rejects the ground clutter and provides the maximum coherent integration gain for all of the target returns from within a single range gate (i.e. neither a collapsing loss from too long an integration time nor a mismatch loss from too short an integration time will occur). The key to this technique is to provide at least two pulse returns (and preferably 3 to 5) in any range gate for the maximum target velocity for which the radar is designed.

The time for which a target return remains in a single range gate, T_G, is given by the equation:

$$T_G = \Delta R/V_R \tag{3.1}$$

where ΔR is the range resolution and V_R is the radial velocity of the target. Hence if ΔR is 0.25 m and V_R is 100 m/sec, then T_G is 2.5 msec. The bandwidth of the Doppler frequency for this target, ΔF_D, is the inverse of the time the target remains in the range gate. Hence:

$$\Delta F_D = 1/T_G \tag{3.2}$$

For the above example, ΔF_D is 400 Hz. Note that the Doppler bandwidth is independent of the radar frequency.

The Doppler frequency of the target return, F_D, is given by the equation:

$$F_D = 2V_R/\lambda \tag{3.3}$$

where λ is the radar wavelength. At S-Band, where λ is nominally 0.1 m, the target in the example would have a Doppler frequency of 2000 Hz. Finally, the Q of the Doppler filter matched to a target is given by the equation:

$$\begin{aligned} Q &= F_D/\Delta F_D \\ &= (2V_R/\lambda)(\Delta R/V_R) \\ &= 2\Delta R/\lambda \end{aligned} \tag{3.4}$$

Thus the Q of each filter is a constant, independent of the target's velocity. This is in contrast to the filters formed by techniques such as the fast Fourier transform (FFT), which increases in direct proportion to the Doppler center frequency of each

filter. Thus for the above example, a filter with a Q of 5 will always be optimal for the given range resolution and wavelength.

Finally, the Doppler-spread factor, caused by the variation in the wavelength, λ, across the UWB pulse must be considered. Because the wavelength changes significantly over the UWB pulse, the Doppler frequency spread will cause significant signal processing problems. Note, however that:

$$\begin{aligned} \Delta F_D &= 2V_R(F_{MAX} - F_{MIN})/c \\ &= 2V_R(BW)/c \\ &= V_R/\Delta R \end{aligned} \tag{3.5}$$

where

F_{MIN} = Lowest frequency within the pulse spectrum
F_{MAX} = Highest frequency within the pulse spectrum
BW = Pulse bandwidth

It is noted that Equation 3.5 is identical to the result obtained by combining Equations 3.1 and 3.2. Thus the constant-Q Doppler filter formed by the wavelet transform is seen to be matched to the Doppler-spread of the UWB target return.

The fact that constant-Q filters are well suited to processing the UWB/HPRF waveform allows a new and innovative area of signal processing to be applied: the wavelet transform [1]. Figure 3.1 presents a bank of constant-Q filters formed by using the Morlet wavelet. As can be seen, the filters having low Doppler center frequencies, i.e. the filters which would be matched to slowly moving targets, are quite narrow, which allows them to reject ground clutter. These filters also provide a large integration gain, as the target will remain within a single range gate for a relatively long time. In contrast, the high Doppler center frequency filters are quite broad, allowing them to respond to high-velocity targets. These filters will also be effective for rejecting stationary and low-velocity clutter, due to the large

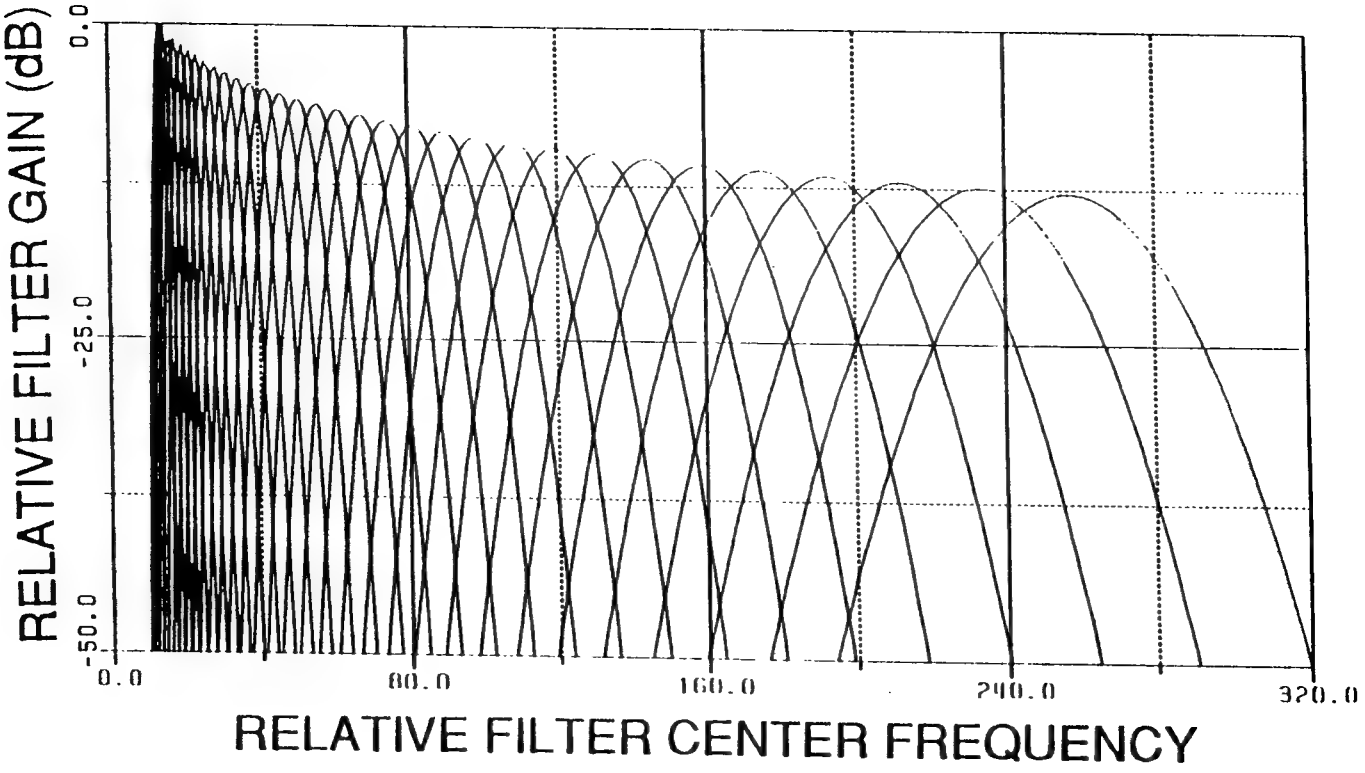

Figure 3.1 Wavelet Filter Bank (32 Filters)

Doppler frequency separation.

The wavelet filtering concept thus provides nearly optimal one-dimensional processing of the target return. All of the signal energy from within a single range gate can be coherently combined, and the clutter can be effectively rejected by either the filters alone or by a cascade of an MTI filter and the wavelet transform. A fast algorithm for performing the wavelet filtering will be presented in the following section. The combination of the signal return for the multiple range gates which the target traverses during a radar dwell will be discussed in Section 5. This combination is necessary to achieve the SNR necessary to detect a LO target.

4.0 Fast Wavelet Processing Algorithm

Unlike the FFT, which efficiently forms constant-width Doppler filters, the wavelet transform must form constant-Q Doppler filters. Fast wavelet algorithms have been described in the literature; however these were found to be unsuitable for the UWB/HPRF waveform application, as they were designed for real (as opposed to complex) data, and as they only allow a filter Q value of two to be used.

The transform that TSC has initially tested is based on the Morlet wavelet, which is of the form:

$$w(t) = \gamma \exp\left(-\frac{1}{2}\gamma t^2\right) \exp(j\gamma g t) \tag{4.1}$$

where γ is the dilation factor and g is the modulation factor. The set of wavelets described by Equation 4.1 (i.e. one for each Doppler center frequency) can be applied to the received radar data in the following manner:

1. Form the FFT of all samples from a coherent dwell.
2. Apply each wavelet by multiplication in the frequency domain.
3. Zero all Doppler filters beyond nominally $\pm 2\Delta F_D$.
4. Form the (smaller) inverse FFT for the truncated data.

The algorithm gains efficiency because only one large forward FFT is required, and the inverse FFTs are, on-average, much shorter. This algorithm also automatically decimates the data rate to a level consistent with the bandwidth of each Doppler filter's output. The decimated data rate is nominally $4/T_G$.

It should be understood that a fundamental difference exists between conventional, narrow band FFT processing and UWB wavelet processing. This is that each Doppler filter formed by an FFT will produce only one output per range-Doppler cell during a coherent processing interval (CPI), while the number of decor-related outputs produced by a wavelet filter during a CPI will equal $\Delta R/V_R$. Thus the low- velocity wavelet filters will only produce a few independent output samples for each CPI, while the high-velocity filters can produce many tens of independent output samples. Also, while the filter (or window) function that is applied to the data is of fixed length for all of the Doppler filters formed by an FFT, its length is inversely proportional to the Doppler center frequency for each wavelet transform filter. These factors restrict the computational efficiency that can be achieved by a wavelet transform.

Figures 4.1 and 2 illustrate how the wavelet filter function is applied to the data for a target that moves through range gates as a function of time and how the sign output evolves over time. In this example a 100 m/s velocity target, which has a Doppler frequency of 2000 Hz, traverses four range gates during the CPI. The amplitude window for each range gate that is applied to the data in the time domain by the algorithm is seen to move to the right to match the target's range migration. Figure 4.2 illustrates how the wavelet processed data peaks in time as the target moves through the range gates.

The deterministic relationship between the target's radial velocity and Doppler frequency allows the processor to correctly associate the amplitude peaks for each gate. In this example for a 2000 Hz Doppler frequency, the peak is shifted by 50 time samples per range gate; thus samples S(R,T), S(R + 1, T + 50), S(R + 2, T

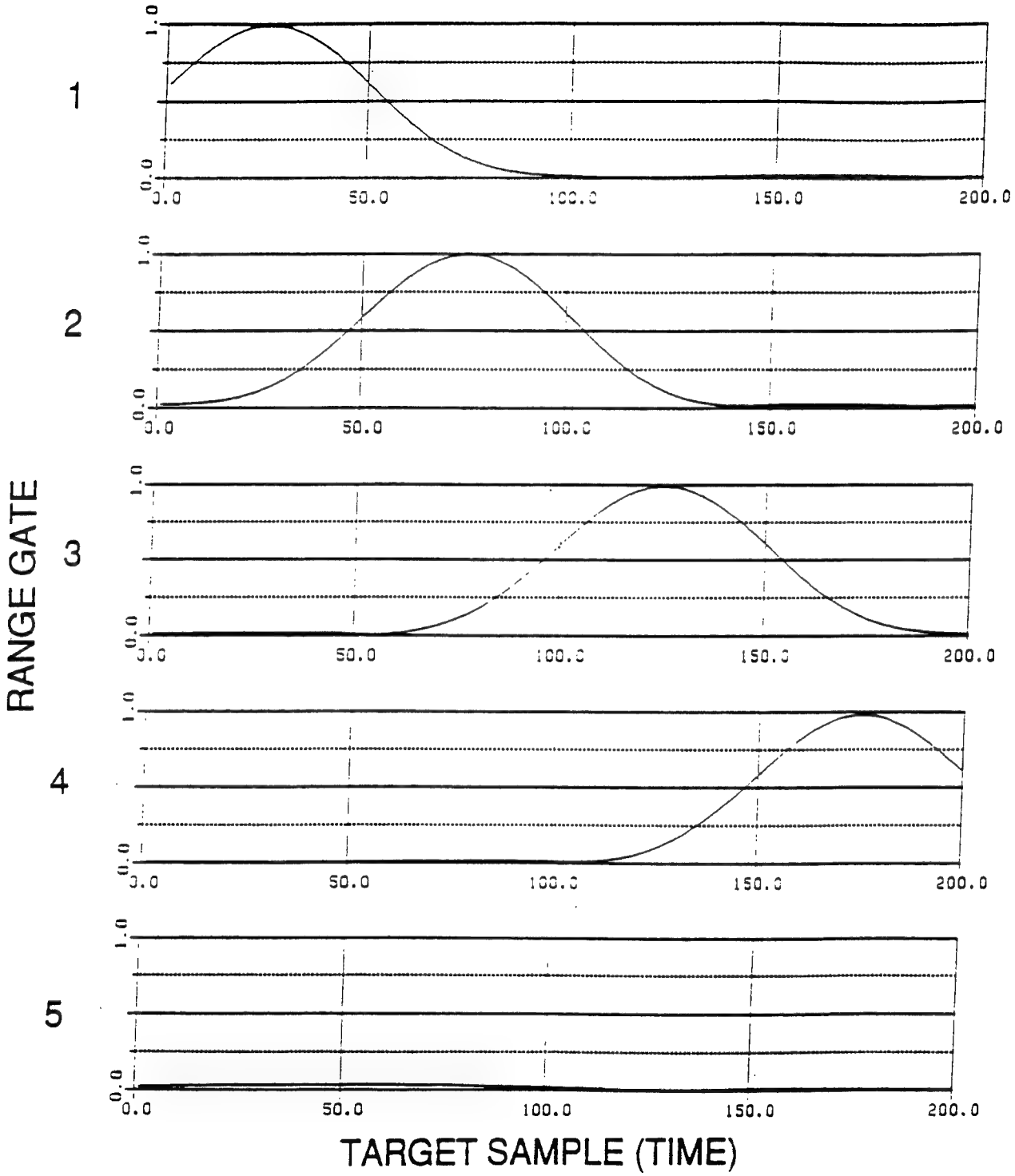

Figure 4.1 Wavelet Filter Function Versus Time

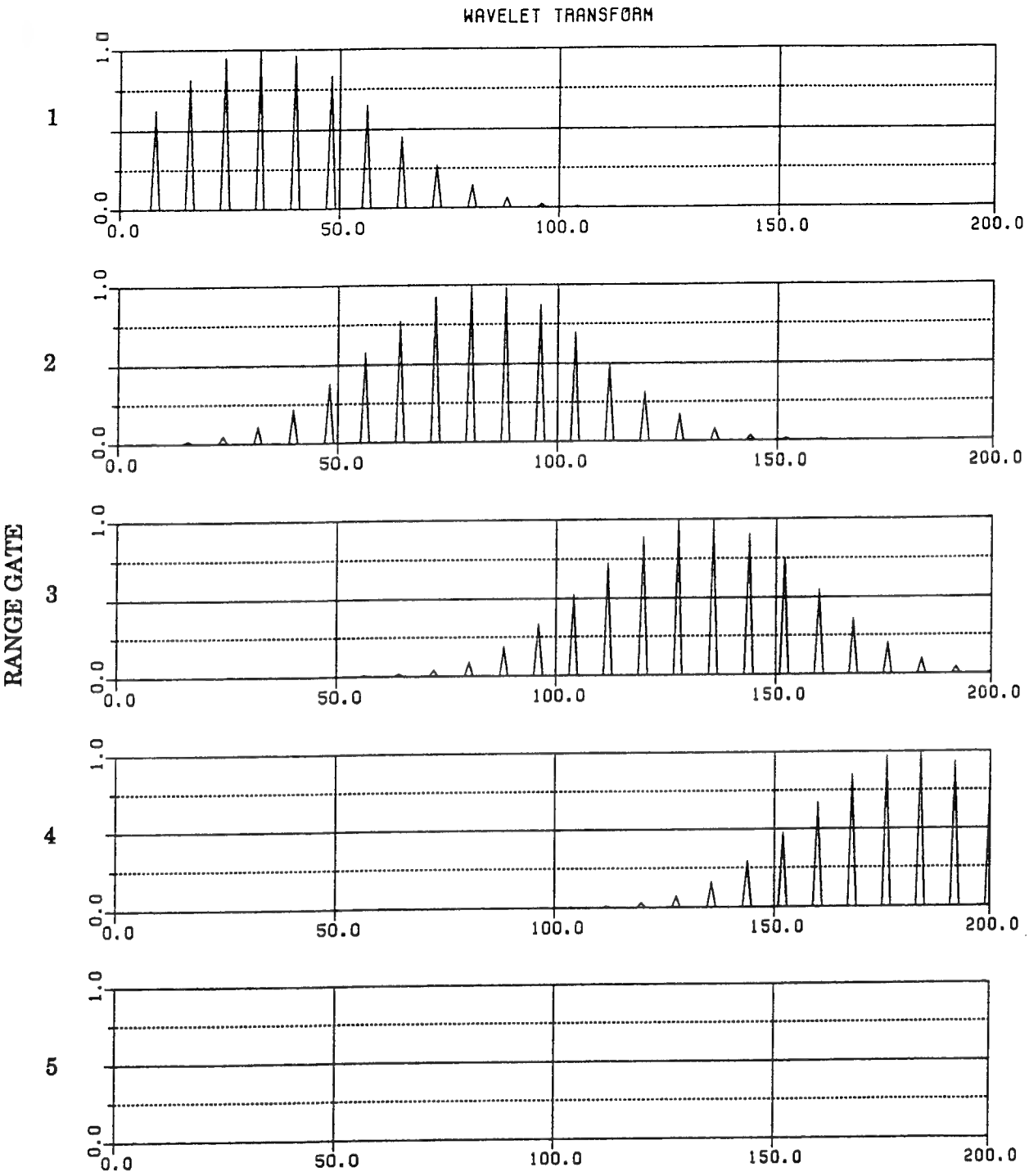

Figure 4.2 Signal Response Versus Time

+ 100) and S(R + 3, T + 150) would be combined after the wavelet processing, where R is the initial range gate number and T is the initial time sample number.

Figure 4.3 illustrates how the wavelet filters of different Doppler frequencies respond for a particular range gate, which in this case is Range Gate 3 from the previous example. It is readily apparent that the filtered response for Range Gate 3 peaks at the appropriate time (i.e. sample number 125), and that the magnitude of this response is significantly greater in the Doppler filter centered at F_D = 1934 Hz than in the adjacent Doppler filters. The filters have been designed to overlap at their 3 dB points, and hence there is a noticeable target response in the adjacent Doppler filters. For filters further away from the one centered at 1934 Hz, the Gaussian weighting of the wavelet significantly attenuates the target response, which provides effective pulse-Doppler processing.

5.0 Multiple Range Gate Target Return Processing

Because of the high range resolution, a target can conceivably traverse many tens of range gates during a CPI. However, due to the design of the UWB/HPRF waveform, no gaps can exist between the range cells containing the target return, i.e. all data samples are sequentially obtained from contiguous range gates. Additionally, as has been shown in previous TSC work, for the typically short time duration CPI, the target's velocity will be essentially constant, even during high-G maneuvers. Therefore a number of techniques exist for combining the signal energy from each individual target scatterer. Finally, as there is a deterministic relationship between the target's Doppler frequency and its range migration within a CPI, the number of range gates that are traversed and the time between the decorrelated output samples of the wavelet filters which perform the coherent integration will be known. These factors will allow the efficient combination of the multiple range gate data.

The maximum SNR can be achieved through coherent integration. The outputs of the wavelet filters at the same Doppler center frequency for the consecutive

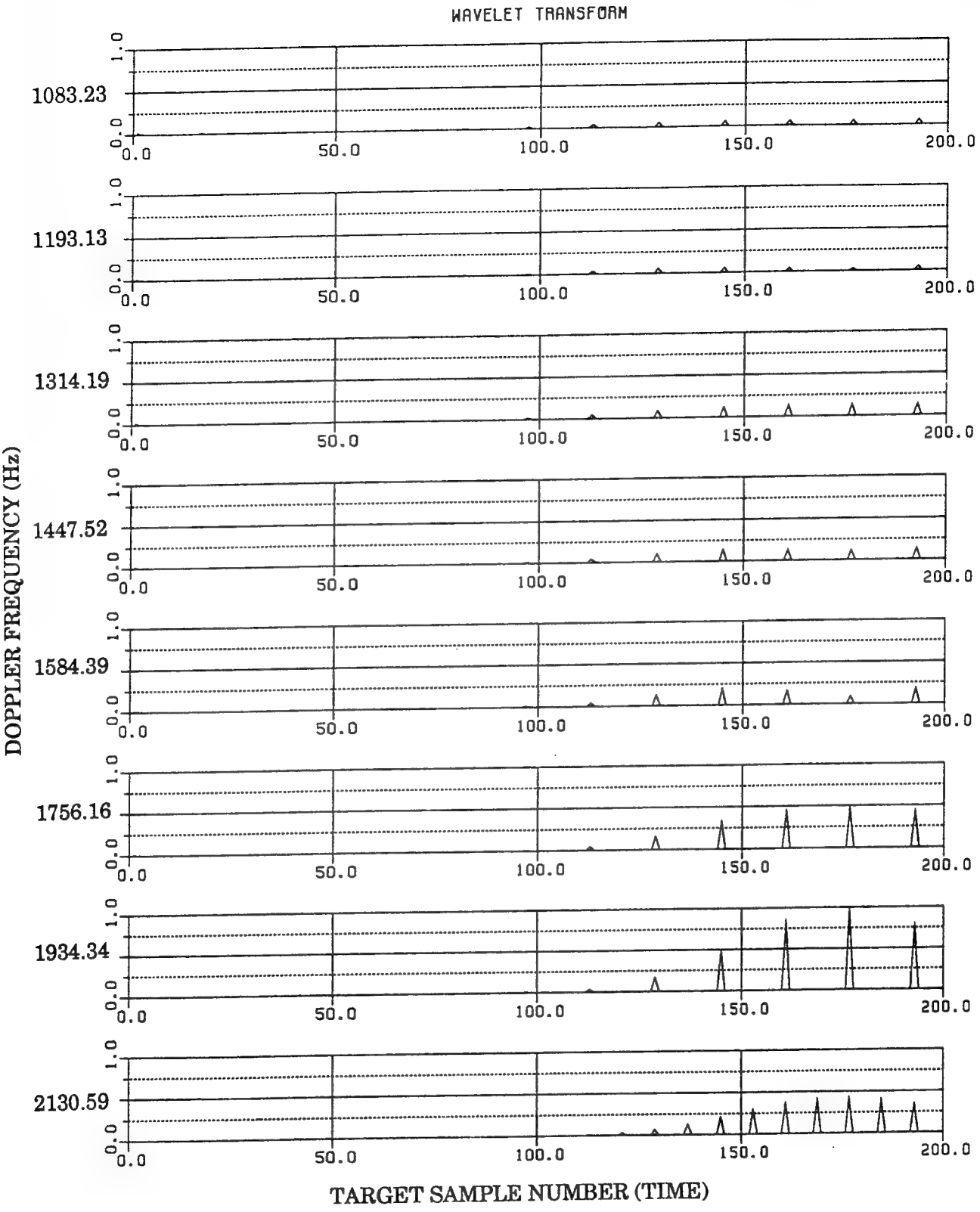

Figure 4.3 Wavelet Transform (Range Gate 4)

range gates traversed by the target will be phase coherent. Therefore a sliding window Fourier transform could be performed over the range dimension for each wavelet filter's output. Only one output sample is required from each range gate within the sliding window. The window must slide because the initial range to the target is unknown.

A Fourier transform is necessary because a difference of only $\lambda/2$ in the range traversed by the target during a CPI will induce a 360 degree phase rotation over the signal return. Therefore a significant number of different Doppler frequencies may have to be processed for each set of wavelet transform output data within the sliding window. An FFT would probably be the most efficient computational technique for performing this operation.

If the window slides by one range gate per FFT, there will be virtually no processing loss due to range mismatch; however, the signal processing requirements will be quite large. If the window is allowed to slide by as much as 50% of the target migration distance (i.e. by half the number of range gates within the window), the loss will be 3 dB; however, the signal processing requirements will be much less.

For example, consider a radar having a wavelength of 0.1 m, a range resolution of 0.25 m, and a CPI of 10 msec. The wavelet filter Q value will be 5; hence a Doppler filter centered at 20,000 Hz will have a bandwidth of 4000 Hz. Target velocities of 900 to 1100 m/sec will fall within the 3 dB width of this filter. Therefore a target whose Doppler frequency falls within this filter could traverse from 36 to 44 range gates within a CPI, and produce from 180 to 220 cycles of Doppler. The wavelet filter processing would be matched to 200 cycles of Doppler, leaving a residual of ± 20 cycles over a 40 range gate window. The signal processor could therefore perform a 64-point FFT on the 40 data samples from these range gates to achieve nearly the maximum coherent integration gain.

Although optimal, such coherent processing is computationally very intensive. An alternative approach is to use TSC's hybrid regression algorithm (HRA). This sequential-detection technique applies a first-threshold to the outputs

of each Doppler filter, and then performs M-of-N processing over the contiguous range gates. The range gates that are used for this process are the same as would be in the sliding window described above, only now much simpler processing is being performed. As explained in Reference [2], a detection can either be declared directly from the target traces identified by the HRA (e.g. meeting an M-of-N criterion for one scatterer, or for two scatterers that are displaced in range but which are at the same Doppler frequency), or the HRA can be used to cull the data so that coherent processing is performed only at locations for which possible target returns are detected.

TSC has shown that the HRA technique can reduce the processing requirements by several orders-of-magnitude with only a small decrease in detection performance. Additionally, the increased SNR provided by the wavelet filtering should improve the results that have been previously reported for the HRA by TSC.

6.0 Concept Validation

To validate the wavelet processing concept, TSC first synthetically generated a high-PRF, UWB radar signal. The eight pulse returns of 320 MHz bandwidth, 250 Hz PRF, 640 MHz sampling rate data shown in Figure 6.1 were collected using the Air Force Rome Laboratory S-band radar. TSC time-shifted and interpolated the data to effectively create a scenario in which a target that is traveling at 156 m/s is sampled by an UWB radar with a 20 kHz PRF, as is shown in Figure 6.2 for every 20th pulse return.

In the scenario that TSC created there are 400 radar pulse returns. The range gates are spaced by 0.25 m. As the radar burst duration is 20 msec, the target will traverse 12.5 range gates during the burst duration. The 0.5 m range resolution results in nominally 64 target samples per range gate.

Figure 6.3 illustrates the output of the wavelet processor for the Doppler filter containing the target. To generate this figure, a threshold 3 dB below the

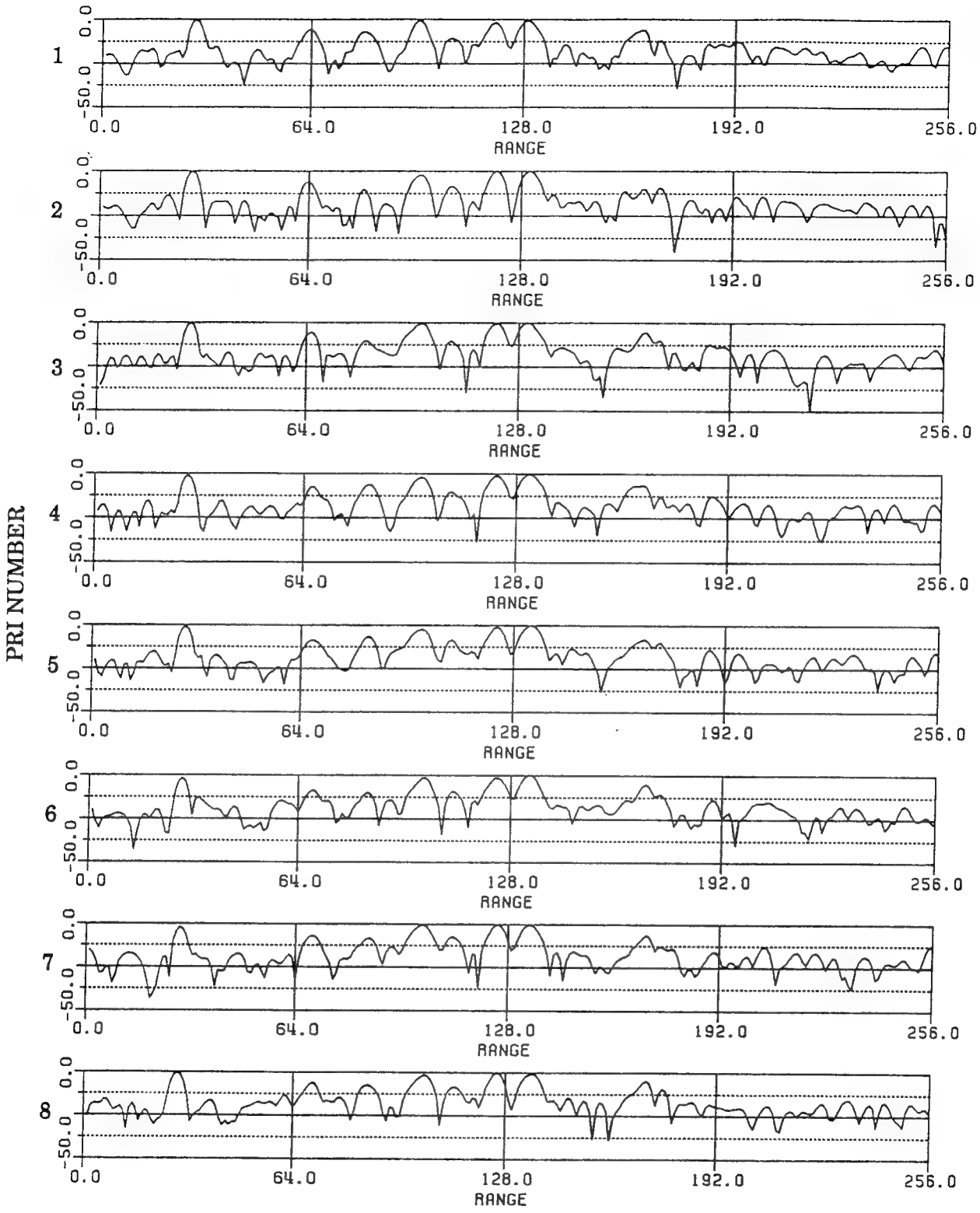

Figure 6.1 Input Data for Wavelet Processing Validation (PRF = 250 Hz)

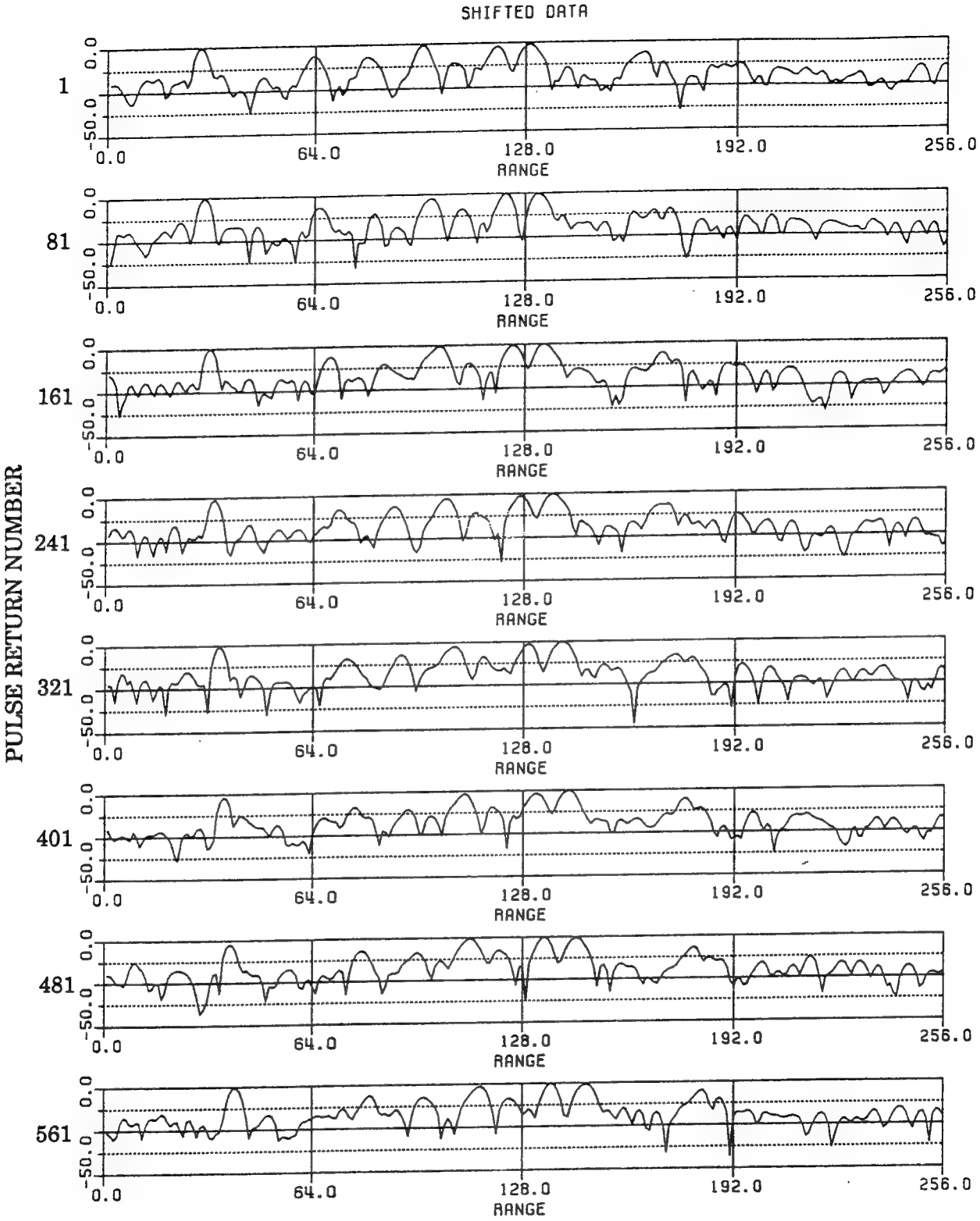

Figure 6.2 Time-Shifted Data to Create High-Velocity Target

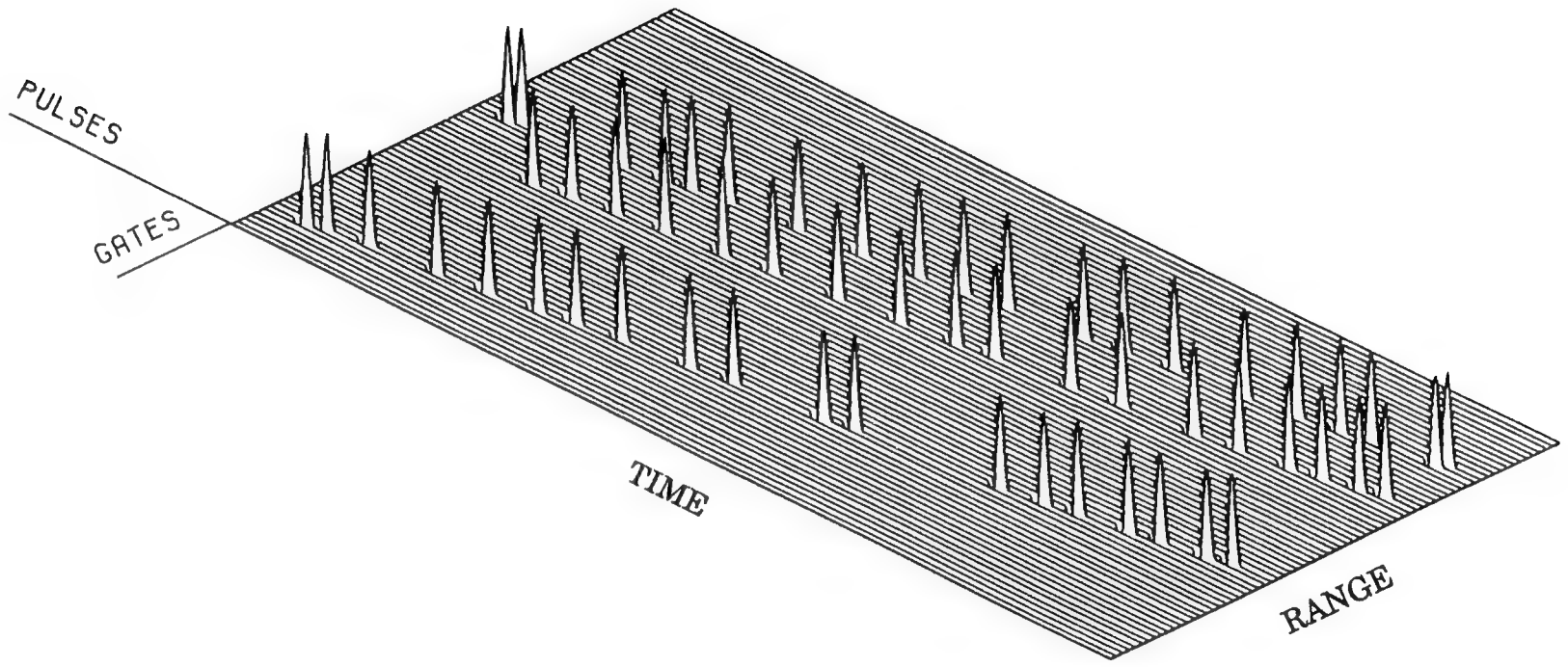

Figure 6.3 Wavelet Processed High-PRF UWB Radar Data

peak target response was used, and the centroid of all time-sequential threshold crossings within each range gate was created. The range versus time progression of the dominant target scatterers after wavelet processing is clearly evident in this figure. Note that some data drop-outs occur for the weaker scatterers.

The linear relationship between the pulse return number and the range gate containing the centroid is readily apparent in Figure 6.3. The HRA described in the previous section would readily detect and associate the three dominant scatterers that are present in this figure. Thus TSC is highly encouraged that the wavelet processing technique will be an effective technique for high-PRF UWB radar processing.

7.0 Conclusions

The UWB/HPRF waveform is potentially a very viable concept for both ground-based air surveillance and AWACS radars. Its signal processing requirements are intensive; however, algorithms have been identified that appear to be compatible with state-of-the-art signal processors. As the use of the UWB/HPRF waveform could reduce or eliminate the large number of parallel receiver channels and the extremely powerful signal processors required for the space-time processors being considered for ADI airborne radars, TSC feels that additional research and experimentation is warranted in this area.

8.0 Demonstration Concept

TSC believes that the UWB/HPRF waveform concept should be carried forward into an experiment. A ground-based radar is recommended for initial testing. The test location should provide a variety of clutter conditions (e.g. urban, rural, hilly-terrain) to test the robustness of the UWB/HPRF concept.

It would be desirable that the test radar system be capable of producing a pulse bandwidth on the order of 250 to 1000 MHz, a pulse width in the range of 0.1 to 10.0 μsec, and a PRF of 5 to 20 kHz. A pulse-burst waveform could be used in

regions where the clutter horizon was equal to only a few range ambiguities.

It would not be necessary to process the data in real-time. Therefore either a high speed waveform digitizer or a very fast ADC and a high speed data buffer could be employed. All pulse compression and Doppler processing could be performed off-line.

The validation would require both a test target and flight testing. The test target must produce the Doppler frequency and range migration necessary to validate the algorithm. This could be done by scaling the PRF so that a low velocity target can be utilized. The flight testing would use the actual parameters.

The demonstration program could provide much valuable data, including the UWB characteristics of target returns, the statistics of clutter returns, and the validation of the signal processing concept. This data would supplement that which was previously obtained and reported on in Reference [2].

The initial tests would be limited in their scope, but would provide significant data of a relatively low cost for assessing the performance of the UWB/HPRF waveform and determining whether it warrants further investigation.

9.0 References

1. Rioul, O. and Vetterli, M., "Wavelets and Signal Processing," IEEE Signal Processing Magazine, Oct. 1991.

2. Moyer, L. and Corbeil, A., Ultra Wide Bandwidth Radar Detection Algorithm Analysis and Demonstration Program, Phase 1, Final Technical Report, Contract No. F30602-91-C-0035, April 1992.

Rome Laboratory

Customer Satisfaction Survey

RL-TR-_____

Please complete this survey, and mail to RL/IMPS, 26 Electronic Pky, Griffiss AFB NY 13441-4514. Your assessment and feedback regarding this technical report will allow Rome Laboratory to have a vehicle to continuously improve our methods of research, publication, and customer satisfaction. Your assistance is greatly appreciated.
Thank You

_____

_____

Organization Name:_____(Optional)

Organization POC: _____(Optional)

Address:_____

1. On a scale of 1 to 5 how would you rate the technology developed under this research?

5-Extremely Useful 1-Not Useful/Wasteful

Rating_____

Please use the space below to comment on your rating. Please suggest improvements. Use the back of this sheet if necessary.

2. Do any specific areas of the report stand out as exceptional?

Yes___ No_____

If yes, please identify the area(s), and comment on what aspects make them "stand out."

3. Do any specific areas of the report stand out as inferior?

Yes___ No___

If yes, please identify the area(s), and comment on what aspects make them "stand out."

4. Please utilize the space below to comment on any other aspects of the report. Comments on both technical content and reporting format are desired.

*U.S. GOVERNMENT PRINTING OFFICE: 1995-610-126-50201

MISSION

OF

ROME LABORATORY

Mission. The mission of Rome Laboratory is to advance the science and technologies of command, control, communications and intelligence and to transition them into systems to meet customer needs. To achieve this, Rome Lab:

a. Conducts vigorous research, development and test programs in all applicable technologies;

b. Transitions technology to current and future systems to improve operational capability, readiness, and supportability;

c. Provides a full range of technical support to Air Force Materiel Command product centers and other Air Force organizations;

d. Promotes transfer of technology to the private sector;

e. Maintains leading edge technological expertise in the areas of surveillance, communications, command and control, intelligence, reliability science, electro-magnetic technology, photonics, signal processing, and computational science.

The thrust areas of technical competence include: Surveillance, Communications, Command and Control, Intelligence, Signal Processing, Computer Science and Technology, Electromagnetic Technology, Photonics and Reliability Sciences.